FTD-HC-23-385-71

FOREIGN TECHNOLOGY DIVISION

FORMATION OF NANOSECOND PULSES OF HIGH VOLTAGE

by

G. A. Mesyats, A. S. Nasibor
and V. V. Kremnev

Security Classification

DOCUMENT CONTROL DATA - R & D

(Security classification of title, body of abstract and indexing annotation must be entered when the overall report is classified)

1. ORIGINATING ACTIVITY (Corporate author) Foreign Technology Division Air Force Systems Command U. S. Air Force	2a. REPORT SECURITY CLASSIFICATION UNCLASSIFIED 2b. GROUP

3. REPORT TITLE

FORMATION OF NANOSECOND PULSES OF HIGH VOLTAGE

4. DESCRIPTIVE NOTES (Type of report and inclusive dates)

Translation

5. AUTHOR(S) (First name, middle initial, last name)

Mesyats, G. A.; Nasibor, A. S. and Kremnev, V. V.

6. REPORT DATE 1970	7a. TOTAL NO. OF PAGES 175	7b. NO. OF REFS 176
8a. CONTRACT OR GRANT NO. F33657-71-D-0057 b. PROJECT NO. 7JJ c. d.	9a. ORIGINATOR'S REPORT NUMBER(S) FTD-HC-23-385-71 9b. OTHER REPORT NO(S) (Any other numbers that may be assigned this report)	

10. DISTRIBUTION STATEMENT

Approved for public release; distribution unlimited.

11. SUPPLEMENTARY NOTES	12. SPONSORING MILITARY ACTIVITY Foreign Technology Division Wright-Patterson AFB, Ohio

13. ABSTRACT

The book is devoted to the design and construction of devices producing pulses lasting from one to hundreds of nanoseconds of voltage ranging up to 1000 kV. A survey is given of the existing methods for producing short high-voltage pulses. Various types of circuitry for generators of high-voltage nanosecond pulses are discussed. An analysis is given of transient processes within the framework of equivalent circuits. Engineering calculations are included for the formative elements of various types of generators. Consideration is given to circuits correcting pulse waveforms, and also to circuits used to measure pulse parameters. This book is intended for experimental physicists, specialists in the area of electrical and radio engineering, and for students majoring in engineering.

DD FORM 1 NOV 68 1473

UNCLASSIFIED

Security Classification

KEY WORDS	LINK A		LINK B		LINK C	
	ROLE	WT	ROLE	WT	ROLE	WT
Nanosecond Pulse						
Pulse Signal						
Circuit						
Design						
Pulse Laser						

EDITED TRANSLATION

FORMATION OF NANOSECOND PULSES OF HIGH VOLTAGE

By: G. A. Mesyats, A. S. Nasibor and
V. V. Kremnev

English pages: 175

Source: Formirovaniye Nanosekundnykh Impul'sov Vysokogo Napryazheniya 1970, pp. 1-153

Translated under: F33657-71-D-0057

UR/0000-70-000-000

PREPARED BY:

TRANSLATION DIVISION
FOREIGN TECHNOLOGY DIVISION
WP-AFB, OHIO.

TABLE OF CONTENTS

ABSTRACT

The book is devoted to the design and construction of devices producing pulses lasting from one to hundreds of nanoseconds of voltage ranging up to 1000 kV. A survey is given of the existing methods for producing short high-voltage pulses. Various types of circuitry for generators of high-voltage nanosecond pulses are discussed. An analysis is given of transient processes within the framework of equivalent circuits. Engineering calculations are included for the formative elements of various types of generators. Consideration is given to circuits correcting pulse waveforms, and also to circuits used to measure pulse parameters.

The book is intended for experimental physicists, specialists in the area of electrical and radio engineering, and for students majoring in engineering.

Foreword

The interest in nanosecond high-voltage pulse generators is rapidly increasing. At the present time, they are used in quantum radio physics, in nuclear physics, in particle accelerators, in x-ray defectoscopy, in high-speed photography, etc. The possibility of applying nanosecond generators to solve certain problems in experimental physics such as the production of powerful pulse lasers, strong-current accelerators of charged particles, and fast heating of plasma is of extreme interest.

The bright prospects for nanosecond high-voltage generators are due to the fact that they are capable of producing within a short time interval (10^{-8} - 10^{-7} seconds) enormous energies ranging from hundreds of Joules to megajoules, and thus are sources of energy of colossal densities. Even now it seems realistic to build devices which would produce pulses up to 10^{13} Watt.

Unfortunately, the technical literature devoted to power pulse techniques sheds little light on the problems of producing nanosecond high-voltage pulses. This situation gave the authors the idea of sharing with the reader the experience accumulated in this area in the Soviet Union and abroad.

Keeping in mind the small size of this book, we attempted to avoid laborious calculations, to facilitate as much as possible the understanding of the various methods of producing nanosecond pulses, and to determine a procedure which should be followed by an engineer in selecting a circuit and computing its elements.

The first and second chapters are devoted to the fundamental problems involved in producing nanosecond pulses of high voltage. The third and fourth chapters contain essentially the original

handbook-type material which is necessary in computing and constructing elements of nanosecond generators. The last chapter is devoted to applications of nanosecond high-voltage pulses. Greatest emphasis has been laid on those prospects which are opening up with the application of nanosecond high-voltage pulses to the rapidly developing areas of contemporary physics. In this chapter, we felt it was permissible to deviate slightly from the main theme and to dwell in more detail on the physical principles underlying the operation of semiconductor and gaseous pulse lasers, so that specialists in high-voltage nanosecond techniques could more clearly see those trends and problems whose solution will apparently largely determine the development of the technology for producing high-voltage nanosecond pulses in the years to come.

A substantial portion of the monograph has been written on the basis of work done by the authors at the Nuclear Physics Scientific Research Institute at the Tomsk Polytechnical Institute and at the P. N. Lebedev Physics Institute of the USSR Academy of Sciences.

G. A. Mesyats wrote the Introduction, Sections 2-5, 3-4, 4-5, 5-2 and 5-3; A. S. Nasibov wrote Sections 1-1, 1-5, 2-4, 2-6, 2-7, and 4-2; V. V. Kremnev wrote Sections 1-3, 3-1 - 3-3, and 3-5; Sections 1-2 and 2-3 were written jointly by the authors; Sections 1-4, 2-1, 2-2, and 4-4 were written by V. V. Kremnov and G. A. Mesyats; Section 4-1 was written by A. A. Dul'zon jointly with G. A. Mesyats; Section 5-1 was written by A. S. Nasibov in collaboration with G. G. Petrov; Section 5-4 was written by N. S. Rudenko.

The authors will feel that they have achieved their goal if, upon reading the book, the reader will not only become acquainted with the great opportunities which are opening up before engineers when it comes to the selection of circuitry and constructing high-voltage nanosecond pulse generators, but in addition will be able to select a circuit and compute the parameters of the basic elements of the generator circuit.

The authors would like to thank Academician N. G. Basov whose ideas stimulated the development of research on techniques of high-voltage nanosecond pulses, to Professor A. A. Borob'yev for support given to the work, and Professor G. A. Vorob'yev for useful discussions and help in the work. The authors will be grateful to the readers for critical remarks and desiderata.

The Authors

INTRODUCTION

Nanosecond pulse techniques generate low-power voltage pulses of several hundred volts and below, and produce high-voltage and powerful pulses of voltage ranging from 10^4 to 10^7 V [1,3]. Low-power nanosecond pulse technology owes its existence to experimental nuclear physics, radio engineering, and computer technology [2, 6]. The principal difference between the two types of pulse technology consists of the character of the active elements used. If in the first case these include tunnel diodes, secondary-emission tubes, low-voltage high-speed thyratrons, etc., then in the second case they include various types of spark gaps, ferrite elements, powerful hydrogen thyratrons, lines carrying shock electromagnetic waves, etc. Many papers in the periodicals as well as monographs have been devoted to the methods of generating low-power nanosecond pulses [2, 6]. The generation of powerful nanosecond pulses, however, has not received as much space in the technical literature. This is due, on one hand, to the fact that until the beginning of the 1950's there had not been too much interest in such pulses, and, on the other, to the great difficulties involved in their generation and recording. The spectrum of the harmonics of nanosecond pulses extends through super-high frequencies. Therefore, to generate and transmit such pulses it is necessary to use the kind of equipment that will pass wide frequency bands and will simultaneously sustain high voltages without a breakdown. The pulse parameters are strongly affected by the capacitance and inductance of the generator's discharge circuit. The latter are determined by the dimensions of the apparatus, and increase with the growth of these dimensions. Therefore, the requirements of steep front and pulse shortness (particularly as applied to rectangular wave forms) are contrary to making its amplitude as large as possible. The reason for this is that, as the voltage and current increase, the size of the pulse generator shows a similar tendency which leads to an increase of parasitic capacitance and

inductance. These contrary tendencies can be resolved by using coaxial structures involving distributed parameters and switching devices in a medium with high electric strength. Buravoy [5] was the first to describe a method for generating 100 kV pulses lasting 10^{-8} seconds. It was the year 1926. To shorten the pulse front, he used a peaking spark gap in oil which was used earlier by Hertz to obtain short electromegnetic waves. The duration of the pulse is shortened by means of a device called Binder's loop. The computations of the wavefront parameters were done considering the resistance of the spark from Tepler's formula. These studies made it possible to establish a relationship between the curvature of the wavefront and the line parameters, breakdown voltage of the spark gap, and the pressure at the gap. In particular, these studies resulted in the very important conclusion that, at constant breakdown voltage of the switching gap and low self-inductance of the circuit, the curvature of the pulse front is proportional to the pressure in the spark gap. This permitted Schering and Raske [25] to build a five-stage Marx pulse generator which made use of low-inductance plate capacitors and spark gaps in an atmosphere of compressed CO_2 gas. At 400 kV, the pulse front lasted 10^{-8} seconds.

A further contribution to the technique of high-voltage nanosecond pulses was made by Fletcher [26]. He was the first to use a gaseous peaking spark gap. He proposed a method for correcting the top of the pulse by including a capacitance in parallel with the generating line, and developed several types of voltage dividers for nanosecond pulses. He was the first to obtain a 20 kV pulse with a 0.4 nanosecond front. This work had a great influence on the subsequent development of the technique of powerful nanosecond pulses.

A substantial contribution to the development of high-voltage nanosecond pulse technology was made by I. S. Stekol'nikov [27] and by the work done at the Institute of Nuclear physics of the Siberian Division of the USSR Academy of Science [28, 29, 38, 159]. A survey of the work done up to 1963 was made in the monograph [1] . However,

[1] is devoted to the methods of generating voltage pulses of amplitude on the order of 10^4 V. The present work deals mainly with the methods of generating nanosecond voltage pulses of amplitude up to 10^6 V.

CHAPTER ONE

HIGH-VOLTAGE PULSE TRANSFORMERS

1-1. Transformer with Windings Made of Coaxial Cable

The formation of nanosecond pulses with amplitudes up to 100 kV involves considerable difficulties when it comes to choosing the right type of transformer. The ordinary pulse transformers, used in the microsecond range, are in this case inapplicable, since an increase in the amplitude of the pulse entails an increase in the thickness of insulation. This results in greater dimensions of the transformer and greater values of the parasitic parameters which distort the pulse. Therefore, at present, to transform nanosecond pulses, wide use is made of pulse transformers connected between long lines (discussed in Section 1-2) placed in parallel before the primary and in series after the secondary. However, a drawback of this transformer is that it needs a large number of uncoupling impedances. The number of impedances $m = n - 1$ and their magnitude increase rapidly with an increase in the number of lines n. This entails complications in the design and an increase in the size of the transformer. These drawbacks can be easily eliminated by making the windings of an ordinary pulse transformer with a ferromagnetic

core out of coaxial cable [7, 8]. A schematic showing the connections among the windings of such a transformer for n = 3 is given in Figure 1-1.

Figure 1-1. A schematic showing the connections of the windings of a "cable" pulse transformer with the transformation ratio n = 3.

The windings consist of three pieces of coaxial cable. The ends of the sheath of the pieces of coaxial cable are connected in parallel and form the primary of the transformer. The center wires of the pieces of cable are connected in series, and form the secondary. The transformation ratio n is equal to the number of pieces of the cable.

To increase the inductance, the cable windings are wound around a ferromagnetic core. In the case of short pulses, ferrite can be considered a better material for the core.

The parasitic parameters of a transformer can be determined with an accuracy sufficient for the purpose of experiments in terms of the running parameters of coaxial cable. The high pulse electric strength of coaxial cable permits one to obtain at the output of such a transformer short high-voltage pulses with amplitudes of tens of kilovolts. An important advantage of cable transformers is that they are stable under strong dynamic perturbations, which occur when large pulse currents pass through the windings. This is due to the fact that windings are coaxial. This property makes it possible to use the transformer also in producing large pulse currents.

The maximum amplitude of the pulse at the output of a "cable" pulse transformer is determined by the pulse electric strength, and for coaxial cables produced at the present time it may reach approximately 100 kV.

Below we give the basic considerations relating to the computation of the parameters of the "cable" pulse transformer, and we show that using it, it is possible to form high-voltage nanosecond pulses.

a) Computation of the elements of an equivalent transformer circuit.

The capacitance of a "cable" pulse transformer is determined mainly by the running cable capacitance C_0. For convenience in analysing the processes occurring in the transformer circuit, the distributed capacitance of the windings is replaced by the equivalent (dynamic) capacitance, as applied to the turns of the primary (divided by the voltage in the primary U_1).

The dynamic value of the capacitance differs from the static value, and is determined in terms of the energy stored in the windings. From the general considerations involving the definition of the dynamic capacitance, it is easy to show [7, 8] that in the case of a "cable" pulse transformer the dynamic capacitance is

$$C = \frac{n(n \pm 1)(2n \pm 1)}{6} C_0 l_k \qquad (1\text{-}1)$$

where n — is the transformation ratio; l_k — is the length of a cable segment. The sign " — " in Equation (1-1) corresponds to the case where the transformer does not change the polarity of the pulse.

For n = 1, and assuming that the polarity of the pulse is not changed by the transformer, the dynamic capacitance is by (1-1) equal to zero. The physical meaning of this fact is that the potentials on the primary (sheath) and secondary (center wires) are equal in terms of value and sign, and thus the capacitance of the cable is not charged.

The stray inductance of a "cable" pulse transformer is determined by the distribution of the field between the windings, i.e., between

the sheath and the center wire of a cable. Since the field between the sheath and the center wire of a cable determines the linear inductance of the cable, L_0, it is easy to see that, if a "cable" transformer contains n sections, the stray inductance of the secondary divided by the number of turns in the primary, L, is given by

$$L=\frac{L_0 l_k}{n}, \tag{1-2}$$

where L_0 — is the linear inductance of the cable; l_k — is the length of the cable segment.

In contrast to pulse transformers composed of ordinary windings, the primary (sheath) of a "cable" transformer does not produce any stray flux, since it does not contain any magnetic flux that is not connected with the secondary (center wire).

Equation (1-2) implies that the stray inductance of a "cable" pulse transformer is determined only by the linear inductance of the cable, and for a certain length of the cable it does not depend on the shape of coils and the presence of the core.

To determine the degree of distortion of a pulse front, it is necessary to know the wave resistance of a cable pulse transformer $\rho = \sqrt{L/C}$.

Equations (1-1) and (1-2) easily imply that

$$\rho=\rho_0\frac{1}{n}\sqrt{\frac{6}{(n\mp 1)(2n\mp 1)}}, \tag{1-3}$$

where $\rho_0=\sqrt{L_0/C_0}$ — is the wave resistance of the cable.

The sign " — " corresponds to the case when the polarity of the pulse is not changed by the transformer. The sign " + " corresponds to the case when it is changed.

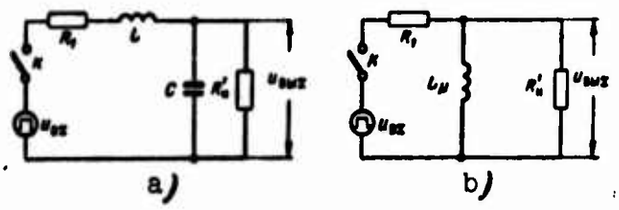

Figure 1-2. Equivalent circuit for a pulse transformer.

a - for high frequencies; b - for low frequencies.

The length of the front of a pulse passing through a cable pulse transformer can be found by considering the transient process in the equivalent circuit for a pulse transformer, Figure 1-2, a, with parameters divided by the number of turns in the primary: R_1 is the internal resistance of the source; $R'_H = R_H/n^2$ is the reduced load resistance.

Using a widely known [4] technique of analyzing the transient processes, for the circuit in Figure 1-2, a, we can easily show that, when a voltage surge is input into the circuit, the duration of the front of the output pulse, t_{f0}, per 1 m of the winding (linear duration of the front) with an accuracy sufficient for engineering calculations is given by an expression in which the values of L, C, and ρ are taken from (1-1) - (1-3):

$$t_{\phi 0} = \theta(1{,}2 + 2\xi^2), \tag{1-4}$$

where

$$\left.\begin{aligned} \xi &= \frac{\sqrt{k}}{2}\left(\frac{\rho}{R'_H} + \frac{R_1}{\rho}\right); \\ \theta &= \sqrt{kLC}; \\ k &= \frac{R'_H}{R_1 + R'_H}. \end{aligned}\right\} \tag{1-5}$$

From (1-5), we find

$$R'_H = \frac{\rho\sqrt{k}}{\xi \mp \sqrt{\xi^2 - \xi^2_{min}}}, \qquad (1\text{-}6)$$

where $\xi_{min} = \frac{R_2}{R_1 + R'_H}$ is the minimum value determined by finding the minimum value of the formula for ξ.

From (1-5) and (1-6), we can find the function $t_{f0} = f(R'_H)$ for given ρ_0, C, n, k.

Figure 1-3 shows a graph of the function $t_{f0} = f(R'_H)$ for a pulse transformer whose windings are made of a coaxial cable with $\rho_0 = 50$ ohms and $C_0 = 100$ pF/m. These values of ρ_0 and C_0 approximately correspond to the wave resistances and the linear capacitance of a majority of coaxial cables which can be used as winding of heavy-duty "cable" pulse transformers. Using the plots given in Figure 1-3, if one is given the length of the cable, l_H, and the reduced resistance, one can find, with an accuracy sufficient for the experiment, the duration of the pulse front from the formula

$$t_\phi = t_{\phi 0} l_H \qquad (1\text{-}7)$$

By analyzing the plots in Figure 1-3, we can arrive at the following conclusions:

1. For a cable with $\rho_0 = 50$ ohms and $C_0 = 100$ pF/m and the transformation ratio n ranging from 2 to 4, the minimum value of the pulse duration is obtained for R_H equal to several hundred ohms which corresponds to the power of several dozen megawatts. The coaxial cable is then fully used as to its electric strength.

2. If the length of the cable in the primary is on the order of several tens of centimeters, the transformation ratio is n = 2 - 3,

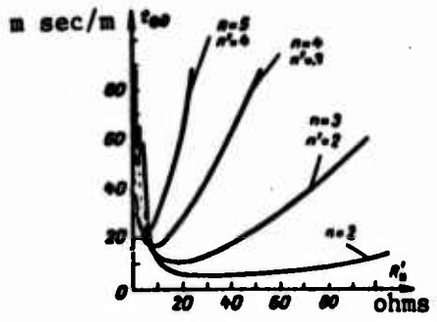

Figure 1-3. Plot of linear length of pulse front vs. converted resistance of load for the values ρ_0 = 50 ohms, C_0 = 100 pF/m, k = 0.5.

n - is the transformation ratio without a change in the pulse polarity;

n' - is the transformation ratio with a change in the pulse polarity.

and the load corresponds to the optimum mode of operation, and the duration of the pulse front cannot exceed several nanoseconds.

It must be noted that for a given amplitude and length of a pulse, the length of the cable in the primary winding depends on the parameters of the core material: magnetic permeability μ and saturation induction B_M, in the following way: with an increase in μ and B_M, the length of the cable l_k decreases. For a given type of core and its material, an and a given amplitude the ratio t_f/t_p will be conserved. For example, for a nickel-zinc ferrite of type F1-1000 for the amplitude U_M = 50 kV, the minimum ratio is $t_f/t_p \approx 0.05$.

Generally speaking, starting with certain values of pulse length (for F_1-1000 ferrites with $t_p \approx 100$ nsec), the value of the magnetic permeability μ depends on the length of the pulse and has a decreasing characteristic. In accordance with this, the ratio t_f/t_p tends to increase.

b) Determination of the number of turns and choice of material and parameters for the magnetic circuit.

An analysis of the effect of a rectangular pulse on the primary winding of a transformer and a study of an equivalent circuit in Figure 1-2, b yield the following formulas for the basic parameters of a pulse transformer [4]. The number of turns in the primary is

$$w_1 = \frac{U_{вх} t_и}{\Delta B S} 10^4. \qquad (1\text{-}8)$$

Magnetization inductance is

$$L_\mu = \frac{4\pi 10^{-8} w_1^2 S}{l_0} \mu, \text{ H}. \qquad (1\text{-}9)$$

The drop of the pulse peak is

$$\lambda = \frac{\Delta U_{вых}}{U_{вых}} = \frac{t_и R_1 R'_н}{L_\mu (R_1 + R'_н)}. \qquad (1\text{-}10)$$

Here U_{in} is the voltage of the primary; U_{out} is the voltage of the load, v; t_p is the length of the pulse, sec; R_1 is the equivalent internal resistance of the generator, ohms; R'_H is the reduced resistance of the load, ohms; S is the cross section of the core, cm^2; l_0 is the length of a mean line of force of the magnetic circuit, cm; μ is the magnetic permeability; ΔB is the value of the magnetic induction within a partial cycle of the hysteresis loop, tesla.

Using (1-8), (1-9), (1-10), we can determine the parameters of the core and the winding. As we can see from the formulas given, the minimum number of turns and the maximum magnetization inductance (and consequently, the minimum front at a minimum drop of the plane section) can be obtained at the maximum ratio S/l_0 of the core. Of course, an annular form of the core is most convenient from all points of view (it fully utilizes the magnetic circuit, it reduces the parasitic parameters, etc.). However, there is a limitation which does not permit S/l_0 to attain a large value for one ring due to the increased ratio of the outer to inner diameters. In fact, for the same magnetization force (m.f.) field intensity will depend on the length of the magnetic path:

$$H = \frac{I_\mu w_1}{l}, \text{ A/cm} \qquad (1\text{-}11)$$

However, due to the large difference in diameters, there will be considerable differences between l_o and l_i for the ring, and thus $H_o << H_i$, which may result in saturation of the inner part of the ring, and thus a reduction of the physical cross-section of the magnetic circuit. An effective way of obtaining large ratios ($S/l_0 \approx 1 - 1.5$) involves constructing the core of several rings.

To construct a pulse transformer, one must choose a magnetic material with the following properties:

1) large value of the maximum induction B_M;
2) large value of the magnetic permeability μ;
3) large value of the resistivity ρ_{sp};
4) small losses due to eddy currents;
5) weak dependence of μ on frequency.

In practice, there is no material possessing all of the above properties. Among the existing materials, it makes sense to consider the possibility of using ferrites and high-quality alloys made of Permalloy. The advantage of Permalloy alloys is that they have a large magnetization induction and magnetic permeability ($B_M = 0.7 - 1.5$ tesla, $\mu \approx 150{,}000$). A considerable drawback of Permalloy alloys is their small resistivity. For small pulse lengths, $t_p \approx 10^{-8} - 10^{-7}$ sec, the eddy currents rapidly lower the value of μ. To reduce eddy currents, the cores are made of a material several microns in thickness. It must be noted that the technology of winding, annealing, and deposition of interlayer insulation involves considerable difficulties, and requires special equipment [10]. Another disadvantage of using Permalloy cores is the fact that one must insulate the winding from the core.

In contrast with Permalloy alloys, ferrite materials have large resistivity which means that they can be used without an additional high-voltage insulation.

The eddy currents and the function $\mu = f(t_p)$ are not expressed as sharply in ferrites as they are in Permalloys. Their drawbacks are the relatively small values of B_M and μ. In the final selection of the material, one must estimate its properties for a given pulse length t_p.

c) Effect of induction rate of increase on the operation of the core.

The rate of increase of the magnetic induction in the core during the formation of high-voltage nanosecond pulses of tens of kilovolts may reach values on the order of $10^7 - 10^8$ tesla/sec. As a result, powerful eddy currents are set up in the core which produce a strong demagnetizing current [11]. To compensate for this field during the magnetization of the core, one must use an additional current. Therefore, the role of the ordinary magnetization current in the pulse mode of operation is played by the so-called apparent magnetization current $I_к > I_\mu$. The apparent increase in the magnetization current results in an apparent reduction of the magnetic permeability of the core, $\mu_к < \mu$.

The apparent permeability of the magnetic material depends basically on the thickness δ_{th} of the core strip and the pulse length t_H. In general, the relative value of the apparent permeability is a function of the ratio of the pulse length to the eddy time constant θ_B.

$$\mu_к = f\left(\frac{t_н}{\theta_в}\right), \qquad (1\text{-}12)$$

where

$$\theta_в = \frac{\mu_\Delta \delta_{th}^2}{\pi \cdot 10^9 \rho_{sp}};$$

δ_{th} is the thickness of the core sheets, cm; ρ_{sp} is the specific electric resistance, ohm·cm; μ_Δ is the magnetic permeability within a partial cycle of the hysteresis loop.

The dependence of the relative magnetic permeability μ_Δ/μ_0 on the relative length $\tau_p = l_p/l_0$ has been considered in [4].

In addition to the effect of the demagnetization field of eddy currents, one must also consider the nonuniform distribution of the magnetic flux over a section of the sheet, by virtue of which the maximum increase ΔB_M on the surface of the sheet exceeds the average value of the increase given by (1-8).

The ratio of the maximum value of the induction increase on the surface of the sheet to the average increase within the sheet as a function of τ_p is given by the formula

$$\frac{\Delta B_M}{\Delta B_{av}} = 1 + \frac{1}{\tau_p}\left(\frac{\pi^2}{3} - 2\sum_{k=1}^{\infty}\frac{1}{k^2}e^{-k\tau_p}\right). \qquad (1\text{-}13)$$

For example, for $\tau_p = 0.2$ $\Delta B_M \approx 10\ \Delta B_{av}$. Such a high value of ΔB_M leads to an additional increase of the magnetization current, and lowers the value of μ_K. In general, an exact calculation of μ_K is difficult, and usually the actual value of the magnetic permeability is computed experimentally. In [13], the values of μ_K were experimentally determined for various alloys. The author stipulates that investigations designed to determine the function $\mu_K = f(t_p)$ for $t_p = 3\cdot10^{-8}$ sec have shown that in a majority of Permalloys $\mu_K = 400 - 600$ for sheet thickness of $\delta_{th} = 10 - 15$ micrometers. Thus, we see that an advantage of Permalloys is their large value of ΔB_M. However, this property, which permits one to raise the potential U_{in} to hundreds of kilovolts [see Equation (1-8)], is not realized in practice. It must be noted that the values of the magnetic permeability μ_K and the maximum value of ΔB_M refer to the portion of the magnetization characteristic that has the largest curvature. For operation in this portion, one must introduce an additional magnetization which produces a number of additional difficulties related to the decoupling of the magnetization winding from the effect of the high pulse voltage, and to the necessary elimination of the effect of parasitic parameters.

When operating without additional magnetization, the values of the magnetic permeability μ_K and the increase of the magnetic induction ΔB_M within a partial cycle of the hysteresis loop for Permalloys decrease sharply.

Let us consider the characteristics of ferrites. Out of ferrite cores whose production has been mastered by domestic industry, nickel-zinc ferrite is most convenient as to the dimensions of the ring and the physical characteristics. The magnetic permeability of ferrites falls off at frequencies higher than the gyromagnetic frequency of the electron spin f_{gy} [14 - 17]:

$$f_{gy} = \frac{gB_M}{\mu}, \qquad (1\text{-}14)$$

where $g = 2 \cdot 10^{10}$ 1/tesla sec.

Figure 1-4 gives the plot of $\mu = F(f)$ for ferrites with different values of μ [15]. The plot shows that the nickel-zinc ferrite with $\mu = 1{,}000$ is most suitable for making cores. To this ferrite there corresponds a domestic ferrite material of the type F1-1000 ($B_M = 0.25$ tesla, $\mu = 1{,}000$). The boundary frequency for this ferrite (1-14) is equal to 6 MHz. In the case of pulses with $t_f \approx 0.2t_p$, the upper limiting frequency for $t_p = 2 \cdot 10^{-7}$ sec is determined using the formula [4]

$$f_в = \frac{0.4}{t_ф} = \frac{0.4}{4 \cdot 10^{-8}} = 10 \text{ MHz} \qquad (1\text{-}15)$$

In this case, the corresponding value of the magnetic permeability is $\mu_B \approx 300$. The lower limiting frequency can be found from the formula

$$f_н \approx \frac{1}{t_н} = 5 \text{ MHz} \qquad (1\text{-}16)$$

The μ_H corresponding to this frequency is approximately equal to 500. The value of μ_B must be taken into consideration when analyzing the transient process occurring during the formation of the pulse front.

The value of μ_H must be taken into consideration when analyzing the distortion of the pulse peak.

The value of μ can be found more accurately using experimental methods. Then the additional effects of the magnetic field, etc. can be taken into consideration. It follows from the values of f_{gy} found by computation that nickel-zinc ferrites should be used for $t_p \geq 10^{-7}$ sec.

d) Construction of a "cable" pulse transformer.

The core of a "cable" pulse transformer is built using individual ferrite rings. To eliminate the cracking of rings, pressboards are placed between rings during the winding of the cable. The core ends are fitted with rings made of insulating material whose radius of curvature is such as to eliminate the possibility of the cable cracking. To reduce the insulating distances, the windings are made from one piece of cable, and then the sheath is separated into sections. Thus, the secondary (center wire) does not suffer a gap in insulation along its entire length. An example of a design of a pulse transformer with the transformation ratio n = 3 is given in Figure 1-5. The transformer is built on ten 120 x 80 mm nickel-zinc ferrite rings.

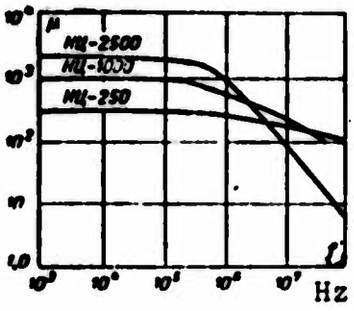

Figure 1-4. Dependence of magnetic permeability on frequency

Figure 1-5. General view of a "cable" pulse transformer with the number of cables n = 3, power 15 megawatts at the voltage of 50 kV; pulse length is 100 nanosec.

To reduce its size, the transformer is mounted on a high-voltage pulse separator made of an insulating material. Under optimal conditions, the transformer can transmit a pulse with the following parameters:

Maximum voltage	50 kV
Maximum power	15 megawatts
Pulse length	100 nanoseconds
Front length[1]	15 nanoseconds

1-2. Transformer Built of Sections of Coaxial Cable

Transformation of short pulses with voltages up to hundreds of kilovolts entails considerable difficulties.

An impulse transformer with windings made of coaxial cable (see Section 1-1) is in this case inapplicable due to the following factors:

1. The pulse electric strength of coaxial cables that are produced today and are suitable for use as pulse transformer windings is limited by the insulating strength of the cable and does not exceed 100 kV.

2. As the transformation ratio increases, the dynamic capacity grows in proportion to the sum of a numerical series, $\frac{n(n+1)(2n+1)}{6}$, which leads to the distortion of the pulse waveform. Therefore, in transforming pulses with voltages up to hundreds of kilovolts, one uses a pulse transformer made of sections of coaxial cable. This type of transformer, proposed by Lewis [18], represents a device made of several busbars (generally, n) which at the input are connected in parallel, and at the output in series (Figure 1-6). The voltage pulse fed into the input of the transformer during a time $t_3 = l/v$ (where l is the length of the lines; v is the speed of propagation of electromagnetic waves), reaches the output of the transformer. If a load

Footnote (1) appears on page 38a.

$R_H = h\rho$, where ρ is the wave resistance of an individual line, is placed at the output, then at the load the amplitude of the voltage in the absence of distortions increases n times compared to the input voltage. To reduce the frequency distortions of the transformed pulse and heighten the transformation ratio up to its ideal value, equal to n, the input of the transformer should be separated from its output by means of large uncoupling impedances. This is why, to increase the inductance, the transformer lines are wound on a coil. To increase the transformation ratio, it is also necessary to reduce the capacitances and inductances which couple the coils. Therefore, the coils are made so that the winding pitch is not uniform, and are placed as far as possible from each other. To increase the inductance of the coil, one can use ferrite cores or cores made of other ferromagnetic materials. In this case, however, one must keep in mind a reduction of the effective magnetic permeability with an equivalent frequency (for more details, see Section 1-1).

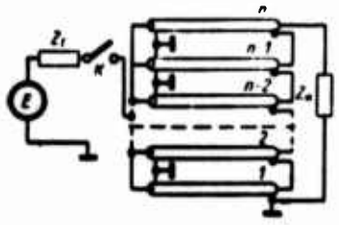

Figure 1-6. A schematic showing principal parts of a transformer built from sections of long lines.

To reduce high-frequency distortions, one also makes use of coaxial transformer designs [18]. In this case, the transformer lines are made in the form of n coaxial cylinders contained within one another. In another version of this construction, all lines are wound around individual cylinders made of an insulating material and placed in grounded metallic cylinders. The sheath of each line forms a spiral with each cylinder.

In the case of transforming very short pulses (approximately 10^{-8} sec), it is possible to reduce pulse distortion no less effectively by using ferrite cores which are put on cable sheaths [21].

An advantage of a transformer built on sections of long lines is the relatively uniform distribution of voltage along the lines at the output of the circuit and small values of parasitic parameters (compared to the ordinary pulse transformers on ferromagnetic cores). This makes it possible to transform with small distortions pulses tens of nanoseconds in width and hundreds of kilovolts in voltage [19, 20].

The drawback of this transformer is that it is necessary to use with it decoupling impedances whose sizes increase with an increase of the transformation coefficient.

a) An equivalent circuit for a transformer built from sections of long lines (cables).

Upon the arrival of the pulse at the output leads of the transformer built from sections of long lines, the sheaths of the lines on the output side are at different pulse potentials, i.e., electromagnetic signals begin to propagate from the output of the transformer toward its input along the sheaths and inside the lines. The character and the magnitude of these signals, as well as the form and amplitude of the output pulse, are determined in a general case by the number of lines in the transformer, amplitude, and form of the input pulse, wave resistances of the lines, mutual positioning of the lines, the design of the transformer, and the load resistance. If one considers the output end of each cable at a time when a voltage pulse arrives at it as a pulse source of voltage 2E, then the equivalent network used in the analysis of the processes distorting the pulse is as is shown in Figure 1-7, c. In this case, Z and Z_0 are determined by various transformer parameters when the pulse front is analyzed (parasitic parameters) or when analyzing the flat part (inductance of the uncoupling impedances), n is the number of cable sections. For $Z_0 >> nZ$, the maximum transformation ratio for the network is

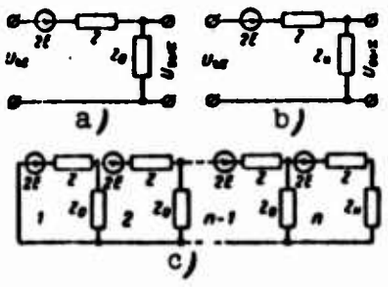

Figure 1-7. Schemes for designing transformers built from sections of long lines.

a - active Γ-shaped four-terminal network of general type;
b - n^{th} four-terminal network;
c - equivalent transformer network.

$$N = 2n \frac{Z_0}{nZ + Z_0},$$

where $Z = \rho$.

In an actual case, due to parasitic parameters and a finite value of the uncoupling resistance Z_0, both the front and the peak of the pulse are distorted. In addition, a certain distortion of the pulse depends on the transmission band of the coaxial cable, i.e., the dependence of ρ on the frequency. However, in a majority of cases the cut-off frequency of the cable (see Section 4-1) is much higher than the equivalent cut-off frequency of the pulse, and therefore, distortions introduced by the cable can be neglected.

b) Transformation ratio.

Now we shall proceed to analyze the equivalent network. As noted earlier, the uncoupling resistance Z_0 can be made in the form of a line with a wave resistance $Z_0 = \text{const}$ or in the form of a coil with inductance L whose resistance Z_0 is a function of time $Z_0 = f(t_p)$.

In the first case, the transformation ratio of the output pulse changes; in the second — there is a voltage drop along the flat portion of the pulse.

Let us consider the first case. The load resistance may in general not be matched with the transformer output. To simplify the analysis, we assume that: Z_0, Z and Z_H are ohmic resistances; E is the input impulse; Z_g is the internal resistance of the pulse generator (Figure 1-6). It is easy to see that the network in question

consists of n - 1 active L networks, shown in Figure 1-7, a, loaded at the output by the n^{th} four-terminal network, shown in Figure 1-7, b. A derivation of the formula for the potential at the load is given in [22]. In this case, the voltage at the load is defined as (in a general case in the operator form)

$$U_n = \frac{2E(\lambda_1^n - \lambda_1^{-n})Z_n}{\lambda_1^n[Z + Z_n(1-\lambda_1^{-1})] - \lambda_1^{-n}[Z + Z_n(1-\lambda_1)]}. \qquad (1\text{-}17)$$

where

$$\lambda_1 = 1 + \frac{Z}{2Z_0} + \sqrt{\frac{Z}{Z_0}\left(1 + \frac{Z}{4Z_0}\right)}.$$

If hyperbolic functions are introduced, then (1-17) becomes simplified:

$$U_n = \frac{2E}{\frac{Z + Z_n}{Z_n} - \frac{\operatorname{sh}(n-1)\varphi}{\operatorname{sh} n\varphi}}. \qquad (1\text{-}18)$$

where $\varphi = \lg \lambda_1$.

From (1-18) for $Z_H = \infty$ we obtain:

$$U_{n\infty} = \frac{2E}{1 - \frac{\operatorname{sh}(n-1)\varphi}{\operatorname{sh} n\varphi}}. \qquad (1\text{-}19)$$

From (1-19) for $n \to \infty$ we have in the limit $U_{H\infty} = U_{H.max}$, and [22, 23]

$$U_{H \cdot max} = \frac{2E\lambda_1}{\lambda_1 - 1}. \qquad (1\text{-}20)$$

Figure 1-8, a and b give plots of $U_H/E = f(n)$ for various values of the ratio Z_0/Z for $Z_H = nZ$ and $Z_H = \infty$, computed using (1-18) and (1-19), respectively. The functions U_H/E initially grow almost proportionally to n, and the growth of U_H/E for the open-circuit case proceeds much faster. Then the increase slows down, and the functions

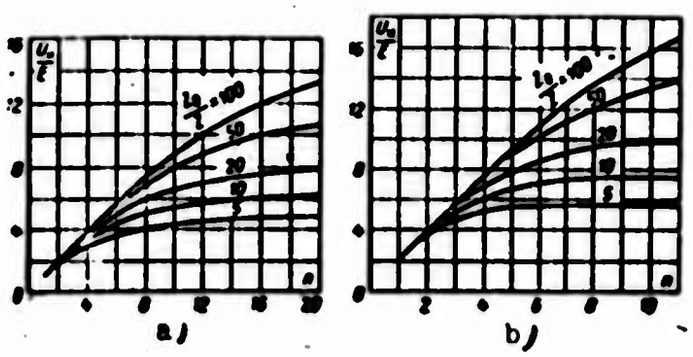

Figure 1-8. The transformation ratio as a function of the number of lines.
a - for $Z_H = nZ$; b - for $Z_H = \infty$.

tend toward saturation, which can be found from (1-20). For each specific ratio Z_0/Z, there is a certain number of lines $n = n_{opt}$ starting at which the transformation ratio U_H/E does not grow appreciably with an increase in n, and the increase is of no practical importance. In accordance with Figure 1-8, a and b, one can recommend that n_{opt} be found as a point of intersection of the horizontal line drawn at the level of the limiting value of the voltage on the load, $U_{H.max}$, and the tangent to the plot of U_H/E at $n = 1$. It is easy to show that the equation of this tangent for $Z_H = nZ$ has the form $U_H/E = n$, and for $Z_H \to \infty$ $U_H/E = 2n$. Consequently, for $Z_H = nZ$ [33]

$$n_{opt} = \frac{2\lambda_1}{\lambda_1 - 1}, \tag{1-21}$$

and for $Z_H \to \infty$

$$n_{opt} = \frac{\lambda_1}{\lambda_1 - 1}. \tag{1-22}$$

c) Distortion of the peak of the pulse

If lines are wound into coils with large numbers of turns, then in this case Z_0 will vary in time. In the approximate analysis of the effect of Z_0 on the pulse form, we can assume that the form of the pulse front is influenced by the capacitance, and the form of the peak — by the coil inductance. Let us assume that we are given the coil inductance L, capacitance C, the time needed for the transformed pulse to grow from 0.1 to 0.9 of the amplitude value t_f. Then Equation (1-15) is valid for the upper cut-off frequency f_B.

The inductive and capacitive reactances of the coil at this frequency can be found from the relations

$$X_L = \frac{j2\pi 0{,}8L}{t_0}; \qquad (1\text{-}23)$$

$$X_C = \frac{0{,}2t_0}{j\pi C}, \qquad (1\text{-}24)$$

where $j = \sqrt{-1}$.

If $|X_L| > |X_C|$, then when analyzing the front of the transformed pulse, we can neglect the effect of the coil inductance.

On the other hand, we have Equation (1-16) for the lower frequency f_H of the transformed impulse. Substituting (1-16) into the formulas for reactances X_L and X_C, we obtain, respectively:

$$X_L = j2\pi L/t_n, \quad X_C = \frac{t_n}{j2\pi C}. \qquad (1\text{-}25)$$

If $|X_L| < |X_C|$, then in the analysis of the distortions of the pulse peak, we neglect the effect of the capacitance. To simplify the analysis, we consider the open-circuit mode of the transformer under the influence of a drop at the input, $U_{in} = E$.

For the calculation of the pulse peak, we have:

$$Z_0 = Lp; \quad Z = \rho, \tag{1-26}$$

where ρ is the wave resistance of the cable; p is the operator. When making a transition from the operator expression for the voltage on the load (1-18) to its original, we obtain, in view of (1-26), the following expression for the relative value [22, 23]:

$$u_{вн}(\tau) = \frac{u_н(\tau)}{E} = 2 + \sum_{x=0}^{n-2} \frac{2\operatorname{ctg}^2 \frac{\varphi_x}{2}}{2n-1} e^{-0{,}25\left(\operatorname{ctg}^2 \frac{\varphi_x}{2} + 1\right)\tau}, \tag{1-27}$$

where $\varphi_x = \frac{\pi(1+2x)}{2n-1}$; $\tau = \frac{t_p}{L}$.

The analysis [30] of Equation (1-27) implies that, with an error no greater than 15% for $n \leq 20$, the value of the relative drop of the pulse, λ, for the case $Z_H \to \infty$ can be written as

$$\lambda = \frac{n-1}{n}\left\{1 - \exp\left[-0{,}25\tau \Big/ \sin^2 \frac{\varphi_0}{2}\right]\right\}, \tag{1-28}$$

where $\varphi_0 = \frac{\pi}{2n-1}$; $\tau = \frac{t_p}{L}$.

Using (1-28), we can find the inductance of a coil if we are given the number of lines in the transformer n, the width of the transformed pulse t_p, the wave resistance of the line ρ, and the maximum permissible value of the drop of the pulse peak, λ. In this case, we obtain

$$L > \frac{t_{и}\rho}{4\sin^2 \frac{\varphi_0}{2} \ln\left(1 - \frac{2n}{n-1}\right)}. \tag{1-29}$$

Equation (1-29) shows that the inductance of the coil must increase in proportion to the pulse width, the wave resistance of the lines used, and the square of the number of lines (for $n > 4$), since $\sin^2 \frac{\varphi_0}{2} \sim n^2$.

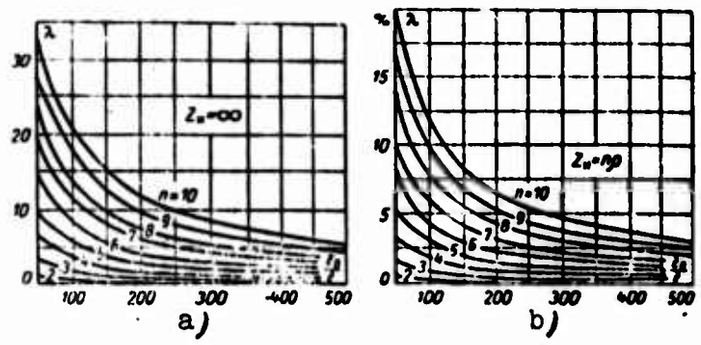

Figure 1-9. Dependence of the relative reduction of the pulse amplitude λ on the parameter $\bar{Z}_0 = Z_0/Z$ for various n.

a - for an open-circuit transformer $Z_H = \infty$;

b - for a loaded transformer, $Z_H = nZ$.

If the condition $Z_0/Z >> 1$ is satisfied, then — with an accuracy sufficient for engineering calculations — we have the relation

$$Z_0 = \frac{L}{t_u}. \qquad (1\text{-}30)$$

from which we can determine L.

In [24] the value of λ has been found following a different line of reasoning. According to the analysis given there

$$\lambda = \frac{U_u(0) - U_u(t_u)}{U_u(0)}.$$

It is assumed that $Z_0 = \infty$ at $t = 0$, and for $t > 0$ Z_0 has a finite value.

The plots of $\lambda = f(Z_0/Z)$ for various n for $Z_H = \infty$ and $Z_H = nZ$ are given in Figure 1-9.

d) Distortions of the pulse front.

In calculating the distortion of the front of the transformed pulse for the open-circuit mode of the transformer, we shall consider the self-capacitance of the winding, C. Then

$$Z_0 = \frac{1}{Cp};\ Z = p. \tag{1-31}$$

In this case, the voltage at the output of the transformer becomes [22, 23]:

$$u_{вых}(\tau_1) = 2n - 2(n-1)\exp\left[-4\sin^2\frac{\pi\tau_1}{2(2n-1)}\right]. \tag{1-32}$$

where $\tau_1 = t/\rho C$.

Assuming the width of the front, t_f, to be the time needed for the voltage to increase to the level of 0.9 times the amplitude, from (1-32) we determine the maximum permissible value of the self-capacitance of the coil as

$$C \leq \frac{-4l_0\sin^2\frac{\pi}{2(2n-1)}}{\rho\ln\frac{0.1n}{n-1}}. \tag{1-33}$$

Equation (1-33) implies that the width of the front increases in proportion to the coil capacitance, wave resistance of an individual transformer line, and the square of the number of lines (for $n \geq 4\sin^2\frac{\pi}{2(2n-1)} \approx \frac{\pi^2}{4(2n-1)^2}$).

1-3. Transformer Based on Coupled LC-Circuits.

One of the methods of obtaining high voltages for generators of nanosecond pulses involves voltage transformation in a system composed of two oscillating circuits L_1C_1 and L_2C_2 with an inductive coupling (Figure 1-10). Nanosecond pulses are generated by connecting C_2 in

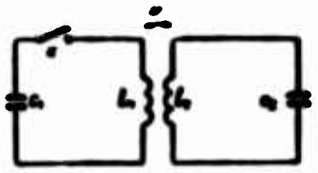

Figure 1-10. A circuit of a transformer based on coupled LC-circuits.

the second circuit as a load through a high-speed spark gap (for more details, see Section 5-2). To stimulate oscillations in the first circuit, it is necessary to charge C_1 to a certain voltage U_1. After the commutator K is closed, the free oscillations that occur are transmitted to the L_2C_2 circuit. In order for the transmission of energy from the first circuit to the second to occur with maximum efficiency, it is necessary that the frequencies of oscillations in the circuits be equal, i.e.,

$$f_1 = \frac{1}{2\pi\sqrt{L_1C_1}} = f_2 = \frac{1}{2\pi\sqrt{L_2C_2}}.$$

Analyzing the transient process in these circuits without considering the losses, we can obtain the following for the voltage on the capacitor C_2:

$$u_2 = -\frac{U_1}{2}\sqrt{\frac{C_1}{C_2}}(\cos\omega_1\tau - \cos\omega_2\tau), \tag{1-34}$$

where $\tau = t/\sqrt{L_1C_1}$; $\omega_1 = 1/\sqrt{1+k}$;

$$\omega_2 = 1/\sqrt{1-k}; \quad k = M/\sqrt{L_1L_2}.$$

M — is the mutual induction coefficient for the circuits;
t — is the time.

The maximum possible value of u_2 for fixed circuit parameters L and C and variable k will be

$$u_{2m} = -U_1\sqrt{\frac{C_1}{C_2}}. \tag{1-35}$$

i.e., the voltage on the capacitor C_2 is greater than the voltage on the capacitor C_1 for $C_1 > C_2$. If $C_1 = n^2 C_2$, then at the output the voltage will be multiplied n times.

Equation (1-34) then implies [31]:

$$k = \frac{(l+1)^2 - l^2}{(l+1)^2 + l^2}, \tag{1-36}$$

where $l = 1, 2, \ldots, \infty$. For these values of l, we obtain several values of the coefficient k: 0.6; 0.385; 0.28; ...; 0. The maximum possible voltage on the capacitor C_2, given by (1-35), corresponds to the maximum coefficient of energy transmission from the first circuit to the next. In the case of undamped oscillations in the circuits, this coefficient is equal to 1.

When considering the resistances r_1 and r_2 in the first and second circuit, respectively, the output will be in the form of damped oscillations. The period of these oscillations, assuming weak damping in the circuits, can be determined from (1-34). The magnitude of damping can be determined principally by the ratio r/L in each circuit. Therefore, for $L_2 = n^2 L_1 (n \gg 1)$ the first circuit has a great effect on the damping of oscillations. The time until the first large maximum of oscillations in the presence of weak damping in the circuits is determined approximately from (1-34) as

$$t_m \approx \pi \sqrt{(1+k) L_1 C_1}. \tag{1-37}$$

The relative decrement of the amplitude, λ, is in this case determined by the quantity

$$\lambda \approx \frac{\pi [(l+1)^2 + l^2]^{3/2}}{\sqrt{2}\, l (l+1)}, \tag{1-38}$$

i.e., with an increase of l (or a decrease of k) damping tends to intensify. In this connection, one must obtain a large value of k on the order of optimal coupling coefficients (especially k = 0.6).

A transformer based on coupled LC circuits differs conveniently from the Marx generator by the absence of a large number of spark gaps, and from the ordinary pulse transformer by the absence of the ferromagnetic core. These facts favor this method of stepping up the voltage when the generators operate at increased pulse frequencies.

Transformers based on coupled oscillatory circuits are becoming more and more widespread [31 - 34]. In [33] the secondary winding of the transformer was made in the form of a flat spiral wound on a squirrel-cage carcass. In this cage the output voltage reached 1 MV. The use of the secondary winding in the form of a flat spiral is convenient in that it is possible to obtain a voltage from it which varies uniformly from zero on the outer turn to a maximum on the inner one. To reduce the electric field in the transformer, the entire block was placed in a deionized water with a specific resistance from 2 to 10 megaohm·cm. The transformation ratio obtained is approximately 10. The coupling coefficient is chosen approximately as 0.6. Reference [31] presents the theory of the transformer and describes the design by means of which it was possible to obtain 1.5 MV at the output. However, the coupling coefficient in this case was equal to only 0.18.

On the basis of the calculations given in this section, and handbook data on self- and mutual inductances of single-layer coils [14], one can compute the basic elements of the transformer construction, being given the transformation ratio, amplitude of the output voltage, and the value of one of the capacitances.

The basic parameters of the generator of nanosecond pulses can be computed using the formulas of Section 2-2 if, as the formative capacitor, one takes C_2, and as the charging inductance one takes L_2. One of the generators involving the use of such a transformer was described in Section 5-2.

1-4. Transformers with Inhomogeneous Lines

This type of transformer represents in a general case a section of line with linear parameters L and C varying along the length, which has at the input a small value of the wave resistance $\sqrt{L/C}$, and at the output — a large one. The character of the pulse distortion during transformation depends on the type of the inhomogeneous line used (spiral, flat, stepwise, etc.), and on the degree of variation of the wave resistance per unit length of the line.

The simplest transformer made on the base of an inhomogeneous line consists of segments of homogeneous lines with various wave resistances. These segments are connected in a cascade one behind another as the wave resistance increases. The theory of such a transformer is presented in [2]. The transformation ratio has in this case a maximum value if the reflection coefficient, when a pulse is reflected from any point of the connection between the lines, is held constant.

The maximum transformation ratio n_M is given [2] as

$$n_M = \frac{\theta^N}{(1-e^{-\ln\theta/N})^N}. \qquad (1\text{-}39)$$

where N is the number of line sections; θ is the ratio of the wave resistance at the output of the transformer to the input resistance. Using this type of transformer, a pulse was obtained with an amplitude up to 1 MV for the front width of $5 \cdot 10^{-9}$ seconds [35].

The basic drawback of a network composed of homogeneous lines is that, when a pulse passes through the line junction, its front is lengthened. In addition, it is difficult to produce a set of line sections with various wave resistances, determined by the condition of a maximum transformation ratio. In devices of this type, the basic pulse on the load is followed by additional pulses if the pulse width is less than twice the transition time of an electromagnetic signal over a line section. If the pulse width is greater

than the interval indicated, then a pulse of stepwise form will be obtained as output. The envelope of the pulse is approximately determined by an analysis of a distributed inhomogeneous line, described below.

If the number of line sections is increased to infinity, in the limit reducing the length of each segment to zero, then a distributed inhomogeneous transformer line is obtained. The theory of such lines is most completely presented in [36, 85]. Such lines have found use both in transformation and as generating and correcting pulse networks [36, 37] for microsecond and nanosecond pulses. An advantage of transformers built from inhomogeneous lines is a considerable reduction of their geometrical size with a simultaneous decrease of the transformed pulse width. The basic distortion of the pulse in the transformer is manifested in the form of a gradual drop of the flat part. The value of the drop, λ, expressed as a percentage of the pulse amplitude, can be found from the relation [6]

$$\lambda = \frac{50 (\ln n_T)^2}{(T_0/t_p)}, \qquad (1\text{-}40)$$

where t_p is the width of the transformed pulse; T_0 is the delay time for the pulse in the transformer line, determined by its length; n_T is the transformation ratio. This property of an inhomogeneous line is used for transforming with a simultaneous correction of pulses with a smoothly increasing flat portion [2, 36].

Equation (1-40) implies that, in order that the decrement of the flat portion of the pulse be small, it is necessary to reduce the width of the transformed pulse, to increase the delay time of the inhomogeneous line, T_0, and to decrease the transformation ratio. If one desires to increase the output voltage several times, keeping λ and t_p constant, then in accordance with (1-40) the minimum delay time for the line increases and so does its size, and the use of a transformer on ordinary inhomogeneous lines may entail difficulties. In this case, one uses transformers with spiral inhomogeneous lines

[2, 4, 39, 120]. The transformation ratio for transformers with spiral inhomogeneous lines usually does not exceed 4 due to large distortions of the front of the pulse

1-5. Autotransformer Made of Foil Winding

Martin and Smith [40] proposed a pulse autotransformer design that would generate high-voltage pulses of amplitude about 1 MV. The design is distinguished for its simplicity and exceptional compactness. Windings of the autotransformer are made of copper foil strip 80-100 microns in thickness which narrows down toward the ends, as shown in Figure 1-11. D and C are the primary leads, and A and B — secondary leads. Before the foil is twisted into a cylinder, it is covered with an insulating layer made of polyethylene or lawsan, and the etched spots are filled with absorbing paper. The paper thickness is chosen equal to the foil thickness. Then the foil strip with insulation is wound around a cylinder made of insulating material. The cylinder with foil is placed in an evacuated volume, and then is immersed in a degassed $CuSO_4$ solution. The copper sulfate solution plays an important role, since with its relatively high specific resistance (up to 10^4 ohm) it makes it possible to obtain a uniform distribution of magnetic field intensity.

Figure 1-12 shows various versions of autotransformer circuits [40]. The autotransformer design discussed corresponds to Version 3 in Figure 1-12. An equivalent network for a pulse autotransformer, with values divided by the number of turns in the primary winding, is given in Figure 1-13, where C_1 is the reservoir capacitor; C_2n^2 is a recalculated load capacitance; L_K is the commutator inductance; L_C is the reservoir capacitor inductance; L_p is the stray inductance; L_2/n^2 is the recalculated load inductance; L_l is the line inductance; L_1 is the inductance of the primary winding; n is the transformation ratio. The stray inductance is defined according to the formula [40].

$$L_p = k\frac{36\delta r\cdot 10^{-9}}{2b_{изол}+b_{пров}}, \text{ henrys}, \qquad (1-41)$$

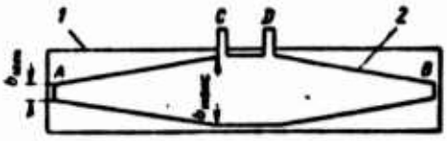

Figure 1-11. Configuration of winding made of foil with superimposed insulation.
1 - insulation; 2 - foil tape.

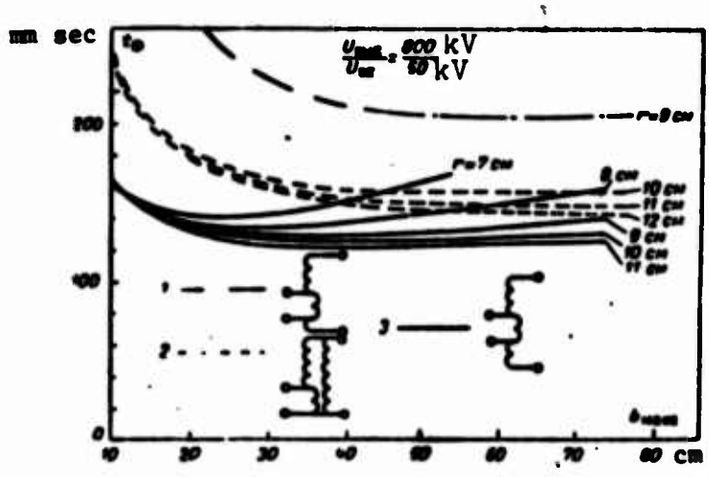

Figure 1-12. Dependence of the front width t_f on the value b_{max} at fixed transformer parameters for autotransformer versions 1, 2, 3.

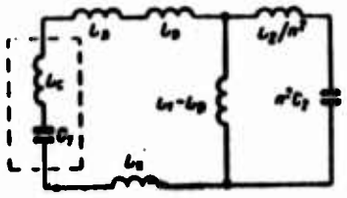

Figure 1-13. An equivalent autotransformer network.

where Δ is the total winding thickness, cm; b_{max} and b_{min} are the maximum and minimum foil widths, cm; r is the radius of the winding, cm.

The coefficient k is determined by the network showing how the autotransformer windings are coupled (Figure 1-12). For network 1: k = 1; for network 2: k = 2; for network 3: k = 0.5.

The inductance of the primary winding can be found from the formula

$$L_1 = \frac{40r^2 \cdot 10^{-9}}{r + b_{max}}, \text{ H}. \qquad (1\text{-}42)$$

Without taking L_2/n^2 into consideration, the ratio of the output voltage to the input voltage is given by the formula

$$\frac{U_{out}}{U_{in}} = \frac{n \cdot 2(L_1 - L_p)C_1}{(L_1 + L_a + L_c + L_k)(C_1 + n^2 C_2)}. \qquad (1\text{-}43)$$

The width of the pulse front is given by the formula

$$t_\phi = \pi \left[(L_a + L_a + L_c + L_p)\left(\frac{C_1 n^2 C_2}{C_1 + n^2 C_2}\right)\right]^{1/2}. \qquad (1\text{-}44)$$

The formula is valid for $2r > b_{max}$ and $r >> \Delta$. Reference [40] calculates t_f as a function of b_{max} for the three versions of a generator with an autotransformer for fixed parameters:

C_1 = 0.5 μF; $L_c = 1 \cdot 10^{-9}$ henrys; C_2 = 900 pF; U_{in} = 50 kV; $L_K = 4 \cdot 10^{-9}$ henrys; Δ = 1.5 cm; U_{out} = 800 kV; $L_l = 6 \cdot 10^{-9}$ henrys; n = 16.

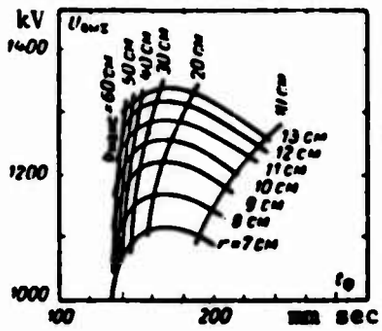

Figure 1-14. The output voltage U_{out} and the time t_f as functions of r and b_{max}.

The plots obtained are shown in Figure 1-12. Figure 1-14 gives the plots of the maximum output voltage in kilovolts and the time of voltage rise, t_f, as functions of r and b_{max} for fixed values of the following parameters:

$C_1 = 0.25\,\mu F$; $C_2 = 900$ pF; $L_l = 6 \cdot 10^{-9}$ henrys; $L_K = 4 \cdot 10^{-9}$ henrys; $L_c = 2 \cdot 10^{-9}$ henrys; $\Delta = 3$ cm.

FOOTNOTE

1. on page 20. The length of the fro. ,rresponds to an ideal voltage jump at the transformer input.

CHAPTER TWO

GENERATORS OF NANOSECOND PULSES OF HIGH VOLTAGE

There are two basic principles of designing high-voltage nanosecond pulse generators. In the first case, given pulse parameters (front, width, decline, and flat part) are obtained by reducing parasitic parameters of the discharge circuit to desired values and by using high-speed commutators. In the second case, first a high-voltage pulse is produced without strict requirements as to its form followed by its transformation. The transformation is achieved with the aid of low-inductance reservoir capacitors, peaking discharge circuits, and nonlinear elements. This principle is ordinarily used to obtain voltage pulses of 10^5 V and more with the front on the order of 10^{-9} seconds. To obtain a starting high-voltage pulse, one can use any method of obtaining high voltage pulses, including th se involving the use of step-up transformers, described in Chapter I.

2-1. Marx Generators

To obtain voltage pulses with an amplitude up to 10^6 V and more, one often uses the Marx circuit (Figure 2-1). The circuit operates basically as follows. Several capacitors (in general n) of capacitance C each are connected in parallel, and are charged through a

resistance R_3 and charging resistances R_0 by a direct voltage source to a voltage U_1. If all spark gaps are closed simultaneously, then the capacitors C are connected in series, and a voltage pulse with an amplitude close to nU_1 flows through the resistance R_p. The resistances R_0 are selected subject to the condition $R_0C >> t_p$ (t_p is the pulse width). In its turn, the pulse width t_p is determined by the value of the capacitance at "pulse breakdown", C/n, and the resistance R_p. The resistances r are necessary to damp the oscillations at the pulse peak, and the resistance R_f and capacitance C_f are included for pulse front correction.

Usually, to initiate a discharge in the first spark gap P_1, one uses an additional electrode or ionizing radiation falling on the gap and the cathode. All the other spark gaps are discharged consecutively as a result of the surge in the spark gap. It is important to note that the breakdown and the maintenance of discharge in spark gaps are possible in the presence of parasitic capacitances, one of which, C_4, is shown in Figure 2-1. The parasitic capacitances must be able to support the development of a discharge until the next spark gap suffers a breakdown and discharges into a load. The problems involving the design of charging and discharging systems and the determination of pulse parameters for the case when the Marx circuit operates in the microsecond range have been analyzed in detail in [3, 41].

To increase the voltage on one step of the Marx circuit to $2U_1$ and thus to increase the output pulse amplitude to $2nU_1$, one uses a pulse voltage generator circuit with a two-sided charging arrangement. In this design, the capacitors are charged using both semiperiods of rectified voltage.

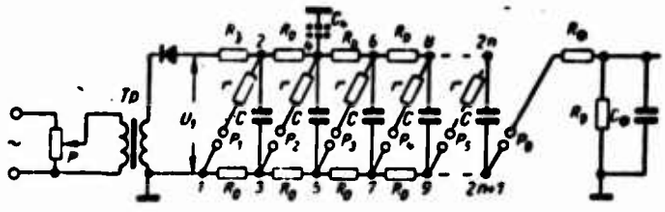

Figure 2.1. Diagram showing the principle of the Marx generator.

a) Equivalent network for the discharge circuit of a pulse voltage generator.

An equivalent network for the discharge circuit of the generator is shown in Figure 2-2. Here $C_0 = C/n$ is the capacitance at breakdown, $U_0 = nU$ is the output generator voltage; C and U are the capacitance and voltage of the pulse voltage generator step; n is the number of the pulse voltage generator steps; L is the inductance of the discharge circuit; C_H and R_H are the capacitance and active load resistance; R_{sp} is the nonlinear resistance of the commutators; R_l is the active resistance which is sometimes included to damp off oscillations at the pulse peak; K is a key corresponding to an ideal commutator.

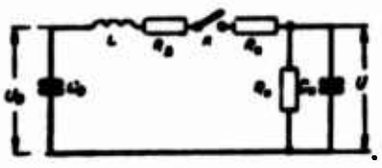

Figure 2-2. An equivalent network for the discharge circuit of the Marx generator.

Depending on the specific conditions (pressure in spark gaps, dimensions of the circuit, working voltage, load character), the value of this or another circuit element can be neglected. We shall assume that gaps are broken down under conditions close to static. Then the spark resistance R_{sp1} for a single spark gap, according to the spark theory by Rompe and Weizel, can be written as [1, 42]:

$$R^2_{sp1}(t) = \frac{pd^2}{2a\int_0^t i^2 dt}, \qquad (2\text{-}1)$$

where p is the gas pressure, at; d is the gap width, cm; i is the current, A; t is the time, sec; a is a gas constant. For the air and nitrogen, the value of the coefficient $a \approx (0.8-1)$ atm cm^2/V^2 sec [43]. At a constant gap breakdown voltage, we have pd = const (Paschen's law). Therefore, for U = const, as the gas pressure increases, the spark resistance grows smaller. The spark resistance cannot generally be neglected in determining the amplitudes and pulse widths. If one

fails to consider the effect of L and C_H on the pulse parameters (then also the resistance R_d cannot be considered), then taking the spark resistance into consideration according to (2-1) the pulse amplitude will have the form [44]:

$$U = U_0\left(1 - \frac{1}{\sqrt{1+2B}}\right)^{3/2}\sqrt{\frac{1+2B}{2B}}. \qquad (2\text{-}2)$$

and the pulse width at half height for $B \leq 20$ will be

$$t_w \approx 2.20 + 1.3R_H C_0. \qquad (2\text{-}3)$$

where $B = R_0 C_0/\theta$; $\theta = 2pd^2/aU_0^2$. If B >> 2θ, then the effect of the spark on t_{sp} will not be apparent, and $t_{sp} \approx 0.7\ R_H C_0$.

The pulse front width t_f can be more conveniently defined here as the ratio of the pulse amplitude to the maximum curvature of its front. For $B \geq 5$ the value of t_f can be found [44] from the formula

$$t_f \approx \frac{128}{27}\theta\frac{[1-(2B)^{-1/3}]^{3/2}}{1-\varphi(A)}, \qquad (2.4)$$

where $A = L/\theta R_H$. L is the inductance of the discharge circuit. For $0 \leq A \leq 25$ the function φ can be found [1] using the empirical formula

$$\varphi(A) = 0.157A - 0.0108A^2 + 0.00017A^3. \qquad (2\text{-}5)$$

Formulas (2-2) - (2-4) imply that the amplitude, front width, and pulse width depend not only on the discharge circuit parameters R, L, C, but also on the value of θ which will be called the spark time constant. The smaller the value of θ, the larger the pulse amplitude, the shorter its front and width. At constant voltage $U_0 \sim pd$, we have $\theta \sim p^{-1}$. Consequently, the higher the gas pressure, the smaller the value of θ. In the air at atmospheric pressure and $d \approx 1$ cm, we have $\theta \approx$ nanosec, i.e., the pulse front width according to (2-5) even in the absence of inductance (L = 0) cannot be less than 10 nanosec. Consequently, to obtain pulses with nanosecond

front widths, it is necessary to place the spark gaps in a compressed gas.

At high gas pressure, the value of θ becomes so small that the spark gap can be considered an ideal switch. The pulse front is in this case determined only by the parasitic parameters of the discharge circuit, L and C_H. If one neglects the effect of C_H, then the pulse front width between the levels 0.1-0.9 of the amplitude will be $t_f = 2.2\ L/R_H$. If $R_H \gg 2\sqrt{L/C_0}$, then the pulse width at the half height will be $0.7\ R_H C_0$. Consequently, to obtain the pulse front on the order of 10^{-9} sec, it is necessary that the inductance of the discharge circuit, L, not exceed $10^{-9}\ R_H$ henrys. For $R_H \gtrsim$ 100 ohms, we must have $L < 10^{-7}$ henrys. The inductance of the discharge circuit, L, is essentially determined by the dimensions of the generator. The latter, for a given value of the pulse amplitude, are determined by the insulating strength of the medium in which the generator is located. To increase the insulating strength of the medium, it is necessary to place the entire generator in a compressed gas atmosphere, since in this case we obtain a simultaneous reduction of the values of θ and L for the discharge circuit of the generator.

b) <u>Short pulse generators made on the basis of the Marx circuit</u>.

Several versions of Marx high-voltage nanosecond voltage pulse generators are available. One of the first was a 400 kV generator built by Schering and Raske [25]. To reduce the switching time, the spark gaps were placed containing carbon dioxide at 13 at. pressure. The generator consisted of five stages, each stage containing two 50 kV capacitors connected in series. Low-inductance plate capacitors were built out of a large number of aluminum foil sheets with paper insulation connected in parallel. To reduce the inductance of the discharge circuit, the capacitors were connected in a "zig-zag", forming at discharge a bifilar conductor. The generator produced 375 kV pulses with $1.1 \cdot 10^{-8}$ sec front width.

In the second version of the generator, coaxial lines were used as reservoirs in order to reduce the inductance of the discharge circuit of the nanosecond pulse generator. This type of generator, involving six coaxial lines, was used to obtain 80 kV rectangular pulses whose width was 0.8 microsec and front width was 10^{-8} sec . A description of this generator was given in [3, 45].

In [46] keep-alive electrodes were placed in the spark gaps to reduce the formation time of a nanosecond pulse generator.

We know that the stability of the spark gap operation depends on the intensity of the ultraviolet radiation incident on the cathode. To increase the stability of spark actuation of nanosecond pulse generators, the study [47] proposed shunting the first spark gap of the generator with a capacitance whose value is comparable with the capacitance of one of the generator stages. In this case, intensive radiation from the powerful spark forming in the first gap has the effect of considerably shortening and stabilizing the breakdown of all the consecutive spark gaps.

The work [48] describes the Marx generator in which 160 stages were used to obtain 2 mV $50 \cdot 10^{-9}$ sec pulses. The capacitors of each stage had a small self-inductance. To reduce the size and the gap breakdown time, the generator elements were placed in a compressed gas.

Reference [49] contains a design for a small-size, high-voltage nanosecond pulse generator in which the inductance of the discharge circuit was made small by placing the entire structure in compressed gas. The generator was used to power a spark chamber, and consisted of ten Marx stages placed in a cascade. The generator produced a pulse with a front and decline of 2 nsec. The pulse amplitude was up to 200 kV. The lag between the application of the triggering pulse and the formation of the output pulse was about 10 nanoseconds, and its time scatter was no more than 1 nsec. The discharge circuit of the generator is given in Figure 2-3, a. In contrast with an

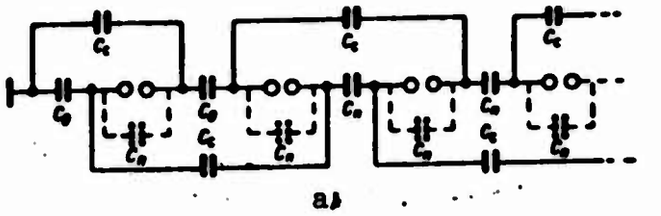

Figure 2-3.
a - Schematic diagram of a generator discharge circuit with coupling capacitors; b - design diagram of a short-pulse generator.

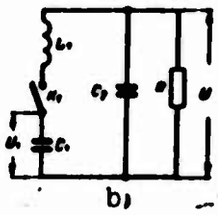

ordinary generator circu. t, a coupling capacitance C_c is used here in addition between the individual generator cascades. The capacitances make possible significant acceleration of the spark gap breakdown process. In this case, we must have $C_0 >> C_c >> C_g$, where C_0 is the capacitance of an individual generator stage, C_g is the gap capacitance. For $C_c = 0$ in the case of breakdown of the first generator gap, if one neglects the breakdown time, a parasitic pulse of peak form will appear on the load.

After such a pulse appears on the load, each of the remaining unpunctured gaps is charged up by $\Delta U_1 \approx \frac{U_0}{n-1}$, where n is the number of gaps, U_0 is the voltage of one generator stage. It can be shown that, after the breakdown of each consecutive i^{th} gap, the n - i remaining ones are charged up by an increasing amount $\Delta U_i = \frac{U_0}{n-i}$, and the time constant of each charging process is $\tau = \frac{RC_g}{n-i}$, where R is the load resistance. This implies that the voltage surge at each of the remaining gaps, assuming a large number of gaps, n, and a small number of discharged gaps, i, will be inconsequential, and as a whole this will result in large delay times between breakdowns. Introduction of the coupling capacitors, C_c, makes it possible to transmit a 100% voltage surge to the second gap, no matter what the number of cascades is, assuming discharge occurred in the first gap. To eliminate statistical fluctuations of the gap breakdown delay time, use was made of an auxiliary corona discharge from spikes which were placed against discharge gaps, and thus provided a steady supply of free electrons at the cathode. The diameter of the spikes which produced a corona discharge was approximately 0.01 mm, and the

corona current did not exceed a value on the order of 1 μA. Polystyrene was used as a dielectric in the coupling capacitors, and barium titanate served in the same capacity in reservoir capacitors. The corona-producing spikes were placed between the spark gaps, and the latter were placed so that they would irradiate each other at breakdown. The entire device, together with spark gaps and charging resistances, was placed in nitrogen at 7 at. In the generator under consideration, the breakdown time of all gaps is much less than the length of the transient provess in the circuit. This case corresponds to the equivalent circuit of Figure 2-3, b in which all gaps were replaced by an ideal switch K_1; L_1 is the total inductance of all sparks and capacitors; $C_0/n = C_1$ is the capacitance at breakdown; C_2 is the capacitance of the load; R is the load resistance. The source voltage U_g is in this case determined by the formula

$$U_r = nU_0 \frac{C_0}{C_0 + 2nC_0}.$$

An analysis of the above connection scheme does not entail too much difficulty. To obtain rectangular pulses, one can use a cut-off discharge circuit. For analysis of this case, one must include C_2 and R, connected in parallel, and the inductance of the spark gap, L_2 with the switch, K_2. A design analogous to the generator described is given in [50]. This generator was used to investigate the operation of streamer chambers.

The study [51] gives a design for a 100 kV pulse generator (Figure 2-4). To stabilize the gap breakdown, use was made of a light guide formed by chamber walls with a reflecting cover 1. High-voltage (400 pF, 30 kV) barium titanate capacitors, 2, were placed in a cylinder of organic glass, 3, and attached with nylon screws, 4. The cylinder walls had through slits for admitting ultraviolet radiation and for providing access to the electrodes. The capacitors were charged through charging resistances, 5. The electrodes 6 were made of polished bronze hemispheres which were attached to the capacitors with brass threaded rods for clearance adjustment. A tungsten keep-

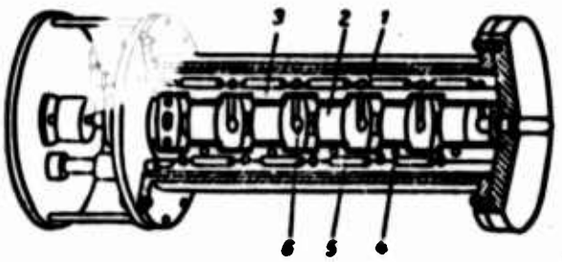

Figure 2-4. Design of a small-scale generator.

alive electrode passed through an opening in the flange of the chamber, so that its end was flush with the level of the inner surface of the flange. The nitrogen pressure in the chamber was approximately equal to 3 at. The pulse front had the width of 3 nsec on the ohmic load.

The basic advantages of small-scale generators are seen to include: reliability of operation, high triggering stability, small width of the pulses generated.

2-2. Generators Charged by Marx Circuits

a) Enlargement of the pulse front curvature in the Marx circuit.

Analysis of the Marx discharge circuit implies that the pulse parameters are, even at high gas pressure in the discharge circuit, determined by the inductance of the discharge circuit and the load capacitance. To eliminate the effect of these factors on the pulse front, it is necessary to include an inductance-free capacitor of capacitance C_2 between the high-voltage electrode of the cut-off discharger of the nanosecond pulse generator and the ground [52]. The operation of the circuit (Figure 2-5, a) is based on the pulse charging of the reservoir capacitor C_2 followed by its discharge through the gap P_2 into the load R_H.

Let us assume that the reservoir element C_2 is charged sufficiently long, so that — after all the dischargers of the generator are punctured — the switching process in them is practically finished. With a fast breakdown of the cut-off gap P_2 and a small value of the

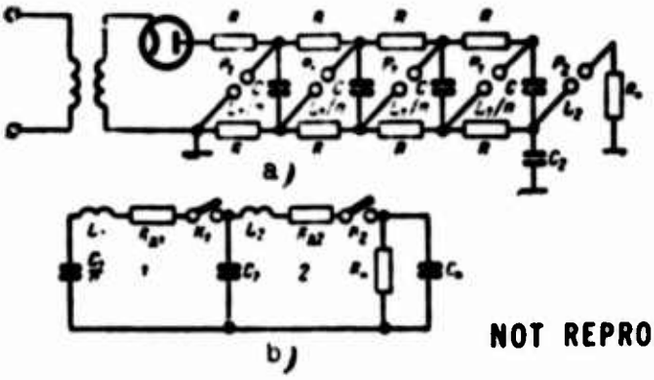

Figure 2.5. a - Marx generator with an inductance-free reservoir capacitor; b - design diagram of the generator.

inductance L_2 as compared with the inductance L_1, the pulse on the load R_H will be initially primarily determined by the parameters L_2, C_2, R_H and the gap spark resistance P_2, and then by the parameters of the generator discharge circuit. The equivalent circuit for the device is shown in Figure 2-5, b. The closing of K_1 and K_2 corresponds to the breakdown of the gaps P_1 and P_2. The resistance R_{d1} is equal to the sum of the residual resistance of the spark gaps P_1, resistance of the busbars, equivalent loss resistance in the capacitors C and C_2, and damping resistance. To simplify the analysis of the circuit, we assume that the pulse front is determined — due to the effect of the shunt capacitor C_2 — only by the parameters of the discharge circuit 2 (L_2, C_2, R_{d2}, R_H, C_H) and the spark resistance, and the peak and amplitude of the pulse — by the parameters of circuit 1 and R_H. This assumption is valid only when, during the formation of the pulse front, the capacitance C_2 fails to discharge itself to any great extent into the load R_H. An analysis of the transient process in the discharge circuit 2, taking into account the nonlinear spark resistance in the gap P_2, is complicated. Basic design relations, given at the beginning of Section 2-1, can be used to estimate the pulse front width.

Below, we give an analysis of the double-circuit network of Figure 205, b, taking into account the above assumptions. In many cases the capacitance at breakdown of the nanosecond generator is $C/n >> C_2$. Therefore, in the analysis we can replace it by a source of infinitely large power. When the switch K_1 is closed, the voltage U_c on the capacitor C_2 and the current i in circuit 1 are determined as follows

$$U_c(t) = U_r\left[1 - e^{-\beta t}\left(\cos \omega t + \frac{\beta}{\omega}\sin \omega t\right)\right]; \tag{2-6}$$

$$i(t) = \frac{U_r}{L_1 \omega} e^{-\beta t}. \tag{2-7}$$

where $U_g = nU_0$ is the voltage obtained from the open-circuited Marx network,

$$\beta = \frac{R_{\Sigma_1}}{2L_1}; \quad \omega = \sqrt{\frac{1}{L_1 C_2} - \frac{R_{\Sigma_1}^2}{4L_1^2}}; \quad R_{\Sigma_1} < 2\sqrt{\frac{L_1}{C_2}}.$$

After the key K_2 is closed, the voltage on the load will become [53]:

$$u_n(\tau) = \frac{U_r}{d}\left[1 - \frac{U_C(t_3)\,d/U_r - 1}{\sin \varphi} e^{-\beta_1 \tau}\sin(\omega_1 \tau - \varphi)\right], \tag{2-8}$$

where

$$\tau = \frac{R_n}{L_1} t; \quad \beta_1 = \frac{1+\gamma}{2B}; \quad \gamma = R_{\Sigma_1} R_n C_2 / L_1;$$

$$\omega_1 = \sqrt{\frac{d}{B} - \beta_1^2}; \quad d = 1 + \frac{R_{\Sigma_1}}{R_n}; \quad B = \frac{R_n^2 C_2}{L_1};$$

$$\operatorname{tg} \varphi = \frac{2B\left[U_C(t_3)\,d - U_r\right]\omega_1}{(1+\gamma)\left[dU_C(t_3) + U_r\right] - 2d\left[\frac{R_{\Sigma_1}}{R_n} BU_C(t_3) + i(t_3) R_n\right]}.$$

t_3 is the delay in the closing of key K_2 after K_1 has been closed.

Let us consider some cases that are most interesting from the practical point of view.

1. Let us set $R_{\Sigma_1} = \sqrt{2\frac{L_1}{C_2}}$, $t_3 = \infty$. Then the voltage on the capacitor C_2 will practically monotonically increase to U_g (overshoot

at the peak is less than 4%). The second condition means that the key K_2 is closed when the voltage on C_2 is stabilized. One should not allow the process to be completely aperiodic, since this leads to an increase in R_d and a reduction of the amplitude of the output pulse. A plot of the voltage $h = u_H/nU_0$ on the load versus time is given in Figure 2-6, a.

The voltage on the load under steady-state conditions, $u_{H\infty}$, according to (2-8) has the form $u_{H\infty} = U_g/d$. Using the value of $u_{H\infty}$ from (2-8), we can write

$$B = \frac{2u_{H\infty}}{(U_r - u_{H\infty})^2}. \qquad (2\text{-}9)$$

To obtain a pulse whose form would be close to rectangular, the value of $u_{H\infty}$ must be close to $U_g = nU_0$. For example, for $u_{H\infty} \geq 0.9\ U_g$ the parameter $B \geq 162$. The voltage pulse has oscillations at the top. Therefore, to have a comprehensive concept of the function $u_H(\tau)$ it is necessary in addition to know the voltage $U_{H.M}$ at the nearest minimum point which is determined from the condition $du_H(\tau)/d\tau = 0$. Then from (2-8) for $B > 100$, we obtain the ratio of the dip to the overshoot

$$\xi = \frac{u_{H\infty} - u_{H.M}}{U_r - u_{H\infty}} \approx 0{,}07,$$

i.e., the voltage stabilizes with practically no oscillations.

2. Now let us consider the case when $R_{d1} = 0$, $t_3 = \infty$.

The condition $R_{d1} = 0$ determines the oscillatory mode in circuit 1, and the condition $t_3 = \infty$ postulates a controlled breakdown of the gap P_2 after the transient process ends in circuit 1. From (2-8), we obtain

$$u_H(\tau) = U_r\left(1 - \frac{e^{-\tau/2B}}{B\omega_1}\sin\omega_1\tau\right). \qquad (2\text{-}10)$$

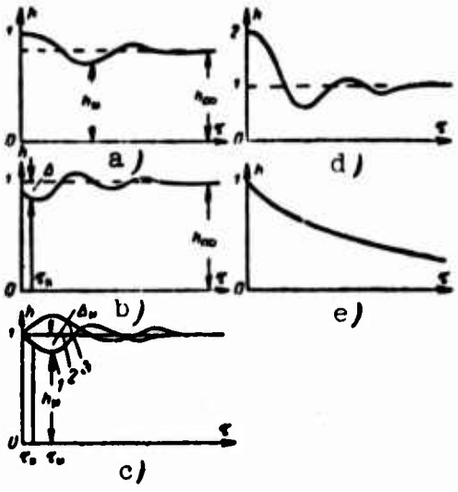

Figure 2-6. Normalized voltage on the load $h = u_{H\infty}/nU_0$ as a function of normalized time τ with the generator under various operating conditions.

a - for $R_{d1} = \sqrt{2\frac{L_1}{C_2}}$, $t_3 = \infty$; b - for $R_{d1} = 0$, $t_3 = \infty$; c - for $R_{d1} = 0$, $t_3 = \frac{\pi}{2\omega}$ (curves 1, 2, 3 correspond to $B<1$, $B=1$ and $B>1$); d - for $R_{d1} = 0$, $t_3 = \frac{\pi}{\omega}$; e - $\frac{C}{n} = C_2$, $t_3 = \frac{\pi}{\sqrt{2}}\sqrt{L_1 C_2}$.

i.e., after K_2 is closed, we obtain an oscillatory form of the pulse on the load (see Figure 2-6, b). If we are given a certain value of the voltage drop $\Delta = [U_g - u_H(\tau_{sp})]/U_g$ at $t = t_{sp}$, we can find $\tau_{sp}(B)$ from (2-10). These functions are plotted in Figure 2-7, a $\left(\tau_{sp} = \frac{R_H}{L_1} t_{sp}\right)$. From the plots of $\tau_{sp}(B)$, we can find C_2 if we are given t_{sp}, Δ, R_H and L_1. With an increase in B — i.e., with a decrease in L_1 and increase in C_2 — the magnitudes of the dips grow smaller. Therefore, it is desirable to increase the capacitance C_2. The value of L_1 is usually limited by the self-inductance of the generator discharge circuit.

3. If $R_{d1} = 0$, $t_3 = \pi/2\omega$, then the key K_2 will be closed when the current in the first circuit attains a maximum.

Then (2-6) and (2-7) imply that

$$\omega = \frac{1}{\sqrt{L_1 C_2}};\quad \beta = 0;\quad U_C = U_r;\quad i(t_3) = \frac{U_r\sqrt{C_2}}{\sqrt{L_1}}.$$

Formula (2-8) gives the following expression for the voltage on the load:

$$u_H = U_r\left[1 + \frac{e^{-\tau/2B}}{\omega_1 B}(\sqrt{B} - 1)\sin\omega_1\tau\right]. \qquad (2\text{-}11)$$

where $\omega_1 = \sqrt{\frac{1}{B} - \frac{1}{4B^2}}$ for $B > \frac{1}{4}$; for $B < \frac{1}{4}$ sin becomes sh. Plots of the voltage on the load for B < 1, B = 1 and B > 1 are given in Figure 2-6, c.

To obtain pulses of width t_{sp} less than the time until the first maximum (or minimum), t_M, at the top of the pulse, one should not limit the value of the overshoot by $|\Delta_M| \leq 0.1$. In this case, the region of the permissible values of the parameter B is extended. When calculating the generator parameters to obtain the minimum value of C_2, it is necessary to take the smallest value of B for a permissible value of the amplitude of oscillations at the top of the pulse. Therefore, in practice one takes C_2. For this case Figure 2-7, b gives plots of $B(\tau = \tau_{sp})$ according to Equation (2-11) for a permissible relative voltage drop Δ = const when $\Delta \leq \Delta_M$. The graphs in Figure 2-7, b make it possible to determine the value of the capacitance C_2 if we know the values of the parameters L_1, R_H, Δ and t_{sp}. If, in the course of calculations, it turns out that $\tau_{sp} > \tau_M$, then one can decrease the parameters B, without at the same time reducing the voltage Δ.

It will be noted that, in the operational mode of the transformer that we are considering here, a considerable portion of the pulse energy comes directly from the basic source — the discharge capacitance of the Marx generator through the inductance L_1. This makes it possible to considerably reduce the necessary value of C_2 as compared with the previous cases.

4. Let us consider the most interesting operational mode of the Marx circuit when $R_{d1} = 0$, and $t_3 = \pi/\omega$.

This case corresponds to the closing of the key K_2 when the voltage on the capacitor C_2 reaches a maximum, i.e., when $U_c(t_3) = 2U_g$. When K_2 is closed, a voltage is applied to the load which is twice the operating voltage obtained from the Marx circuit. Then,

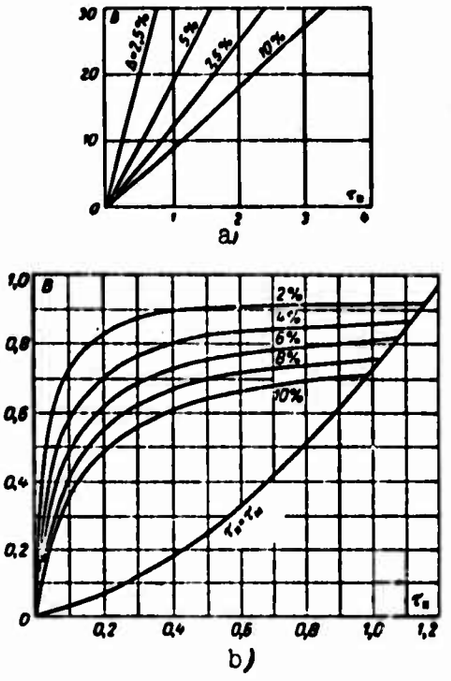

Figure 2-7. Plots of the parameter B vs. τ_{sp}.

a - for $R_{d1} = 2\sqrt{\frac{L_1}{C_2}}$, $t_3 = \infty$; b - for $R_{d1} = 0$, $t_3 = \frac{\pi}{2\omega}$.

as the capacitor C_2 is discharged, the voltage on the load falls off. The pulse form can be computed from a formula that can be obtained from (2-8) by setting $t_3 = \pi/\omega_1$, $R_{d1} = 0$:

$$u_n = U_r\left[1 - \frac{\exp(-\tau/2B)}{\sin\varphi}\sin(\omega_1\tau - \varphi)\right], \quad (2\text{-}12)$$

where $\omega_1 = \frac{\sqrt{4B-1}}{2B}$; $\operatorname{tg}\varphi = \frac{\sqrt{4B-1}}{3}$.

The plot of the variation of voltage on the load is shown in Figure 2-6,d. If we assume that $\tau/2B = \text{const}$, then with an increase in B, the value of the voltage drop Δ, as implied by (2-12), will increase. This means that, with a decrease of L_1, the voltage on the capacitance C_2 falls off faster. Therefore, to reduce the drop in the pulse peak a choke coil with high inductance is included in the discharge circuit of the generator. If $L_1 \to \infty$, then for fixed values of t, R_H, and C_2 the value of the drop $\Delta = \frac{u_n(0) - u_n(t)}{u_n(0)}$ tends to a minimum. In practice, we are usually given the parameters t, Δ and R_H, and the value of C_2 is then computed. If t, Δ and R_H remain unchanged, and $L_1 \to \infty$, then in this case C_2 tends to a minimum

$$C_2 \approx -\frac{t}{R_n \ln(1-\Delta)}. \quad (2\text{-}13)$$

However, the decrease of C_2 with an increase in L_1 occurs nonuniformly. First C_2 falls off rapidly, and then more slowly. Therefore, the inductance L_1 should be restricted to a certain

reasonable interval at whose limit C_2 still decreases substantially with an increase in L_1. Under the condition that $\Delta \leq 0.1$, and C_2 is determined from (2-13), the inductance L_1 can be found from the formula

$$L_1 = 2{,}5 R_{\text{н}} t_{\text{н}}. \qquad (2\text{-}14)$$

It will be noted that the operational mode of the Marx circuit which we have just discussed is a particular case of stepping up voltage by means of a cascade connection of LC circuits (see Section 2-5).

5. If $C/n \approx C_2$, $t_3 = \pi/\omega_2$, $\omega_2 = \sqrt{2}/\sqrt{L_1 C_2}$, $R_{d1} = 0$, then $U_c = U_{c\ max} \approx U_g$, i.e., at $t = t_3$ the electric energy stored in the discharge capacitance C/n goes into C_2. After the key K_2 is closed under the condition that $R_H C_2 \ll t_3$, practically the entire energy stored in C_2 is released on the load R_H. The plot of the voltage on the load is given in Figure 2-6,b. Complete utilization of the energy stored in the Marx circuit will occur under the condition that

$$L_1 \approx 5 R_{\text{н}} t_{\text{н}}. \qquad (2\text{-}15)$$

b) Design of generators.

The Marx generators containing a reservoir capacitor, given in [52], have found wide use [54-56]. A description of the first such generator with a voltage of 150 kV and the front width of $5 \cdot 10^{-9}$ sec is given in [53, 54]. The generator consisted of five stages; each stage consisted of two KBGP 0.01-μF 15-kV capacitors charged on both sides. To reduce the size of the inductive discharge circuit of the nanosecond generator, each KBGP capacitor was shunted off by the inductance-free KOB-3 capacitor. Use was made of the first operational mode, described above. The value of C_2 was determined for given R_H, Δ, t_{sp} and experimentally determined L_1.

To reduce the inductance of circuit 2 (Figure 2-5, b), a coaxial capacitor C_2 was made (Figure 2-8). The resistance R_H was placed along the axis of the capacitor (Figure 2-5,b). The resistor is in the form of a glass tube 4 with a water solution of NaCl (Figure 2-8). Transformer oil 3 served as a dielectric. In this case, the height of the capacitor was chosen such that waves were not allowed to form in it (as in a coaxial line), since they would have the effect of distorting the front. The height of the capacitor C_2 was 20 cm. The voltage pulse on the load had strong oscillatory components due to the inductance L_2 = 0.3 microhenrys and capacitance C_H = 5 pF. It was not possible to eliminate these oscillations by increasing the resistance R_{d_2} (tube filled with water) due to the presence of a capacitance shunting R_{d_2} off.

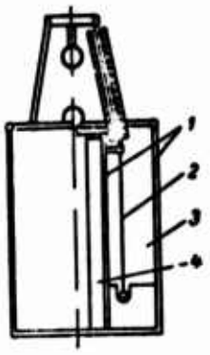

Figure 2-8. Construction of the inductance-free capacitor.
1 - capacitor plate; 2 - screen; 3 - transformer oil; 4 - load.

The oscillations were eliminated by increasing the spark resistance in the discharger P_2 (see the diagram in Figure 2-5,a) by lowering the air pressure or increasing the degree of inhomogeneity of the field at the electrodes of the spark gap P_2 [54, 55]. In the generator design under consideration, the spark gap P_2 consisted of two electrodes in the form of sharp points. This type of spark gap design eliminates oscillations at the top of the pulse. Figure 2-9 shows oscillograms of pulses obtained from nanosecond pulse generators: without using auxiliary capacitances (a); with the KOB-3 capacitors and absence of C_2 (b); with the KOB-3 capacitors and C_2 = 150 pF (c). In oscillography, use was made of an ohmic voltage divider consisting of the resistance R_H and RK-1 cable along which a pulse was passed to the plates of the oscillograph. A design of a 500 kV pulse generator, operating according to a similar scheme, is also mentioned in [50].

Reference [56] gives a description of a 500-kV 1.5 nsec-front voltage pulse generator. The basic elements of this generator were selected, starting from the condition that the voltage be doubled at the output of the generator. Glycerin, which is a liquid with the dielectric permittivity $\varepsilon = 40$, was used as a dielectric in the reservoir capacitor C_2. By means of a brief puncture of C_2 under a high pulse voltage (only during the discharge of the nanosecond generator) it was possible to considerably reduce the size[(1)] of the reservoir capacitor C_2 and the spark chamber P_2 which was designed to contain that capacitor.

Figure 2-10 shows the composition of the generator. An inductance-free capacitor 3 consists of two cylindrical plates, with a space filled with glycerin. Its capacitance is 1 nanofarad. The working capacitance of a nanosecond generator 1, used as a charging device, is 12.5 pF, and the voltage is 150 kV. The inner plate of capacitor 3 serves as a housing for the spark chamber 4, in which a switching spark gap is located in a nitrogen atmosphere at the pressure of 16 at. Due to the presence of seals, the distance between spark gap electrodes can be regulated without disturbing the pressure level in the spark chamber.

The transmission line 5 with a 100 Ohm wave resistance and length of 4 m consists of a Ø 80 mm brass tube filled with transformer oil, and the center wire 8 mm in diameter. When capacitor 3 is connected to the Marx generator output through inductance 2, the capacitance at "breakdown" is discharged in an oscillatory manner. The amplitude of the first oscillation exceeds the operating voltage of the generator not by a factor of 2, but only by a factor of 1.7. The authors claim that, out of 30% lost voltage, 8% is due to the finite value of the generator capacitance at breakdown, and the remaining 22% is due to the damping of oscillations as a result of the conductivity of the glycerin capacitor.

Footnote (1) appears on page 82.

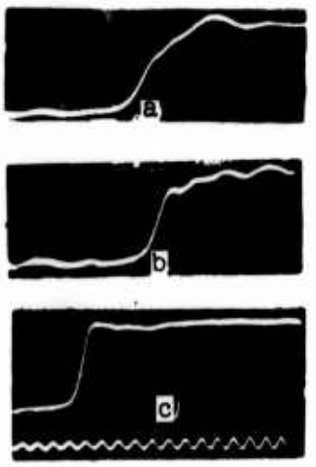

Figure 2.9. Oscillograms of pulses obtained using a Marx generator. The frequency of the calibrated signal was 100 MHz.

The spark gap inside the chamber was regulated to achieve a breakdown at the maximum of the first oscillation, i.e., in order that the amplitude of the pulse, propagating along the transmission line, be 1.7 times greater than the amplitude of the charging generator pulse. The voltage at the open end of the transmission line was doubled, and was 3.4 times greater than the voltage of the charging generator. The output amplitude of the pulse was 500 kV.

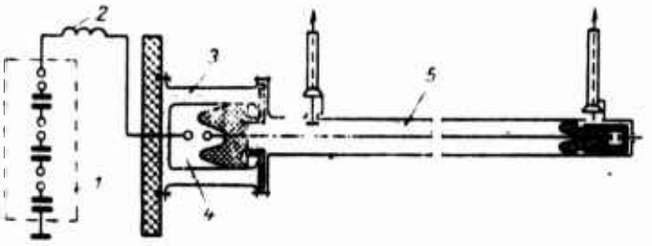

Figure 2-10. Generator of 500 kV nanosecond pulses.

To regulate the width of the pulses supplied to the load, a cut-off spark gap of the tri atron type was developed, which was connected into the coaxial line. The spark gap was filled with nitrogen at 10 at. A keep-alive electrode was placed in a spherical electrode which was grounded. The center wire of the line served as the high-voltage electrode. The spark gap cavity was separated from the line cavity by plastic bushings. The design called for regulation of the clearance between the high-voltage and grounded electrodes. The spark gap was triggered by supplying a pulse produced by the

first stage of the Marx generator to the keep-alive electrode. If the basic pulse had a voltage of 500 kV and width of 10 nsec and was of positive polarity, the scatter of the spark gap actuation time was about 1 nsec. The results of studying the operation of cut-off spark gaps for the nanosecond pulse-width range are also given in [158].

To obtain 1 mV voltage pulses with the front width of approximately 5×10^{-9} sec, instead of line 5 (Figure 2-10) it is possible to use a transformer made out of sections of homogeneous lines with an increasing wave resistance (see Section 1-4) [35]. The transformer was built in the form of a brass tube 80 mm in diameter with the center wire running inside. The wire consisted of six sections of diameters 55, 45, 35, 25, 16, and 3 mm. Transformer oil was used as a dielectric. The wave resistances of the line sections thus formed increased from 16 to 134 ohms. The length of the sections was chosen from the condition that the propagation time of a pulse along a section of the line when multiplied by two must be no less than the width of the pulse front. In the design under consideration, the length of each segment was 60 cm.

[59] describes a generator of 400 kV pulses, with the front of about 10^{-9} sec which also doubled the voltage.

2-3. Generators of High-Voltage Pulses with Transformers Made out of Sections of Coaxial Cable

The transformer discussed in Section 1-2 is used as the basic element of generators involving sections of coaxial cable. Generators of this type are distinguished by simplicity of design, and are used to form pulses hundreds of nanoseconds in width.

a) Circuits and designs.

Figure 2-11 shows a generator of high-voltage pulses involving sections of coaxial cable [19]. The generator consists of three

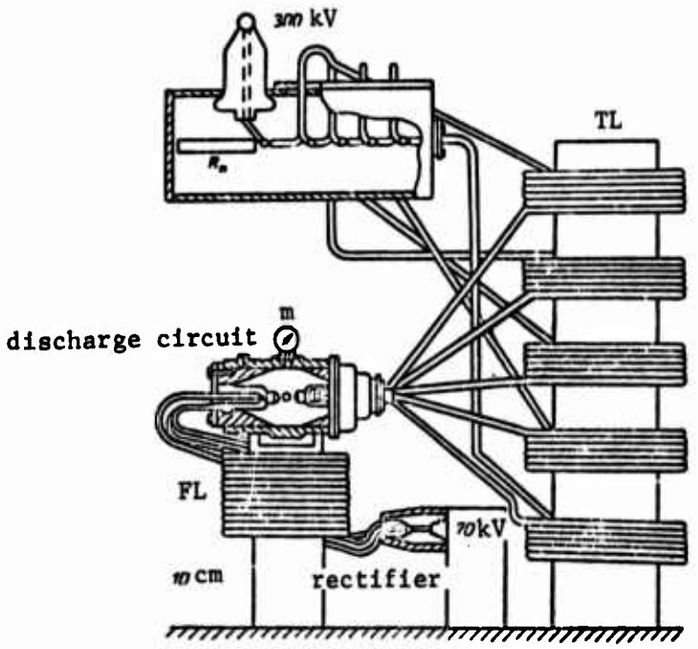

Figure 2-11. A diagram of a 300 kV nanosecond pulse generator.

basic elements: forming line FL, spark gap, and transforming line TL. The forming line is made of five sections of the RK-106 cable, each 25 m long, connected in parallel, and raised to a voltage of 70 kV.

When the spark gap is actuated, a rectangular 0.25-μsec pulse, with a time of increase no more than 5 nsec and an amplitude of 35 kV, was formed on the forming line. The transformer line also consisted of five sections of the RK-106 cable. The input resistance of the transforming line was equal to the wave resistance of the forming line. At the output of the transforming line, all cables were connected in series. The electric length of the transforming line was chosen equal to the pulse width. Cable sections in the transforming line were made in the form of coils lying at a distance no less than 10-20 cm from each other and from the surrounding massive metallic objects. Coils were placed on a bakelite tube 30 cm

in diameter. High-voltage leads were thoroughly sealed to prevent corona discharge and were placed in oil together with the load. Use was made of a spark gap of coaxial structure, operating at a pressure of several atmospheres. A rectangular pulse of amplitude 160 kV and width 0.25 μsec was obtained from the generator after matching the loads. With the load R_H = 2 kohms, a pulse was obtained with an amplitude of approximately 300 kV and a time of increase was about 0 ⁻ μsec.

The study [21] describes a multichannel generator of high-voltage nanosecond pulses. Each of the channels represents a transmission line. To increase the uncoupling impedances, ferrite rings were put on the cables. In this case, pulses with an amplitude up to 130 kV were formed at the output.

To obtain high-voltage (amplitudes up to 300 kV) pulses with a width of 250 nsec and a front width of 20 nsec, a two-stage forming line and a transformer based on cable segments can be used [20]. A diagram of the generator is shown in Figure 2-12. The generator consists of four basic units: forming line FL, commutating thyratron TGI-1-2500/35, transforming line TL, and correcting elements L_{K1}, L_{K2}, C_{K1}, R_{K1}, C'_K.

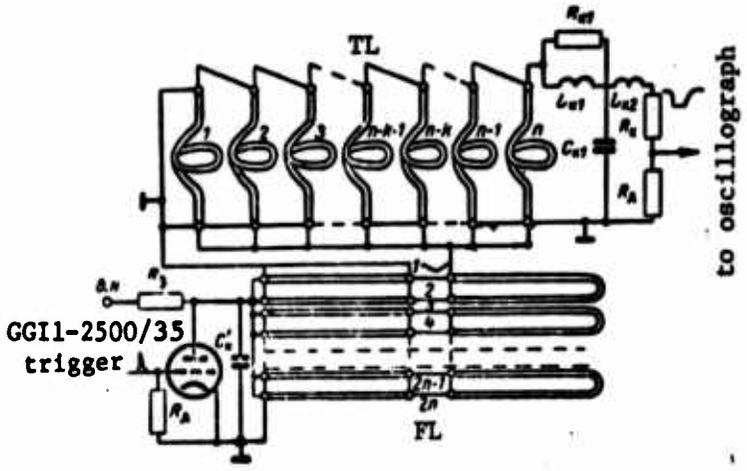

Figure 2-12. Generator of high-voltage pulses with an amplitude of 300 kV involving a transformer based on cable segments.

The circuit operates in the following order. After the thyratron is triggered by a triggering pulse, there is a discharge of the left arm of the two-stage forming line raised to the voltage E. During the time $\tau_1 = l/v$ — where l is the length of the left arm, v is the speed of the voltage wave — a voltage pulse of width $t_{sp} = 2l/v$ is formed at the output of the forming line. The pulse amplitude is equal to E, assuming the shaping line is matched with the input resistance of the transforming line. The pulse formed propagates along cables connected in parallel at the input and in series at the output. Assuming the matching condition is satisfied for the load $R_H = n\rho$ (ρ is the wave resistance of an individual cable; n is the number of cables), the voltage $U_H = nE$ appears on the load.

The shaping line was made of the KPB-1/50 cable. Each arm of the line contained twenty 20 m cable segments connected in parallel. Structurally, cables in the right arm were in the form of ten 40-m segments, each of which was electrically equivalent to two 20-m segments connected in parallel and open at the ends.

The commutating element, i.e., the thyratron, was put in a metal jacket in order to reduce its self-inductance. In that case, the actuation frequency was 13 pulses per second, and the pulse current was up to 12 kA.

The transformer based on segments of coaxial cable consisted of seven 60-m segments of RKG-5 cable with a wave resistance of $\rho = 50$ ohms each. Each cable segment was wound around a carcass made of five vinyl tubes placed in each other, thus forming a five-layer coil. The inductance of the coil was L = 600 microhenrys.

Due to the large self-inductance and significant ionization time (about 50 nsec) of the TGI-1-2500/35 thyratron, the pulse waveform was substantially distorted. To compensate for the distortions, a corrective circuit for correcting L_{K1}, L_{K2}, C_{K1}, R_K, and an additional corrective capacitance C'_K (Figure 2-12) were added to the

generator. The capacitance C'_K designed to correct the flat portion of the pulse was connected in parallel to the thyratron. The value of the capacitance depends on the thyratron parameters (ionization time, inductance) and the discharge circuit, and is selected experimentally between 3 to 5 nanofarads [22]. In the generator under consideration, the inductance L_{K1} composed of 14 turns was based on 8 ferrite F1-100 rings with an internal diameter of 80 mm and an external one of 120 mm. The inductance L_{K2} contained seven turns on twelve F1-1000 rings with an internal diameter of 33 mm, and an external diameter of 55 mm. The capacitor C_{K1} = 30 pF was in the form of 16,470 pF capacitors connected in series. The 9 KV, 3.3-pF, 37-kV capacitor was used as C'_K.

b) The design of a circuit correcting the pulse front.

When a forming device based on thyratrons is used in generators involving sections of long lines, the pulse front width at the output is on the order of tens of nanoseconds and more. To shorten such a front, [63] suggested a correcting circuit composed of nonlinear elements (Figure 2-13,d), connected before the load at the transformer output (Figure 2-12). The basic contribution to the correction of the front is made by a series circuit $L_{K1}C_{K1}$ with the inductance sharply varying as a result of saturation of the inductance. A parasitic resistance capacitance can be used as the capacitance C_{K1} in certain cases. The second inductance L_{K2} serves to sharpen the pulse front even more, and decreases rapidly when the capacitance C_{K1} is charged to the voltage amplitude value. The resistance $R_1 = n\rho$ is the output resistance of the generator. To compute these elements of the circuit, a technique was proposed [64] which assumes that ferrites in the pulse mode behave in the same way as in the presence of a relatively slow variation of magnetic fields. According to this technique, first one computes a correcting circuit without considering the inductance L_{K2}. In the calculation, one assumes that the pulse front width t_f at the input to the correcting circuit increases according to a linear law

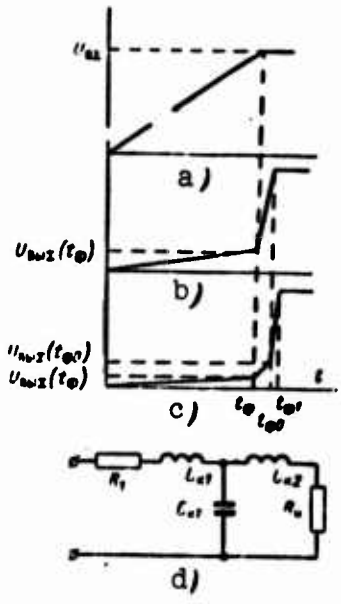

Figure 2-13. A circuit for correcting the front of a high-voltage pulse.

a - input pulse; b - pulse at the output of the correcting circuit for $L_{K2} = 0$; c - final form of the pulse; d - correcting circuit.

(Figure 2-13,a)

$$u_{вх}=mt=\frac{U_м}{t_ф}t, \qquad (2\text{-}16)$$

where U_M is the amplitude of the corrected pulse. The output voltage can be determined using the Duhamel integral.

An analysis of the circuit in Figure 2-13,d, considering (2-16), was given in [64, 107]. In this case, without considering L_{K2} the output voltage was obtained as

$$U_{вых.н}(\tau_ф)=\frac{U_{вых}(\tau_ф)}{U_м B}=1-\frac{1}{\tau_ф}[2-e^{-\tau_ф}(2+\tau_ф)] \qquad (2\text{-}17)$$

for $\xi = 1$, where

$$\xi=\frac{\sqrt{B}}{2}\left(\frac{\rho_н}{R_н}+\frac{R_1}{\rho_н}\right); \qquad (2\text{-}18)$$

$$\tau_ф=\frac{t_ф}{\sqrt{L_{к1}C_н B}}; \qquad (2\text{-}19)$$

$$B=\frac{R_н}{R_1+R_н}; \qquad (2\text{-}20)$$

$$\rho_н=\sqrt{\frac{L_{к1}}{C_н}}. \qquad (2\text{-}21)$$

For $\xi > 1$

$$u_{вых.н}(\tau_ф)=1-\frac{1}{\tau_ф\sqrt{\xi^2-1}}\times \times\left[\frac{q_1}{q_2}(1-e^{-q_2\tau_ф})-\frac{q_2}{q_1}(1-e^{-q_1\tau_ф})\right], \qquad (2\text{-}22)$$

where $q_{1,2}=\xi\pm\sqrt{\xi^2-1}$.

The case of the oscillatory mode ($\xi < 1$) is of no interest. The computed values of $U_{out*}(\tau_f)$ for $\xi \geq 1$ are given in Table 2-1.

TABLE 2-1

τ_f	ξ		
	1	2	3
0,1	0	0	0,005
0,2	0,005	0,005	0,0035
0,3	0,013	0,017	0,00765
0,4	0,022	0,025	0,011
0,5	0,033	0,03	0,0198
0,6	0,045	0,04	0,0265
0,8	0,073	0,07	0,038
1,0	0,104	0,08	0,0562
1,2	0,137	0,1	0,071
1,4	0,17	0,12	0,085
1,6	0,203	0,135	0,1
1,8	0,238	0,16	0,12
2,0	0,271	0,17	0,14

Using the data of Table 2-1 one can compute the necessary value of the corrective inductance L_{K1} if the values of all elements (C_{K1}, R_H and R_1) are given. The order of computation is as follows:

1. We are given the value of $\xi \geq 1$.

2. From (2-18) we determine ρ_K, choosing the larger value, since it corresponds to the smaller values of τ_f, and, consequently, to smaller values of $U_{out*}(\tau_f)$ as indicated by Table 2-1:

$$\rho_K = \frac{R_H}{\sqrt{B}}\left(\xi + \sqrt{\xi^2 - \frac{R_1}{R_H}B}\right). \qquad (2\text{-}23)$$

3. We find from (2-19) and (2-21) the dimensionless front width τ_f, and from Table 2-1 we find $U_{out*}(\tau_f)$:

$$\tau_f = \frac{t_f}{\rho_K C_{K1}\sqrt{B}}. \qquad (2\text{-}24)$$

In actuality, the value of $U_{out*}(\tau_f)$ indicates to what value (as compared with the voltage applied at a given time) the capacitance

C_{K1} became charged. If $U_{out*}(\tau_f) \geq 0.3$, then we repeat the calculation for a larger value of ξ.

4. We determine the value of the corrective inductance

$$L_{K1} = \rho_*^2 C_{K1}. \tag{2-25}$$

5. We find the current in terms of L_{K1}, starting from the following considerations. An analysis of the corrective circuit implies that

$$U_{1x} - I_L R_1 - U_{1MX}(t_\phi) = U_L, \tag{2-26}$$

where U_L is the voltage on the inductance. Assuming that the current through the inductance increases linearly, considering the linear increase of the input voltage, we have

$$U_L = \frac{2I_L L_{K1}}{t_\phi}. \tag{2-27}$$

Substituting this value for U_L into (2-26), we finally obtain

$$I_L = \frac{U_{1x} - U_{1MX}(t_\phi)}{\frac{2L_{K1}}{t_\phi} + R_1} \approx \frac{t_\phi [U_{1x} - U_{1MX}(t_\phi)]}{2L_{K1}}. \tag{2-28}$$

In the case $U_{in} >> U_{out}(t_f)$ and $2L_{K1}/t_f >> R_1$ the expression (2-28) is simplified as

$$I_L \approx \frac{t_\phi U_{1x}}{2L_{K1}}. \tag{2-29}$$

6. Using the formula for the intensity of the magnetic field, we find the number of turns

$$w = \frac{H_M l_0}{I_L}. \tag{2-30}$$

where H_M is the intensity of the magnetic field corresponding to the saturation of the ferrite; l_0 is the average length of the magnetic line of force in the core. The values of H_M, l_0 are determined by

the type and material of the core, and are usually specified earlier (for the core of the F1-1000 ferrite material $H_N \approx 8$--10 A/cm).

7. From the formula for the inductance of the ferrite core, we find the cross-section of the core

$$S = \frac{L_{K1} l_0 \cdot 10^8}{w^2 \mu \cdot 1{,}26}, \ см^2. \qquad (2\text{-}31)$$

In Equation (2-31) it is necessary to consider the dependence of μ on the cut-off frequency (see Section 1-1).

8. Considering the variation of the inductance after saturation $L_{K1} = L_{K10}$, we find the value of ξ_0, and using the formula [4] $\tau_{f0} \approx 1.2 + 2\xi_0^2$ for the case of an instantaneous application of voltage, we find the corresponding value of τ_{f0}.

9. From Equation (2-19), in view of $t_f = t_{f0}$, $\tau_f = \tau_{f0}$, we find the active width of the corrected pulse (Figure 2-13,b):

$$t_{\phi_0} = \tau_{\phi_0} \sqrt{L_{K1_0} C_{K1} B}. \qquad (2\text{-}32)$$

In case it is necessary, a further increase of the front curvature is achieved by connecting an additional saturated inductance L_{K2} in series as shown in Figure 2-13,d.

To a first approximation, the value of the inductance L_{K2} may be estimated under the assumption that the voltage on L_{K2} grows initially according to the law determined by the $L_{K1}C_{K1}$ circuit, and after L_{K1} is saturated — by the $L_{K10}C_{K1}$ circuit.

These time instants are indicated in Figure 2-13,b and c by t_f and t_{f0}, respectively. The transition to the saturation of L_{K2} corresponds to a sharp voltage rise (in time from t_{f0} to t_{f1}, Figure 2-13, c). Therefore, the inductance L_{K2} must be selected in such a way that the core will not be saturated until t_{f0}, when the

voltage on the capacitance C_{K1} reaches its maximum value. A technique of calculating L_{K2} was presented in detail in [107].

Methods of correcting pulse forms in a long line, using concentrated ferrite elements, were described in [172, 173]. These papers, in calculating the effect of correction, took into account the viscosity of ferrites during a sharp variation of the magnetic field.

2-4. Generator of High-Voltage Nanosecond Pulses Involving a "Cable" Transformer

Figure 2-14 gives a version of a generator of high-voltage nanosecond pulses involving a "cable" pulse transformer [65], the design and construction of which are given in Section 1-1.

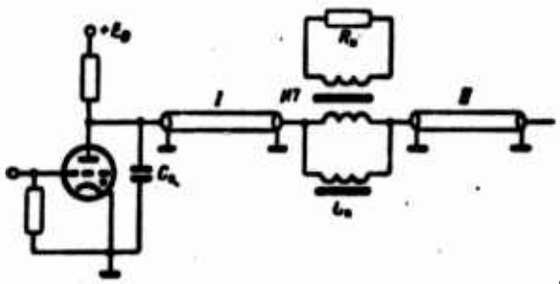

Figure 2-14. Diagram of a generator of high-voltage nanosecond pulses with a "cable" pulse transformer.

A two-stage coaxial line whose principle of operation was described in Section 2-6 serves as a shaping element. A pulse transformer was included in a gap in the center wire, and not in the sheath of the shaping line, in order to eliminate the effect of the parasitic capacitance of the sheaths of arm II on the ground.

The total transformation ratio of the circuit is equal to

$$N=\frac{2R'_{\text{н}}}{2\rho+R'_{\text{н}}}, \qquad (2\text{-}33)$$

where ρ is the wave resistance of a line branch; $R'_H = R_H/n^2$ is the recomputed load resistance.

In case the transformer is not matched with the load, steps may appear at the pulse cut-off. To eliminate the possibility of their occurrence, an inductance L_K which becomes saturated toward the end of the pulse is connected in parallel to the pulse transformer.

The capacitance C_K served to correct the pulse front.

The above circuit is distinguished by its simplicity, and makes it possible to form pulses tens of nanoseconds long, with an amplitude up to 100 kV, and power up to several tens of megawatts [65].

2-5. Cascade Generator of Voltage Pulses

A circuit of a cascade generator, proposed in [66], is shown in Figure 2-15. The circuit consists of several (generally n) LC circuits, connected in a cascade, where

$$\left.\begin{aligned} C_0 \geqslant C_1 \geqslant C_2 \ldots \geqslant C_n; \\ L_1 \leqslant L_2 \geqslant L_3 \ldots \geqslant L_n. \end{aligned}\right\} \qquad (2\text{-}34)$$

where C_0 is the capacitance of the rectifier filter.

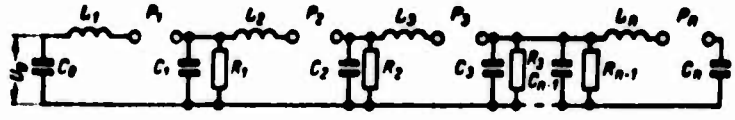

Figure 2-15. Schematic diagram of a cascade pulse generator.

The resistances R_1, R_2, R_3, ..., R_n, which are included in the circuit to provide full discharge of all capacitances before the start of the multiplier, are selected 2 - 3 orders higher than the corresponding wave resistances of the circuits $\rho_1 = \sqrt{L_1/C_1}$, $\rho_2 = \sqrt{L_2/C_2}$, ...

The circuit operates as follows.

The capacitance C_0 charged to the voltage U_0 discharges to an uncharged capacitance C_1 when the gap P_1 is tested. If in this case the ohmic losses in the discharge circuit are neglected, under the condition (2-34), we obtain on the capacitance C_1 a voltage given by

$$u_1 \approx U_0'[1 - \cos(t'/\sqrt{L_1C_1})]. \qquad (2\text{-}35)$$

From (2-35) it follows that at $t = t_1 = \pi\sqrt{L_1C_1}$ the maximum voltage on C_1 will be $U_1 \approx 2U_0$. At t_1, the gap P_2 is punctured, and the capacitance C_1 is discharged into the capacitance C_2 much faster than into the capacitance C_0 due to condition (2-34). In this case, during a time $t = t_2 = \pi\sqrt{L_2C_2}$ after the breakdown of P_2 we have a voltage $U_2 \approx 4U_0$ on the capacitance C_2. After a breakdown of each consecutive gap P_j, the maximum voltage on the capacitance C_j is almost two times greater than that on the capacitance C_{j-1}. Consequently, the maximum voltage on the capacitance C_n will be

$$U_n' \approx 2^n U_0. \qquad (2\text{-}36)$$

In actuality the voltage is stepped up less effectively due to a finite (not infinitely large) ratio of capacitances C_0/C_1, C_1/C_2, ..., C_{n-1}/C_n, the presence of the ohmic losses in the circuits, and a partial precharging of capacitances during the circuit operation. Reference [66] gives an analysis of the circuit under the following assumptions:

(1) ohmic losses in the circuits are not taken into account;

(2) when analyzing the transient process in the j^{th} circuit, the voltage on the capacitance C_{j-2} is assumed to be constant.

Under these conditions, and for

$$\frac{L_1}{L_1} = \frac{L_2}{L_2} = \cdots = \frac{L_{j+1}}{L_j} = \cdots = \frac{L_n}{L_{n-1}} = k_L < 0{,}1$$

and

$$\frac{C_1}{C_0}=\ldots=\frac{C_{j+1}}{C_j}=\ldots=\frac{C_n}{C_{n-1}}=k_C<0{,}1$$

the maximum voltage on the capacitance C_n will be

$$U_n=U_0\frac{2^nC_0}{C_1+C_0}\alpha^{n-1}, \qquad (2\text{-}37)$$

where

$$\alpha=0{,}5\left(1+\frac{1}{k_Lk_C+k_C+1}\right)-\frac{\pi^2k_Lk_C}{4(k_Lk_C+k_C+1)^2}.$$

It must be noted that for small values of k_L and k_C, i.e., when the voltage is stepped up effectively, the energy stored in the capacitance C_n is much smaller than the energy stored in the capacitance C_0. This limits the use of this voltage transformer in pulse devices.

When using this method in [59], pulses were obtained with a front width of approximately 10^{-9} sec and amplitudes up to 400 kV.

2-6. Generators with Shaping Lines Connected in Series

a) Principle of operation

The technique of connecting shaping lines with distributed parameters in series is of extreme interest in the generation of high-voltage nanosecond pulses. The technique was proposed by Blumlein [67], and it is based on changing the voltage polarity on the shaping line when it is short-circuited.

High-voltage nanosecond generator circuits involving shaping lines connected in series make it possible to generate nanosecond pulses with amplitudes of millions of volts and a power of thousands of gigawatts [68].

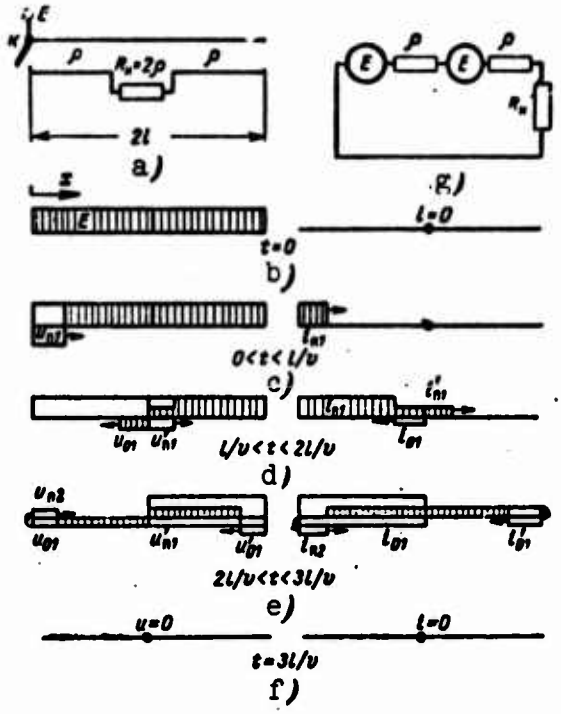

Figure 2-16. a - Connection diagram of two shaping lines; b,c,d,e,f - voltage and current waveforms; g - equivalent circuit.

In order to better understand the process of pulse generation, let us first consider a circuit with two shaping lines connected in series (Figure 2-16,a). The length of each line is l, and the wave resistance is ρ. Initially the lines are at a potential E; the current in lines is $i = 0$ (see Figure 2-16,b).

The process of pulse formation occurs as follows. At a time $0 < t < l/v$ after the switch K is closed, an incident voltage wave propagates in the direction of the load, $u_{gl} = -E$, and the corresponding current wave is $i_{gl} = E/\rho$ (see Figure 2-16,c). At $t = l/v$ incident waves of voltage u_{gl} and current i_{gl} reach the load. This moment corresponds to the end of the full discharge of the active line with the conversion of the electric field energy into the magnetic field energy, and to the start of the reverse process of the conversion of magnetic field energy into electric field energy. Upon reaching the load, the incident wave u_{gl} is partially reflected

without a change in polarity, forming the first reflected wave u_0, and partially passes into the second shaping line, forming the first incident waves of voltage u'_{gl} and current i'_{gl} (see Figure 2-16,d). By examining the equivalent circuit given in Figure 2-16,g, it is easy to find the reflected and incident waves

$$u_{01}=-\frac{E}{2};\ i_{01}=-\frac{E}{2\rho};\ u'_{n1}=-\frac{E}{2};\ i'_{n1}=\frac{E}{2\rho}.$$

The voltage on the load from the time $l/v < t < 2l/v$ is, as we can easily see from the circuit in Figure 2-16, g,

$$u_{\text{ком}}=i_n R_n=\frac{E}{2\rho}2\rho=E.$$

At $t = 2l/v$ (Figure 2-16,e) the voltage wave u_{01} reaches the short-circuited end, and upon reflection with the opposite sign, it forms the incident wave $u_{g2} = E/2$. At the same time, the incident wave u'_{gl} reaches the open end of the right shaping line, and upon reflection with the same sign, it forms a reflected wave $u'_{01} = -E/2$. As both waves move toward the load, the voltage on the line becomes equal to zero. The current wave i_{01}, upon reaching the closed end of the left shaping line, is reflected from it, and — upon forming the incident wave $i_{g2} = -\frac{E}{2\rho}$ without a change in polarity — it propagates toward the load. When the wave i_{01} is reflected from the short-circuited end, the current through the commutator changes its direction.

The current wave i'_{gi}, upon reflection with a change of sign from the end of the right-hand forming line, produces a reflected wave i'_{01}. As the waves i_{g2} and i'_{01} propagate in the direction of the load, the current through the cross-section of the shaping lines becomes zero

$$i_1=i_{n1}+i_{01}+i_{n2}=\frac{E}{\rho}-\frac{E}{2\rho}-\frac{E}{2\rho}=0;$$

$$i_2=i'_{n1}+i'_{01}=\frac{E}{2\rho}-\frac{E}{2\rho}=0.$$

At $t = 3l/v$ the waves of voltage u_{g2}, u'_{01} and current, i_{g2} and i'_{01}, reach the load. Total discharge of the lines is completed, and so is the transition of the energy stored in the lines, W_l, into the load:

$$W_H = I^2 R_H 2\frac{l}{v} = \frac{E^2}{4\rho^2} 2\rho 2\sqrt{LC} = E^2 C$$

or $W_H = W_l$, where C is the capacitance of one line.

In this case, when the switch passes the current only in one direction (for example, thyratron), the processes that take place in the first shaping line are similar to the processes of pulse formation occurring in an ordinary line, raised to the voltage -E after it is connected with a matched load.

b) Generator circuits with shaping lines connected in series.

Let us make some changes in the circuit showing how two shaping lines (two-stage line), given in Figure 2-16,a, are connected.

First of all, we remove the load, and then fold the two-stage line of Figure 2-16,a in two, so that the beginning and the end of the upper general plate coincide. We thus obtain a stack of two lines. In this form, the two-stage line is convenient for use as a standard element in a generator of superhigh voltage pulses.

Figure 2-17,a shows three such shaping lines and the load connected in series [69]. Initially the switches are open and the lines are raised to the voltage E, as shown in Figure 2-17,a with arrows at $t = 0$.

Consequently, the voltage on the load is zero. When the switches are simultaneously closed for a time $t = \tau$, in the ideal case the the voltage at the output of n lines connected in series will be equal to

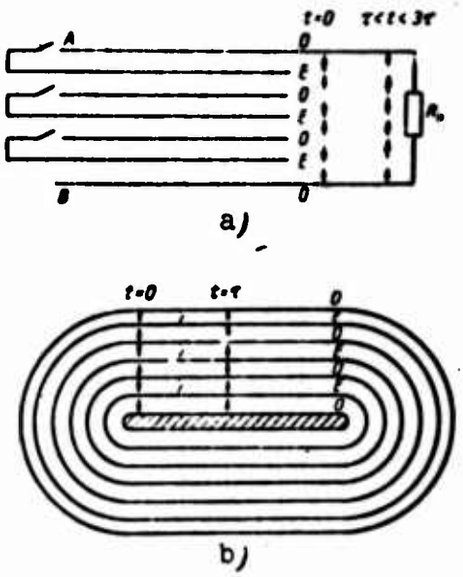

Figure 2-17. Generator with strip lines connected in series.

a - linear design; b - coaxial design.

$$U_{max} = nE\frac{R_н}{n\rho + R_н}. \tag{2-38}$$

The output impedance of the circuit is

$$Z_{вых} = n\rho \approx \frac{n120\pi a}{\sqrt{\varepsilon}(b+a)}, \text{ ohms}; \tag{2-39}$$

and the pulse width is

$$t_и = 2\tau = \frac{2l\sqrt{\varepsilon}}{c}; \text{ sec}. \tag{2-40}$$

In the formulas above:

n is the number of strip lines; a is the distance between strips, cm; b is the strip width, cm; l is the strip length, cm; ε is the dielectric permittivity; c is the speed of light, cm/sec.

In practice, the output parameters of the pulse generated are determined by a number of factors: parameters of the spark gap,

ohmic and dielectric losses when an incident wave is propagating in the line, and parasitic capacitance at the ends of the strip lines. These factors affect both the front width and the amplitude of the output pulse.

A reduction in the pulse front width can be achieved by using special spark gaps, discussed in Section 4-3, and by connecting several spark gaps in each generator stage in parallel. However, it is difficult in practice to trigger in parallel a large number of spark gaps that are raised to a high potential. Ohmic and dielectric losses have a stronger effect on the high-frequency components, and thus also pull on the pulse front. The pulse amplitude for $R_H \to \infty$, taking into account the ohmic and dielectric losses in the interval $l/v < t < 3l/v$, is

$$U_{max} = nE\beta, \qquad (2\text{-}41)$$

where β is a coefficient accounting for a reduction of the pulse amplitude due to line losses.

In [69] it was shown that for $\sqrt{\varepsilon}\frac{l}{a} \approx 5 \cdot 10^4$ the effect of losses may be neglected. To reduce the effect of parasitic capacitance, one must increase the ratio b/a, i.e., decrease the value of ρ and so decrease the time constant $\tau_C \approx \rho C_n$. C_n is the parasitic capacitance.

In this case, we must find a compromise solution between the increase of the time constant of the spark gap, τ_K, and τ_C.

Another method of reducing parasitic capacitance is provided by structuring a strip generator in the form of a set of cylinders placed inside each other as shown in Figure 2-17, b.

Figure 2-17,a and b gives a diagram of a generator with a large number of switches (spark gaps).

In a number of cases, a large number of spark gaps can be replaced by one. For this purpose, a decoupling impedance must be introduced in a generator based on strip lines in order to prevent the discharge of passive lines through a general conductor or busbar.

Two versions of generators based on strip lines with one switch, discussed in [69], are given in Figure 2-18, a and b. The decoupling impedance ρ_0 is selected on the condition $\rho_0 >> \rho$ which corresponds to $a_0 >> a$, where a_0 is the distance between the strips of the decoupling line.

After the switch is closed simultaneously with a total discharge of the active lines, there is a partial discharge of the passive lines. The amplitude of the voltage wave, U_a, propagating in the passive lines toward the load is at the end of the line, as can be easily seen from Figure 2-18,a, equal to

$$U_a = \frac{2E_0}{\rho + 2\rho_0} = \frac{2Ea}{a + 2a_0} \approx \frac{Ea}{a_0}. \qquad (2\text{-}42)$$

The total output voltage is in this case

$$U_{вых} = \frac{nER_н}{R_н + n\rho}\left(\beta - \frac{a}{a_0}\right). \qquad (2\text{-}43)$$

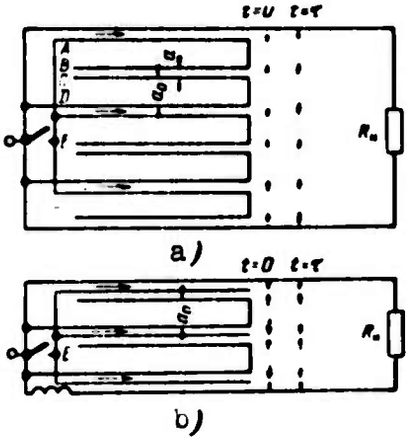

Figure 2-18. Two versions of generators based on strip lines with one switch.

Figure 2-18,b shows a version of a generator with strip lines connected in series which differs from the circuit in Figure 2-18,a by its smaller impedance of decoupling lines. The amplitude of a wave propagating in passive lines is in this case approximately equal to $2E\frac{a}{a_0}$. Generators based on strip lines are at the present time widely used to power spark chambers and accelerating tubes

in strong-current accelerators [40, 48].

In addition to strip shaping lines, generator circuits of the type under consideration may also involve forming lines made out of coaxial cable [70].

2-7. Generator Based on a Strip Line Bent into a Spiral

Fitch and Howell have proposed a spiral generator circuit [69] which is distinguished by its relative compactness and simplicity of fabrication and is capable of generating voltage pulses up to 1 MV.

If a strip line of impedance ρ and length $2l$ is bent into a spiral, then charged and closed at length l, then incident waves will start propagating in either direction from the switch K, as shown in Figure 2-19. As the waves move, the electric energy stored in the line becomes the energy of the magnetic field, and the coaxial capacitances formed by the adjacent turns of the spiral are connected in series. When the incident waves reach the ends of the spiral, the voltage between the beginning and the end of the spiral increases to nE. Upon reflections from the ends, the waves in the active line change their signs, and then there is a reverse conversion of magnetic energy into the electric energy.

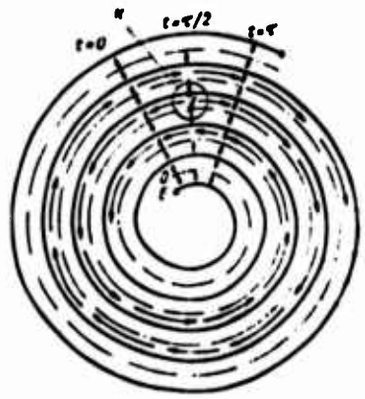

Figure 2-19. Propagation of waves in a strip line bent into a spiral.

When the reflected waves reach the switch, recharging of the active line is over, and the output voltage, assuming $R_H >> n\rho$, reaches the maximum value of 2nE. Then the process of wave reflection is repeated until the entire energy is absorbed by the load or escapes through losses.

The time during which the voltage increases to a maximum is

$$\tau = \frac{\pi n D \sqrt{\varepsilon}}{c}. \qquad (2\text{-}44)$$

where n is the number of spiral turns; D is the average diameter.

The output voltage in the interval $0 < t < \tau$ is

$$u_{вых}(t) = 2\frac{t}{\tau_T} E, \qquad (2\text{-}45)$$

where τ_T is the average time taken by the wave to traverse one turn.

For $\tau < t < 2\tau$, we have

$$u_{вых}(t) = 2\left(n - \frac{t-\tau}{\tau_T}\right) E. \qquad (2\text{-}46)$$

The output capacitance of the spiral generator for $D_o/D_i \approx 1$ is:

$$C_{вых} \approx \left(\frac{1}{n}\right)^2 C, \qquad (2\text{-}47)$$

where C is the total capacitance of the line twisted into a spiral.

It will be noted that the generator of Figure 2-19 with the spark gap attached at the midpoint may be viewed as two spiral generators connected in series.

It is usually more convenient to attach the spark gap at one of the ends of the spiral generator.

All the arguments and formulas presented above are also valid for this case.

In a real generator, the amplitude and the form of the output pulse are determined by the following factors: characteristic of the gap commutation, ohmic and dielectric losses, and by the fact that

the coaxial capacitances connected in series are made out of a single spiral.

If we assume that the switch K has an exponential characteristic of commutation with the time constant τ_K, then the voltage variation with time at any point l_x will be [69]

$$u_{x\max}(t) = U_{l_x}\left[1 - \exp\left(-\frac{t}{\tau_K}\right)\right], \tag{2-48}$$

where t is measured from the moment when the wave passes the point l_x. The voltage distribution along the length is (measurement is made from the switch K)

$$u_l(l_x) = u_l\{1 - \exp[-(l - l_x)\sqrt{\varepsilon}/c\tau_K]\}. \tag{2-49}$$

The coefficient of voltage losses, β_l, related to the variation of voltage along the length l, is determined by the ratio of the areas under the characteristics $u_l = U_\tau(l)$, for the real case with the time constant of the switch τ_K and for the ideal case when $\tau_K = 0$.

$$\beta_l = \frac{1}{El}\int_0^l U_\tau(l)\,dl \tag{2-50}$$

or

$$\beta_l\left(\frac{\tau}{\tau_K}\right) = 1 - \frac{\tau_K}{\tau}\left[1 - \exp\left(-\frac{\tau}{\tau_K}\right)\right].$$

In order that the losses not exceed 10%, it is necessary that

$$L_K < \frac{\tau\rho}{20}, \tag{2-51}$$

where L_K is the inductance of the switch, in henrys [69].

Expressing ρ in terms of the geometric parameters of the strip line, and considering that $a = E/E_a$, the condition (2-51) can be written as

$$\frac{L_K}{E} < \frac{6\pi\tau}{bV\tau E_a}. \qquad (2\text{-}52)$$

where a is the distance between the neighboring turns of the spiral, in cm; E_a is the electric field intensity, V/cm; b is the width of the line, in cm.

If in practice the ratio L_K/E is limited by a value on the order of $2 \cdot 10^{-13}$ henrys/V and $E_a \approx 8 \cdot 10^5$ V/cm, then in order that the losses do not exceed 10%, we must satisfy the condition

$$\tau/h > 10 \text{ nsec/cm} \qquad (2\text{-}53)$$

Ohmic and dielectric losses in a spiral generator can be accounted for using arguments given in Section 4-1.

In addition to the gap characteristic, ohmic and dielectric losses, the pulse form is affected by a number of factors whose total effect on the pulse can be difficult to analyze. Thus, for example, at $t = \tau$ the output capacitance of the spiral generator C_{out} and the spiral inductance L form an oscillating circuit which, in particular, determines the magnitude and the shape of the overshoot after the pulse. In addition, after the switch is closed when the wave passes the first turn, due to the capacitive and inductive coupling the spiral generator may be considered as a pulse transformer.

Fitch and Howell have found that the loss coefficient, accounting for the complex interactions among the spiral turns, depends on the ratio

$$\beta_0 \approx \frac{D}{na}. \qquad (2\text{-}54)$$

The basic parameters of the generator built by Fitch and Howell [69] are: input voltage — 20 kV; output voltage — 750 kV; pulse

width at the base — 500 nsec; C = 0.6 μF; C_{out} = 52 pF; n = 54; D/na = 7.5; β_3 = 0.4.

A convenient insulating material for use in this type of generator may be epoxy resin, chemically pure water, and polyethylene and lawson film.

FOOTNOTES

1. on page 56. For the effect of a strengthening liquid insulation under the influence of short pulses, see Section 4-5.

CHAPTER THREE

METHODS OF MEASURING SHORT HIGH-VOLTAGE PULSES

3-1. Low-Inductance Wire Dividers of Pulse Superhigh Voltages

Voltage dividers are ordinarily used when measuring short high-voltage pulses by means of oscilloscopes. Dividers weaken the signals applied to the deflecting plates of the oscilloscope. Ohmic, capacitive, and mixed (capacitive-ohmic) dividers are in use. The ohmic voltage divider is simple. However, when transmitting short pulses it strongly distorts high-frequency components of the signal due to the influence of the parasitic capacitive couplings between its elements. In a capacitive divider, the division ratio does not depend on frequency within a wide range of values. Therefore, it can be used for recording both fast and relatively slow phenomena. However, when long lines are used as transmitting elements, difficulties arise.

If capacitances are connected in parallel to the resistances of an ohmic divider, a mixed divider is obtained (RC-divider). With fast processes it may be thought of as capacitive, and with slow processes — as ohmic.

In practice we can distinguish between two types of dividers: high-resistance types whose resistance is much greater than the internal resistance of a generator, and dividers which are matched with the load (usually dividers with distributed parameters). It must be noted that designing dividers of the first type for measuring pulses of widths on the order of tens of nanoseconds is an extremely difficult problem which is basically that of searching for ways to reduce parasitic parameters.

In designing dividers of the second type, the parasitic parameters must be taken into account when calculating the distributed parameters of the dividers.

A number of papers [1, 3, 71, 73] are devoted to the design of low-distortion voltage dividers and to the analysis of errors caused by them. In measuring voltage pulses with a front width of 10^{-8} sec and more, and voltages up to 10^{6} V and more, dividers made of a high-resistance conductor have become widely used.

The work [73] describes a high-resistance (about 10 kiloohms) ohmic voltage divider for 350 kV with constant time of increase of about 30 nsec. The inductance-free resistance of the divider is made of two layers of thin Nichrome conductor (0.06 mm in diameter), wound in opposite directions on bakelite rods 9.5 mm in diameter and 140 mm in length. Both layers of the conductor were connected in parallel. The low-voltage end of the divider was attached to a cable which at the output was matched with an oscilloscope. The entire apparatus was placed in a container made of plastic which was filled with nitrogen at the pressure of 8 at.

An analysis in [73] has shown that the lengthening of the front of the pulse being recorded is due to the rapid charging of the parasitic capacitance of the divider elements relative to the ground through the damping resistance and partially through the resistance of the divider itself. To reduce the capacitances relative to the

ground, the dimensions of the divider were reduced, and to eliminate sparkovers over the surface the apparatus was placed in compressed gas. To reduce the effect of the self-resistance on the process of capacitance charging, use was made of screening electrodes in the form of ocnes with rounded edges which straightened out the field along the entire length of the apparatus.

Reference [74] describes an ohmic voltage divider for 2 MV. It is in the form of a tube 2 m in height, around which is wound a high-resistance conductor with a total resistance of 22.5 kohms. To improve the voltage distribution along the length of the divider, a screening system was used which consisted of two disks 80 cm in diameter and four toruses placed every 40 cm. The latter were not connected to the divider resistances. The field distribution between the screening electrodes, determined with the aid of an electrolytic bath, was close to being homogeneous. This helps in evening out the field along the column with the high-resistance conductor.

When a rectangular pulse is used as the input to the divider, the output is in the form of oscillations due to the capacitance between the screening electrodes and the inductance of the connecting wires. When an ohmic resistance was added in series with the upper screen, the oscillations were damped and the pulse at the output of the voltage divider had a front width of 70 nsec. It was possible to shorten the front width to 30 nsec by adding a small inductance, consisting of several turns of copper wire, to the low-voltage arm.

In [75] a 1400 kV ohmic voltage divider transmitted without distortion a pulse front 27 nsec in width. The resistance of the high-voltage arm of the divider was 1000 ohms, and that of the low-voltage arm was 1 ohm. The length of the high-voltage arm was approximately 130 cm, and the arm itself consisted of 10 identical elements. Each element was in the form of a polystyrene rod 12.7 cm in length, and about 1 cm in diameter. Two 0.81 x 0.025 mm^2 strips

made of an alloy of nickel, chromium, aluminum, and iron were wound around the rod in opposite directions. The alloy was characterized by a high specific resistance and a small thermal coefficient. The low-resistance arm of the divider was composed of 1.6 x 0.025 mm^2 strips of the same alloy, and was in the shape of four zigzag loops.

3-2. Dividers Using Lines with Distributed Parameters

In recording voltage pulses with an amplitude up to 10^6 V and a front width of 10^{-9} sec and less, wide use has been made of combined voltage dividers in which a line transmitting the pulse to the load is used as the high-voltage arm of the divider or as the basic element of the apparatus. Ohmic, capacitive, and mixed dividers of this type are in existence..

Reference [26] describes a capacitive divider which is used in oscilloscopes with a high-resistance input. The structure of this divider is shown in Figure 3-1,a. The sheath is removed over a small segment of the cable, and a metallic plate 4 is put on the insulation, which forms a capacitance C_d with the cable center wire. The second capacitance is in the form of the self-capacitance of the oscilloscope plates C_H, which are connected by short wires with plate 4 and the sheath 3. The division ratio of such a divider is given by

$$k \approx \frac{C_H + C_d}{C_d} \qquad (3\text{-}1)$$

The equivalent circuit of the divider is given in Figure 3-2,a [76], where R is the wave resistance of the transmission line; $C = C_H/k$, $L = L_H + L_B$; L_H is the inductance of the leads; L_B is the self-inductance of the leads of the electron-ray tube. It is assumed that the voltage at the front of the pulse varies as in $u = 1 - e^{-at}$ which is an approximation to the pulse front when the pulse is formed during discharge of the line through a spark gap in gas. Damped sinusoidal oscillations, determined by the L and C parameters of the circuit, are then generated on the oscilloscope plates. The amplitude

of the overshoots at the top of the pulse is proportional to [illegible] . The minimum front width τ_f that can be recorded by means of such a divider by an oscilloscope with an error not greater than 10% is given by

[illegible] (3-2)

where $\alpha = \frac{4\pi^2 R^2 C_n^2 f_0^2}{k k_L}$; f_0 is the resonance frequency of the deflecting system of the tube; $k_L = L/L_B$.

For example, for a tube with the parameters f_0 = 600 MHz, k_L = 1, C_l = 5 pF, one can record pulses with the front no less than 10^{-9} sec by means of this type of divider [76].

A divider of a different type is shown schematically in Figure 3-1,b. In this divider, the low-voltage arm C_2 is in the form of a capacitance formed by the metallic foil of electrode 4 and cylinder 3 with a polyethylene film placed in between. The capacitance between the rod 2 and foil 4 makes up the capacitance of the high-voltage arm C_1. The barrier 5 of organic glass is sometimes necessary to eliminate sparkovers between the rod 2 and the foil 4. The diameter of the rod 2 and the internal diameter of the cylinder 3 were chosen so that the wave resistance of the divider is equal to the wave resistance of the cable along which the pulse is sent to the divider. From the divider to the oscilloscope, the voltage is transmitted over another cable. The wave resistance of this cable, R_1, is determined by the requirements on the flat protion of the pulse.

Figure 3-1,a shows another design for a divider of this type [56] designed for measuring pulses with an amplitude up to 500 kV and the front on the order of 10^{-9} sec. Here in addition to the plate 4 producing the capacitances C_1 and C_2 of the divider, there is a screening ring 5 connected to a grounded plate 3. By means of this ring, it is possible to easily regulate the amplitude of the signal

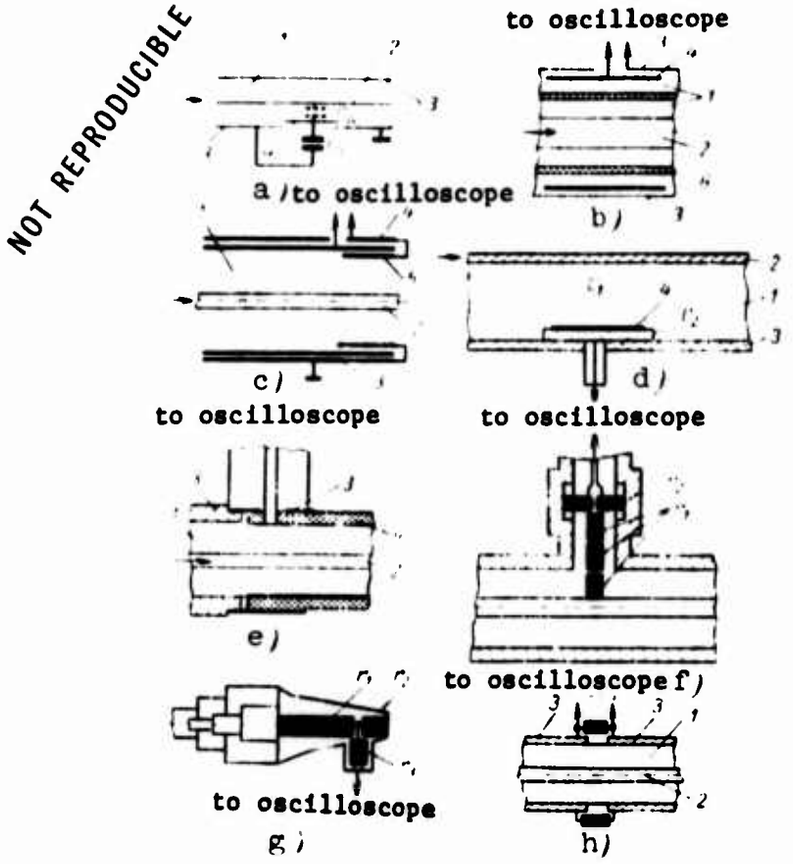

Figure 3-1. Dividers for measuring nanosecond pulses.

1 - line insulation; 2 - high-voltage conductor; 3 - screening conductor; 4 - divider electrode; 5 - screening ring; 6 - barrier; r_1, r_2, r_3 - ohmic resistances.

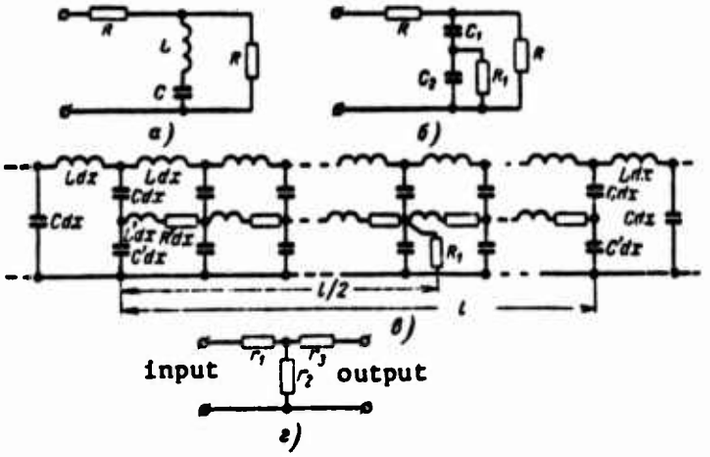

Figure 3-2. Equivalent circuits for dividers of nanosecond pulses.

fed to the plates of the oscilloscope. An equivalent circuit for dividers such as shown in Figure 3-1,b and c, together with lead cables R and R_1, is shown in Figure 3-2, b. For the front width of $t_f \gtrsim 10^{-9}$ sec and less, and for $R_1C_2 \gg t_f$ in the equivalent circuit it is possible to neglect the effect of the resistance R_1 (since it is initially shunted off by the capacitance C_2). In addition, for $C_2 \gg C_1$, the front width t_f at the output of the divider, lying between 0.1 and 0.9 times the amplitude value, assuming an ideal input pulse, is

$$t_\phi \approx 1{,}2RC_1. \tag{3-3}$$

On the other hand, if the pulse width is large, $t_{sp}(t_{sp} \gg t_f)$, the voltage drop at the top of the pulse, defined as the ratio of the difference between the maximum and minimum values of voltage, to its maximum value, will be obtained due to the discharge of C_2 through R_1. Given the permissible value of the drop $\lambda(\lambda \leq 0.2)$, we obtain

$$C_2R_1 \approx \frac{t_u}{\lambda}. \tag{3-4}$$

Formulas (3-3) and (3-4) are useful in computations when the propagation time of electromagnetic waves over the elements C_1 and C_2 of the divider is much less than the front width of the pulse being recorded. The value of C_1 for a divider with a wave resistance of 75 ohms depends only on the length of l_{cyl} of the cylinder of electrode 4, and in the case of air insulation in Figure 3-1,b we have $C_1 = 0.44/_{cyl}$ (C_1 is here in pF, and l_{cyl} is in cm). If $l_{cyl} = 10$ cm, then $C_1 \approx 4.5$ pF and from (3-3), we obtain $t_f \approx 0.4 \cdot 10^{-9}$ sec, i.e., it is possible to record pulses with a front of less than 1 nsec.

The study [49] describes a capacitive divider, built into a strip line, designed for measuring pulses with a front up to 10^{-10} sec, amplitude up to 200 kV, division ratio 10^4, and the time constant $R_1C_2 \gg t_H$. The design of the divider is shown in Figure 3-1,d.

The low-voltage element of the divider, C_2, was made so thin (about 0.1 mm) that no inhomogeneity would be created to stand in the way of a voltage wave propagating along the line, and at the same time the necessary ratio of capacitances C_1/C_2 was obtained. This is achieved by depositing a metallic film 4, serving as an electrode, on an insulating substrate. The depth of penetration of the current into the electrode 4 at the highest frequency in the pulse spectrum, ω, was much higher than the thickness of the conductor, δ, i.e.,

$$\delta \ll \sqrt{\frac{2\sigma}{\omega\mu}}. \tag{3-5}$$

where σ and $\mu = \mu_0 \cdot \mu_r$ are the specific resistance and magnetic permeability of the metallic film. The equivalent circuit for a segment of the divider assumes the form shown in Figure 3-2,c. The following notation is used in the figure: dx - line elements; L, C - linear parameters of the transmission line; L', C', and R' - linear parameters of the line formed by the capacitance C_2. The latter parameters are defined as follows

$$L' = \frac{\mu d}{b}, \text{ henry/m} \tag{3-6}$$

$$R' = \frac{\rho}{bd}, \text{ ohm/m} \tag{3-7}$$

$$C' = \frac{C_1}{l}\frac{ab}{d}, \text{ F/m} \tag{3-8}$$

where $\varepsilon = \varepsilon_0 \cdot \varepsilon_r$ is the dielectric permittivity of the substrate; b is the film width, m; l is the length of the film, m; d is the distance between the film 4 and the lower electrode 3, m (see Figure 3-1,d).

The condition for damping oscillations in the line is

$$R' \gg \omega l. \tag{3-9}$$

At the same time, in order that the recorded pulse not be distorted due to the discharge of the capacitance C_2 through the

wave resistance of the lead cable, R_1, it is necessary to reduce R', so that we have

$$t_n = \left(\frac{l}{\pi}\right)^2 \frac{\sigma}{d\delta} \ll R_1 C_2. \qquad (3\text{-}10)$$

For example, for $\omega = 10^{10}$ Hz in accordance with Equations (3-5) - (3-10) in [49] a divider was built for which $l = 4$ cm, $d = 9 \cdot 10^{-2}$ cm with the relative dielectric permittivity $\varepsilon_1 = 6.5$. The film was made of gold $\delta = 4 \cdot 10^{6}$ cm in thickness. In this case $\sigma/d\delta = 10^5$. For capacitive dividers, discussed above, a good reproduction of all high-frequency components of thepulse is a characteristic trait. However, slower variations of voltage become distorted.

In recording pulses with a large width of the frequency spectrum, use is often made of a divider involving long lines which was first applied by Fletcher [26]. In the design under consideration (Figure 3-1,e), these lines were placed inside each other, and their wave resistances were in the ratio 100:1. A cable along which the signal was fed to the oscilloscope was connected in parallel with the line of lower wave resistance. Ceramics made of titanium dioxide ($\varepsilon = 85$) were used for the line with the smaller wave resistance, and a 52-ohm polyethylene cable was used for the line with the higher wave resistance. The ceramic tube of the low-resistance line had a silver coating 3 and 4 on both sides (Figure 3-1,e). The line with the smaller wave resistance was matched at the end by means of carbon resistors in order to limit reflections from the end. The resistances were in the form of ceramic tubes with a thin carbon layer deposited on the surface. Certain resistors of this type may have the form of disks or cylinders compressed out of a substance which is a mixture of carbon with binding resins. The divider constructed by Fletcher made it possible to observe 20 kV voltage pulses with a front of about 0.5 nsec. It is difficult to build dividers of this type with a large division ratio due to the effect of the inductance of connections in low-voltage line on the front of the recorded pulse. In addition, it is difficult to match such lines perfectly with a load at high

frequencies due to the effect of the inductance of the connection between the line and the load.

In super-high frequency engineering and for nanosecond pulses with the amplitude up to 100 kV, one uses ohmic dividers — attenuators which consist of several resistances. These resistances are chosen in such a way that a matched load is obtained for the signal propagates over the cable into the oscilloscope. The signal has been reduced the desired number of times.

Figure 3-1,f shows the construction of an ohmic divider [26] for recording high-voltage nanosecond pulses. The high-voltage arm consists of three 330 ohm r_1 resistances connected in series, the low-voltage arm — two 20 ohm r_2 resistances connected in parallel. The capacitance of the high-voltage arm relative to the ground is the factor that limits the frequency. The divider made it possible to measure a pulse with a 6 nsec front width with a 10% error. The division ratio was also changed due to the heating of the divider.

Figure 3-1,g shows the construction of a load resistance of type NS-1 which is simultaneously a voltage divider for voltage pulses on the order of several kilovolts. The divider r_1, r_2 is obtained by positioning a high-frequency tap to be connected with the cable; the resistance r_3 serves a matching purpose. To reduce the frequency distortions of the divider, the resistances are surrounded by a metallic screen which, together with the former, produces inhomogeneous lines (see Section 4-4). The equivalent circuit for the device is shown in Figure 3-2, d. A common deficiency of such dividers is the fact that the operating voltage is limited due to the poor functioning of the resistances when encountering high voltage pulses with a steep front.

If the ohmic resistance of the high-voltage arm of the divider is replaced by the wave resistance of a transmission line, then we obtain the simplest divider construction of Figure 3-1, h. In this design, the low-voltage arm is in the form of film resistances

connected in parallel which are placed in a gap in the sheath 3. The division ratio may reach 1/100 and less. With a hign ratio of the arm resistances, the distortion of the pulse front is intensified due to the inductance of the connections between the low-resistance resistances. If the low-value resistance of the divider is connected to the sheath of the line, without screening it is the section behind the divider, then it is hard to get rid of distortions.

Measuring voltages by means of dividers has the following drawbacks:

(1) presence of the parasitic inductance in the resistors and capacitors;

(2) presence of parasitic capacitances between each of the divider sections and the ground or grounded objects, between each of the divider sections and the high-voltage parts of the power source and the control circuit, as well as between divider sections;

(3) voltage drop along the conductor running from the point at which the high voltage is measured to the high-voltage tap of the divider;

(4) voltage drop along the conductor in the grounding circuit of the divider due to either extraneous currents in the conductor or divider currents;

(5) occurrence of oscillations in the divider circuit, due to the presence of a capacitance between the high-voltage tap of the divider and the ground, and due to the inductance of the conductors.

3-3. Measurement of Short Pulses with the Aid of Kerr Cells

As noted in the preceding sections, in measuring high-voltage nonperiodic pulses, as a rule, use is made of oscilloscopes with

voltage dividers. In addition, in measuring the amplitudes of pulses of microsecond width, spherical dischargers can be successfully used. There are also methods of measuring pulses with the aid of oscilloscopes of low sensitivity without dividers. However, as yet this has not been sufficiently developed [77].

Oscilloscopes have the drawback that relatively small deflections of the ray correspond to large variations of voltage. In this case, even the width of the track on the oscilloscopes may have a considerable effect on the accuracy of the determining voltage amplitude.

References [78, 79] describe a device for measuring voltages, based on the Kerr effect, which makes it possible to avoid some of the difficulties indicated above.

The essence of the effect is as follows. In a normal state, many substances are isotropic in the optical sense, since the orientation of molecules in any direction is statistically equiprobable. However, under the influence of an applied electric field the equal probability of any direction in the distribution of molecules is no longer in effect. A certain direction in this case becomes dominant. The substance becomes optically anisotropic. The field of the high voltage pulse is used as such an applied field.

The time it takes for the Kerr effect to occur in the substance after the application of the electric field is practically equal to the statistically averaged time it takes for molecules to become oriented in the preferred direction. This time interval can be approximately calculated on the basis of measurements of the dielectric permittivity at various frequencies. Measurements for nitrobenzene [78] have found that the relaxation time is equal to $5 \cdot 10^{-11}$ sec, and the dielectric permittivity of nitrobenzene was found not to depend on frequency up to 100 MHz, but beginning with 1 GHz it would rapidly fall off. Optical anisotropy, caused by the Kerr effect, is proportional to the square of the intensity of the applied electric field.

It is on this relation that the device for measuring high voltage pulses is based [78].

In the device shown in Figure 3-3, an intense light beam from a high-pressure mercury lamp I is collimated and passed through an interference filter F with a transmission band of 20 Å and the maximum transmitted wavelength of approximately 5,461 Å. The light, upon passing through the filter, should be monochromatic, since the Kerr constant depends on the wavelength. Then with the aid of a prism P the light is polarized in a plane making a 45° angle with the direction of the applied electric field. Subsequently, the light passes through the Kerr cell C where polarization changes strongly, and through the analyzer A. Upon passing through the analyzer A, the light is recorded by a photomultiplier FM whose signal is fed into an oscilloscope and photographed. Thus the measured high-voltage pulse produces a modulated light signal which, upon being analyzed, can be obtained in a reconstituted form, and its amplitude can be measured.

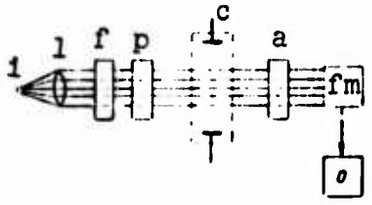

Figure 3-3. Schematic diagram of a measuring device using the Kerr cell.

According to [78] the intensity of the light, J, that had passed through the Kerr cell is for the above apparatus given by

$$J = \frac{1}{2} J_0 \sin^2(\pi j L U^2/d^2), \qquad (3\text{-}11)$$

where J_0 is the intensity of the unpolarized light incident on the polarizer; U is the applied voltage, V; L is the length of the electrodes in the Kerr cell, cm; d is the distance between them, cm; j is the Kerr constant for the medium.

Equation (3-11) implies that the transmission coefficient of the system is maximum for $\pi j L U^2/d^2 = \frac{\pi}{2}, \frac{3}{2}\pi, \frac{5}{2}\pi \ldots$, and that the measurement

accuracy increases with an increase of U, since the maxima will be repeated over increasingly small intervals ΔU. Therefore, by measuring the intensity of light with a small accuracy, it is possible to determine the value of U with a high accuracy. It is, however, necessary to first estimate the amplitude and the width of the pulse being studied. To obtain a higher accuracy, it is recommended to use approximately the value of 5 for the ratio U/U_M, where U_M is the voltage at which the first maximum of the light intensity is observed (3-11). The value of U_M varies with a change of the electrode length or the distance between them. Then one must make a calibrated measurement of U_M. Analyzing the oscillogram obtained using the current from the photomultiplier, one can compute the amplitude of the high-voltage pulse, and — assuming the absence of transient processes in the measuring apparatus and the exact calibration of the oscilloscope scan — one can also determine the form of the entire pulse.

Figure 3-4 shows an example of voltage measurement with the aid of the Kerr cell. At the top we see the form of the applied pulse, determined by means of a precision ohmic voltage divider. At the bottom we see the signal that is the output of the device containing the Kerr cell. One can see that the maximum (peak) of the voltage in the measured pulse (a) is attained after the light signal curve (b) passes the first eight large maxima, the first eight large minima, and 0.2 of the leading edge of the ninth maximum. Upon constructing a graph of J(u) according to (3-11) and comparing it with the lower oscillogram, one can obtain the function u(t) which is analogous to the upper oscillogram.

The advantage of this measurement method is its significantly higher resolution and higher accuracy, and in contrast to other methods the accuracy increases with an increase in voltage. In addition, a total absence of electric coupling between the pulse network and the measuring apparatus excludes the occurrence of any induced voltages.

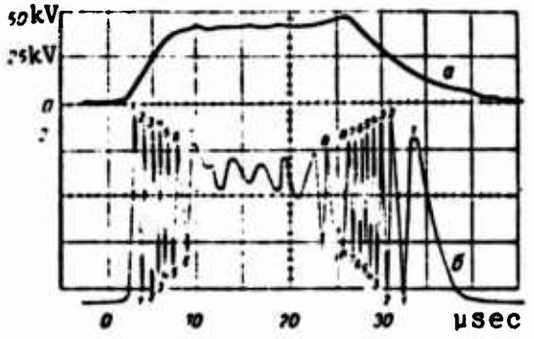

Figure 3-4. Oscillogram of a pulse measured with a precision divider (curve a) and with the Kerr cell (curve b).

The drawbacks of this method are that it is necessary to have monochromatic light, a photomultiplier with the transmission band up to 1 gigahertz, and a traveling-wave oscilloscope. The times of increase and decrease must be sufficiently large, so that the "photomultiplier-oscilloscope" system can follow the oscillations of light intensity caused by the Kerr effect. In addition, the polarity of the pulse is unknown.

3-4. Measurement of Small Voltage Variations at the Top of a High-Voltage Rectangular Pulse by Means of Autoemission Diodes

The magnitude of voltage oscillations at the top of a rectangular pulse can be measured from its oscillogram only to within several percent of accuracy. This is due to the high ratio of an oscillogram line width of the pulse amplitude. For measuring voltage drops to within one percent of accuracy and less, the study [58] has suggested using autoemission diodes with a sharp point cathode.

The density of the autoemission electron current from the cathode is given by [81]

$$j = 1{,}55 \cdot 10^{-6} \frac{E^2}{\varphi} \exp\left(-\frac{6{,}85 \cdot 10^7 \varphi^{3/2}}{E}\right), \qquad (3\text{-}12)$$

where E is the electric field, V/cm; ϕ is the work function, eV.

If a voltage pulse of amplitude U_0 has a rectangular form with a fluctuation at the top $\Delta U << U_0$, then Formula (3-12) may be simplified, replacing j and E with the current i and voltage U,

$$i = Ae^{-\beta U}. \qquad (3\text{-}13)$$

Equation (3-13) implies that small changes in voltage must cause large changes in current. If the relative values of current fluctuation and voltage fluctuation are $\delta i = \Delta i/i_0$ and $\delta U = \Delta U/U_0$, respectively, where i_0 is the current from Equation (3-13) at $U = U_0$, then

$$\delta i = \exp\left[\frac{\beta U}{U_0(1+\delta U)}\right] - 1. \qquad (3\text{-}14)$$

If the exponential is expanded into a series and only the first two terms of the expansion are retained, then

$$\delta i \approx \frac{\beta}{U_0}\delta U. \qquad (3\text{-}15)$$

Consequently, the current fluctuation at the top of the pulse will be magnified B/U_0 times as compared with the voltage fluctuation. The "amplification" coefficient k_y is defined by the formula

$$k_y = \frac{\beta}{U_0} = \frac{6{,}85 \cdot 10^7 \varphi^{3/2}}{\beta U_0}, \qquad (3\text{-}16)$$

where β is the geometric factor which depends only on the dimensions and shape of the sharp point. The larger the radius of the point, the smaller is β [81]. Consequently, to increase k_y it is necessary to increase the radius of the point. Formula (3-12) implies that an increase of k_y results in a strong amplitude decrease of the current i_0. To increase the current amplitude, one must increase the number of points in the autoemission diode.

As an example, Figure 3-5 gives oscillograms of a rectangular voltage pulse 4 μsec in width and 4.5 kV in amplitude, and of the corresponding autoemission current recorded by the OK-17M oscilloscope. At the top of the voltage pulse, it is impossible to determine any change in voltage, and at the top of the current pulse the change can be seen very clearly. As we can see From Figure 3-5, $\delta i = 0.33$. The

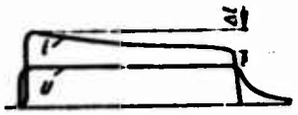

Figure 3-5. Oscillogram of a voltage pulse u and the corresponding autoemission current pulse i.

autoemission diode has a tungsten cathode approximately 10^{-5} cm in radius. B was determined from the slope of the curve lgi = f(1/U) and was $3.1 \cdot 10^4$ V, i.e., for U_0 = 4.5 kV, the "amplification" coefficient was $k_y \approx 6.9$. Consequently, the maximum value of the voltage drop at the top of the voltage pulse (Figure 3-5) is 4.8%.

This method of measuring voltage fluctuations at the top of a rectangular pulse can be easily extended to pulses up to 10^{-8} sec in width and up to 10^5 V and more in amplitude.

3-5. Protection from Disturbances

One of the difficulties that arise in recording high-voltage nanosecond pulses involves shielding recorded signals from parasitic electromagnetic influences. The latter are due to the presence of common resistances in the grounding circuits of measurement and generator networks, and the parasitic electromagnetic couplings between the generator and the measuring device. Couplings result in the occurrence of "negative time" on the oscilloscope screen, "negative" curvature of the pulse, different types of oscillations, wobbles, and other distortions which cast doubt on the reliability of the measurement. To weaken the couplings in the grounding circuit, one can use a decoupling element between the grounded points of the generator circuit and the measuring device in the form of a choke coil or in the form of an active resistance.

To eliminate the electromagnetic couplings, one effective method is to use a screen consisting of a number of parallel metal plates, placed very close to each other [82]. The plates are connected at the center. In this case the large capacitance between the plates

shunts off small capacitances between the generator and divider or the recording instrument. The electromagnetic couplings increase with frequency. The magnitude of the induced voltage is determined not only by the coupling coefficient, but also by the Q factor of a circuit. The most frequently occurring form of the electromagnetic coupling in high-voltage nanosecond technology involves shock excitation of the oscillatory LC circuits in the measurement network by the steep front of an incident wave. Radical methods of protection against interference include a reliable and short grounding, and screening of the measuring apparatus.

In [82] to reduce interferences, the measuring apparatus was screened by metal sheets which were welded together throughout the entire area of the testing region. Copper strips running from suitably located grounding busbars were attached to the sheets at small intervals, and ran farther along all metal blocks of the carcass, screens of the measurement chamber, and the control panel with the oscilloscope screen on it. This type of grounding system is very effective in eliminating random distortions of oscillograms, and in protecting against the influence of usual power units located in the building on the measurement results.

The study [75] describes a device for recording processes occurring at voltages up to 1,400 kV. To eliminate interferences at these voltages, an oscilloscope was put in a separate room with double screening. A cable running from the voltage divider to the oscilloscope had three screens joined together and grounded at the point where the cable was connected to the divider.

Two outer screens were connected to the room screens, and the inner screen — to the oscilloscope housing. The oscilloscope was supplied with power by a motor-generator, where the generator was in the screened room and the motor outside of it. The generator and the motor were linked by a shaft made of an electrically insulating

material. When the oscilloscope was powered by an insulation transformer, a displacement of the zero line was observed, and the voltage drop was distorted during the breakdown of a spark gap.

The entire installation was grounded at the location of the tested object. The screened room in the absence of a separate grounding acquired a potential of up to 35 kV during the acutation of the voltage pulse generator. For this reason, the screened room was connected to the common ground using a separate conductor which did not affect the quality of the oscilloscopic record.

To reduce the influence of currents flowing through the grounding conductors on the quality of the oscillograms, sometimes the floor of the high-voltage room was covered with metal sheets or a metal net which were reliably grounded, and the objects to be grounded were connected with the grounded floor by means of short conductors.

CHAPTER FOUR

ELEMENTS OF GENERATORS OF HIGH-VOLTAGE NANOSECOND PULSES

4-1. Coaxial Lines

In forming, transforming, and transmitting high-voltage pulses, widespread use is made of coaxial cables with polyethylene and teflon insulation, as well as of coaxial lines with liquid insulation (transformer oil, glycerin, water). The operating voltage on such lines may reach 10^6 V and more.

When using coaxial lines and cables in forming and transforming pulses, it is necessary to know the characteristics determining the reliability of lines and cables, and limits of their use. These characteristics include the electric resistance of a cable when operating in the pulse mode and the frequency pass band. Below, coaxial lines and cables will be referred to as coaxial lines.

a) Definitions of the basic parameters of coaxial lines.

Basic formulas to be used in computing coaxial line parameters are listed in the monograph [83]. Here we only give those that are

necessary in designing high-voltage lines. The inductance L of a coaxial line with copper conductors is given by

$$L = 0{,}2 \ln \frac{D}{d} + \frac{13.33}{\sqrt{f}} \left(\frac{1}{d} + \frac{1}{D} \right), \text{ microhenry/m,} \qquad (4\text{-}1)$$

where D and d, mm are the diameters of the outer and inner conductors; f is the frequency of the propagating signal. If the frequency of the signal propagating in the line is large, then the second term in (4-1) may be neglected. The capacitance of a coaxial line, C, is given [83] by the formula

$$C = \frac{\varepsilon}{18 \ln \frac{D}{d}}, \text{ nF/m,} \qquad (4\text{-}2)$$

where ε is the dielectric constant.

If the insulation of a coaxial line is composite along the length of the cable (a cable with air insulation and resistance disks), then

$$\varepsilon = \frac{\varepsilon_1 V_1 + \varepsilon_2 V_2}{V_1 + V_2}, \qquad (4\text{-}3)$$

where quantities with the subscript 1 correspond to the first dielectric, and those with the subscript 2 — to the second dielectric. V is the volume occupied by the insulation.

For an insulation which is composite in the radial direction, we have

$$\varepsilon = \frac{\varepsilon_1 \varepsilon_2 \ln \frac{D}{d}}{\varepsilon_2 \ln \frac{d_r}{d} + \varepsilon_1 \ln \frac{D}{d_r}}, \qquad (4\text{-}4)$$

where the subscripts 1 and 2 refer to the inner and outer dielectrics, respectively. d_r is the diameter of the boundary separating the media.

For the wave resistance Z from (4-1) and (4-2), we obtain

$$Z=\frac{60}{\sqrt{\varepsilon}}\ln\frac{D}{d}=\frac{138}{\sqrt{\varepsilon}}\lg\frac{D}{d},\ \text{ohm}. \tag{4-5}$$

The propagation velocity of tne electromagnetic energy along a coaxial line is given by

$$v=\frac{c}{\sqrt{\varepsilon}},\ \text{m/sec}, \tag{4-6}$$

where c is the velocity of light in vacuum.

Now let us consider the questions involved in selecting the dimensions of a coaxial line to obtain the maximum electric resistance. The intensity E_x of the electric field at a point lying at a distance r_x from the axis of the cable $\left(\frac{d}{2}<r_x<\frac{D}{2}\right)$ is given by [83]

$$E_x=\frac{U}{r_x\ln D/d} \tag{4-7}$$

where U is the voltage applied to the cable. Of course, for $r_x = d/2$ the value of E_x is a maximum, and for $r_x = D/2$ — a minimum. If U and D are given, then (4-7) implies that for $d = D/2.72$ the value of E_x will be a minimum.

To the condition $D/d = 2.72$ there corresponds a coaxial line whose wave resistance is $60/\sqrt{\varepsilon}$. It must be noted that in this case the coaxial line will not be under optimum conditions, as far as wave damping ($D/d = 3.6$ for copper conductors [83] is concerned.

In constructing coaxial lines designed for a transmission of nanosecond pulses, one must keep in mind that they have definite limitations as to frequency. The frequency limitations are due, as shown below, to the damping of waves. In addition, cables with discontinuous insulation (for example, insulating and centering washers at a definite distance in a cable with air insulation) have

limitations related to the inhomogeneity of such lines.

The critical wavelength λ_0 below which transmission over the line is impossible is given by

$$\lambda_0 = 2(a + \Delta\sqrt{\varepsilon}), \tag{4-8}$$

where a is the distance between washers, cm; Δ is the washer thickness, cm; ε is the dielectric constant of the dielectric.

If the wavelength becomes commensurable with the lateral dimensions of a coaxial line, then waves of higher type, such as the TE and TM waves, are set up in the line. For those waves, the theory based on the equations of telegraphy is no longer valid. For this reason, the transmitted pulse becomes distorted. The frequency at which it is possible for higher types of waves to occur in, and be transmitted over, a coaxial line is called the cutoff frequency.

The cutoff frequency for a coaxial line is given by the following formulas:

for TE waves

$$f_0 = \frac{2c}{\pi(D+d)\sqrt{\varepsilon}}; \tag{4-9}$$

for TM waves

$$f_0 = \frac{c}{(D-d)\sqrt{\varepsilon}}, \tag{4-10}$$

where c is the velocity of light in vacuum, cm/sec; D and d are the diameters of line conductors, cm; ε is the dielectric constant.

b) Distortion of pulses by coaxial lines.

When a pulse is transmitted over a coaxial cable, its shape is distorted for three basic reasons: losses in a metal, dielectric

losses in the insulation, and losses related to ionization processes.

Contempory technology of fabricating high-voltage coaxial cables with hard insulation is able to minimize the volume of air bubbles. For this reason, the effect of ionization processes on the deformation of high-voltage pulses may be neglected. In [84] a study was made of the distortion of high-voltage pulses with an amplitude up to 70 kV during their transmission over a RK-103 cable, 530 m in length. It was shown experimentally that the presence of a corona in reality does not have a significant effect on the damping and distortion of high-voltage pulses, and that it is possible to calculate the distortion of high-voltage pulses in coaxial cables with hard insulation at high gradients (up to 50 kV/mm) using the techniques utilized with small gradients. In this case the experimentally obtained damping is 3-8% higher than its computed value. Additional studies have shown that this difference is due to the occurrence of the pulse corona in the air gap between the hard insulation and the cable sheath.

The dielectric losses in the insulation at frequencies up to 50 MHz for cables with polyethylene insulation do not exceed 3-5% losses in the metal, and in the frequency range indicated they may be neglected. With an increase in frequency, the losses in the dielectric increase faster than losses in the metal, and at frequencies above 1.5 - 3 GHz, the losses in the dielectric become dominant [2, 83].

If only the losses in the metal are considered, the deformation of a rectangular pulse ("unit step") may be described [86] by the expression

$$h(l,t)=\operatorname{erfc}(Z)=1-\Phi(Z), \qquad (4\text{-}11)$$

where $h(l,t)$ is the transient response of the cable; $\Phi(Z)$ is the probability integral (Kramp's function);

$$Z=\frac{b_1 l}{2\sqrt{t_1}};\ b_1=\frac{1}{4\pi}\sqrt{\frac{C_0}{L_0}}\sqrt{\mu\rho}\left(\frac{1}{r_1}+\frac{1}{r_2}\right);$$

$t_1=t-t_0$, $t_0=l\sqrt{L_0C_0}$ is the delay time of the cable; $L_0=2\cdot10^{-7}\ln\frac{r_2}{r_1}$, henrys/m, is the inductance of the cable per unit cable; $C_0=\frac{\varepsilon 10^{-9}}{18\ln(r_2/r_1)}$, F/m is the cable capacitance per unit length; ε is the relative dielectric constant of the insulation; r_1, r_2 are the radii of the inner and outer cable conductors, mm; μ, ρ are the magnetic permeability and the specific resistance of the conductors, respectively (for copper conductors; $\mu = 4\pi\cdot10^{-7}$ henrys/m); l is the length of the cable, m; $\rho = 1.75 \times 10^{-2}$ ohm mm^2/m. The probability integral

$$\Phi(Z)=\frac{2}{\sqrt{\pi}}\int_0^Z e^{-x^2}dx$$

cannot be expressed in terms of elementary functions. However, its values can be found in tables [87]. In computing the deformations of nanosecond pulses when it is necessary to consider the losses in the dielectric, the transient cable response should be computed [86] using the formula

$$h(l,t)=\frac{2}{\pi}\int_0^\infty \frac{P(\omega)\sin\omega t_0}{\omega}d\omega, \qquad (4\text{-}12)$$

where $P(\omega)=e^{-\alpha l}\cos(\omega l\sqrt{L_0C_0}-\gamma l)$ is the frequency characteristic of the cable which is the real part of the transmission coefficient; $\alpha=\frac{R_0}{2}\sqrt{\frac{C_0}{L_0}}+\frac{G_0}{2}\sqrt{\frac{L_0}{C_0}}$ is the damping coefficient of the cable (in the high-frequency region); $R_0=b_1\sqrt{2\omega L_0/C_0}$ is the active resistance of the cable per unit length, ohm/m; $G_0=\omega C_0\operatorname{tg}\delta$ is the conductivity of the insulation of the cable per unit length, 1/ohm·m.

Beginning with several hundred megahertz, the function tg δ for polyethylene-insulated cables may be expressed [88] by the formula

$$\operatorname{tg}\delta=\frac{a_1\sqrt{\omega}}{1+m\omega}, \qquad (4\text{-}13)$$

where $a_1 = 1.2 \cdot 10^{-8}$ sec$^{1/2}$/rad$^{1/2}$; $m = 2 \cdot 10^{-11}$ sec/rad;

$$\beta = \sqrt{\omega^2 L_0 C_0 + \left(\frac{R_0}{2}\sqrt{\frac{C_0}{L_0}} - \frac{G_0}{2}\sqrt{\frac{L_0}{C_0}}\right)^2}$$

is the phase coefficient.

A calculation of the transient response from (4-12) can be done analytically [89] or using computers [90, 97]. With a certain approximation, the transient function for the coaxial cable, considering the losses in the dielectric, can be represented [2] by Formula (4-11), whose argument is computed from the expression

$$Z = \frac{\alpha_{cp} l}{2\sqrt{\omega_{cp} l_1}} = \frac{0{,}347}{2\sqrt{\omega_{cp} l_1}}, \qquad (4\text{-}14)$$

where ω_c is the cutoff frequency of the cable pass band; α_c is the damping at the cutoff frequency. The cutoff frequency ω_c is equal to the frequency at which the transmission coefficient $k = e^{-\gamma l}$ (where $\gamma = \alpha + j\beta$) is lowered by 3 decibels as compared with its values at lower frequencies. In accordance with the above definition, ω_c can be calculated using the formula

$$\exp\left[-\alpha_{cp}(\omega_{cp})\, l\right] = \frac{1}{\sqrt{2}}. \qquad (4\text{-}15)$$

Due to the difficulty of solving this transcendental equation, Figure 4-1 gives the plots of the cutoff frequency of the cable pass band versus the cable length for the most widespread types of cables [2].

Figure 4-2 gives the plots of the transient responses for the RK-50-11-13 cable 1, 5, 10 and 30 m in length [2], where A(t) is the ratio of the output voltage u_2 to the input voltage u_1. If it is desired to find the distortion of a pulse whose form differs from a rectangular form, one should apply the Duhamel integral. In this case, the output voltage $u_2(t)$ has the form

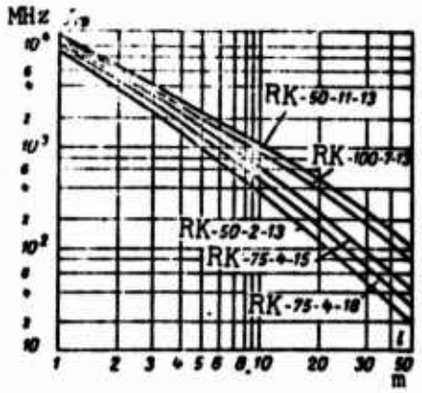

Figure 4.1. Cutoff frequency of the pass band for various types of cable versus their length, considering losses in the dielectric and conductors.

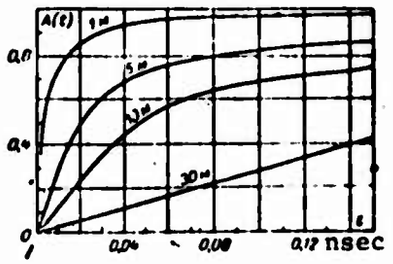

Figure 4-2. Transient response of the RK-50-11-13 cable for various lengths.

$$u_2(t) = \int_0^t u'_1(\tau) h(t-\tau)\, d\tau, \qquad (4\text{-}16)$$

where τ is the running variable; $u'_1(\tau)$ is the derivative of the input voltage.

A technique for an approximate calculation of the Duhamel integral is described in [60, 61].

c) Inhomogeneities in coaxial lines.

In coaxial lines used as forming or transmission elements of the generator of high-voltage nanosecond pulses, it is possible for two types of inhomogeneities to be produced.

First type: inhomogeneities directly related to the electric system of connections among the individual units and circuits of the generator (when additional elements are connected to the line, when the line is connected to a different wave resistance, when the lines branch off, etc.).

Second type: inhomogeneities of the structural-assembly type (sharp variation of the conductor dimensions, inclusion of resistance insulators, line discontinuity, etc.).

In computing the effect of an inhomogeneity of the first type on the waveform, one usually makes use of an equivalent network composed of a two-terminal network and a generator connected in series. The generator consists of a voltage source $2U_{in}$, where U_{in} is the voltage of the incident wave of arbitrary form [1], and the wave resistance Z of the transmission line. The two-terminal network consists of the input resistance of the remaining part of the line, Z, and the input resistance of the added-on element of the circuit, Z_1. The form of the two-terminal network depends on the way the inhomogeneity is connected. For example, when a circuit element of resistance Z_1 (homogeneous line or active resistance) is connected into a gap in the line with the wave resistance Z, the resistances Z_1 and Z are connected in series. If an arbitrary element of resistance Z_1 is included at the end of the line, then the resistance serves as the two-terminal network. In this case, in the short-circuited situation $Z_1 = 0$, and when the end of the line is open $Z_1 = \infty$. It should be kept in mind that the equivalent network is valid only from the arrival of the wave at the inhomogeneity up to the return from the end and beginning of the line of those waves that were refracted and reflected at the location of the inhomogeneity. In computing the effect of the reflected waves, one can use the superposition method.

In analyzing inhomogeneities in transmission lines and their effect on the form of the pulse, it is possible to use the results obtained in the technology of superhigh frequencies. In this case, one must know the maximum frequency f_M in the pulse spectrum which must be transmitted without a substantial change of the amplitude and the phase. t_M may be taken to be the upper cutoff frequency of the frequency response that corresponds to the point at which the amplitude falls off to $1/\sqrt{2}$ of the amplitude at medium frequencies. The relation between f_M and the front width t_f of a pulse, determined between the levels of 0.1 - 0.9 of the amplitude, has the form [6]

$$f_M \approx \frac{0,4}{t_\phi}.$$

The effect of an inhomogeneity of the second type on the form of the voltage wave is generally [6] accounted for by placing a square- or T-form four-terminal network in place of the inhomogeneity, whose parameters depend on the type of inhomogeneity and dimensions of the line. Simple inhomogeneities in which we are interested may be replaced by a capacitance connected in parallel with the line.

Let us consider a discontinuous variation of the radii of the coaxial cable conductors, this being one of the most frequently occurring inhomogeneities.

In practice, we encounter three different cases: 1) diameter of only the inner conductor is changing (Figure 4-3, a); 2) diameter of only the outer conductor is changing (Figure 4-3,b); 3) both parameters are changing simultaneously (Figure 4-3,c). In all cases the inhomogeneity is accounted for by adding a capacitance (Figure 4-3,d):

$$C=FD,$$

where D is the diameter of the outer conductor (in the second case, we may set $D=\frac{D_1+D_2}{2}$).

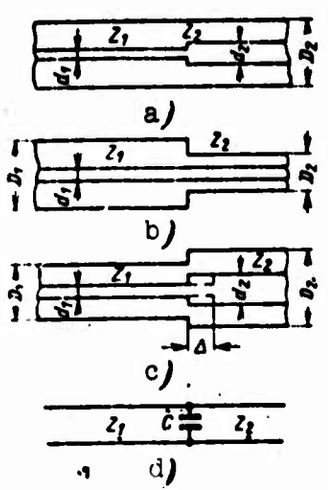

Figure 4-3. Inhomogeneities of the second type (a,b,c) and their equivalent circuit (d).

The plot of the coefficient F as a function of the ratio of diameters is given in Figure 4-4 [14]. The curve $d_1/D = 0$ corresponds to a discontinuance of the inner line conductor. The value of the capacitance for the third case (Figure 4-3,c) is found, starting with the results of the preceding two cases. We first assume the presence of a discontinuity only for the inner conductor, and then only for the outer conductor. The equivalent

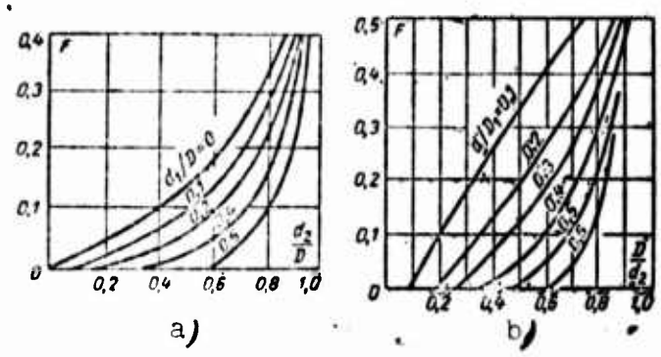

Figure 4-4. Plots for finding the capacitance C corresponding to the inhomogeneities shown in Figure 4-3,a and b.

capacitance can be found by adding the capacitances under the first and second assumption. It is necessary to keep in mind that the data given here can be used only if the wavelength $\lambda > 5D'$, where D' is the larger one of the diameters of the line. The curves given in Figure 4-4 to aid in finding F are applicable to air-filled lines. If a cable is filled with a dielectric, the capacitance C must be multiplied by the dielectric constant ε. If the dielectric fills only the line whose inner conductor is of smaller diameter, then the value of C found with the aid of the plots in Figure 4-4 must be multiplied by ε. If a line with a large diameter of the inner conductor is filled with a dielectric, then in the first approximation it can be assumed that the value of C found for the air-filled line remains unchanged. For lines in which the diameter of the inner conductor is changing, it can be assumed that — when the line with the large diameter is filled with a dielectric — the value of C increases ε times, and, when the line with the smaller diameter is filled, the value of C remains unchanged. If the dielectric fills a portion of a coaxial line whose dimensions are constant, then this is equivalent to a jump in the wave impedance.

In certain cases, a discontinuity in line dimensions may occur at constant wave impedance. In this case, one must observe the

condition $d_1/D_1 = d_2/D_2$. An inhomogeneity at a point of contact is accounted for by adding a capacitance C in the equivalent circuit. The effect of the capacitance can be substantially weakened by shifting the inner conductor by $\Delta = D_2/10$ from the location of the inhomogeneity (in Figure 4-3 indicated with a dotted line). The shift is equivalent to an addition of a series inductance which compensates for the effect of the capacitance C. At high voltages in the line, the electric resistance of such a connection is small due to the presence of sharp angles. To increase the electric resistance, it is better to use a smooth conical connection between the lines. The length of the connection should be chosen using the relation

$$l \geqslant 2D_2.$$

A conical connection is often used when constructing discharge devices, peaking circuits, etc. A detailed analysis of this type of connection is given in [1]. Methods of eliminating inhomogeneities produced by the resistance elements from the dielectric are described in [6].

d) Electric resistance of a coaxial cable in the pulse mode of operation.

Polyethylene is most widely used as an insulator in radio-frequency and pulse cables. Flat specimens of polyethylene possess a very high electric strength (300-600 kV/mm). For short segments of cable devices, the maximum breakdown strength in single-pulse breakdown is of the same order. However, in multi-pulse breakdown it is lowered to 10-20 kV/mm, and strongly depends on the method of applying insulation, presence of semiconductor layers, diameter of the inner conductor, etc.

A study of polyethylene has shown that the basic factor responsible for the lowering of the electric resistance of cable insulation is the presence of air and gas bubbles of various sizes in the insulation.

At high voltages, electric discharges occur in the bubbles that result in a rapid rupture of the insulation and cable breakdowns. The insulation is ruptured near the air bubbles, and then discharge channels gradually penetrate deeper into the insulation. For a breakdown to occur, one needs a definite number of pulses which depends on the number of air bubbles, their size, amplitude and form of pulses, as well as a number of other factors.

No reliable data are available on the electric resistance of coaxial cables in the presence of voltages corresponding to the operational parameters of high-voltage nanosecond generators. It is only possible to make an approximate guess as to the service life of cables under those conditions. The most correct information is given by the so-called "life curve" for a cable which represents an experimentally obtained relationship between the number of pulses resulting in a breakdown and the amplitude of the pulses. A characteristic "life curve" for the IK-2 cable, obtained using 10.6 m cable specimens acted upon by pulses with a front width of 0.8 μsec and the width of 3 μsec, according to the data of [92], is shown in Figure 4-5. The question of how the "life curve" of a cable changes when varying the form of the pulses thus far remains open. One can assume that the change will not be very large [98]. A large reduction of the service life can be expected only with bipolar pulses.

It was experimentally established that for t_{sp} = 100 nsec, U = 50 kV; f = 50 Hz the mean service life of the RK-106 cable is largely determined by the quality of the cable, and in certain cases amounts to 1000 hours [107].

An experimental determination of the "life curve" of a cable requires a great investment of time and materials. For this reason, it is of interest to consider the procedure of [93, 94] in which it is sufficient to determine experimentally two or three points on the life curve, and the remaining points can be obtained analytically.

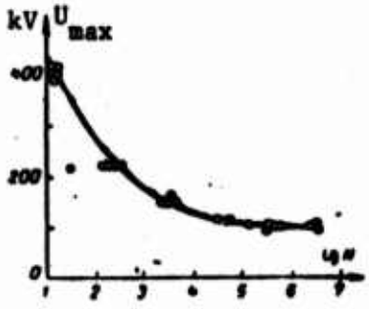

Figure 4-5. Plot of the life of a IK-2 cable segment 10.6 m in length.

In approximately determining the number of unipolar pulses which can be endured by the polyethylene cable insulation until breakdown, use can be made of the empirical formula [95]:

$$N = 7{,}2 \cdot 10^{10} \left(\frac{2U_к}{U}\right)^{9{,}6},$$

where U_K is the amplitude of the initial corona voltage; U is the amplitude of voltage pulses.

For example, for the RK-50-9-11 (RK-106) cable in the case of unipolar pulses with the amplitude U = 50 kV, we have

$$N = 7{,}2 \cdot 10^{10} \left(\frac{2\sqrt{2} \cdot 5}{50}\right)^{9{,}6} \approx 1{,}6 \cdot 10^{9} \quad \text{pulses}$$

It must be noted that for one of the mass produced radio-frequency cables with polyethylene insulation the voltage of the ionization start is no larger than 10 - 12 kV.

The most radical method of increasing the ionization start voltage is to use semiconductor layers on the inner conductor and underneath the screen. The necessary condition for the semiconductor layers to be effective is that they have to be bonded tightly to the insulating layer. In selecting the specific resistance of the semiconductor layer, we are guided by the requirement that the air bubble at the boundary with the conductor be reliably shunted off.

The use of semiconductor layers made it possible to produce a series of polyethylene-insulated high-voltage KPV cables (KPV-1/20, KPV-1/50, KPV-1/75, KPV-1/300). Experiments at the Tomsk Polytechnical Institute have shown that the KPV-1/300 cable in pieces up to several tens of meters is able to resist 6 to 10 thousand pulses with

the amplitude of 250 kV, and 100-200 thousand pulses with the amplitude of 180 kV. The IK-4 cable, produced in the USSR, which has semiconductor layers, is rated for long-term service in the region of of 75 kV unipolar pulses. The USA produces a series of special pulse cables with polyethylene insulation and semiconductor layers designed for voltages from 20 to 100 kV, and a service life of no less than 10^6 pulses (maximum field intensity in the insulation is taken as equal to 20-25 kV/mm [96]).

Coaxial systems involving liquid insulation are very promising for high-voltage nanosecond generators. They possess a number of advantages as compared with polymer-insulated cables: higher reliability, better cooling, automatic return of liquid insulation to previous state after breakdown, smaller damping [97]. The high reliability of such coaxial systems is due to the small volume of hard insulation which has to be thoroughly checked and tested. Tests made at the Tomsk Polytechnical Institute have shown that, when insulators are subject to strict quality control, the coaxial line up to several tens of meters in length sustains no less than 10^6 pulses with an amplitude up to 300 kV, the conductor diameters being 20 mm x 10 mm and 40 mm x 200 mm.

4-2. Pulse Thyratrons

The use of pulse hydrogen thyratrons as commutating elements increases the reliability of high-voltage generators and simplifies their operation.

The advantages of pulse thyratrons include: possibility of parallel triggering of a large number of thyratrons (small instability in triggering); operation at high repetition frequency; long service life.

The drawbacks of thyratrons include: large inductance; switching time is much larger compared with spark gaps; restrictions on switching current and voltage; use of power for incandescence.

These drawbacks impose definite limitations on the range of applicability of thyratrons when dealing with short pulses and large currents. To determine the range of thyratron working parameters, one must know such their characteristics as inductance, switching time, triggering instability. Unfortunately, these parameters are not usually indicated in the technical description of a thyratron.

As shown in § 2-1, the pulse front width is determined by the inductance of the commutator and the switching time. The switching time in a hydrogen thyratron is determined basically by the pressure in the bulb which depends on the temperature of the hydrogen generator. With strict requirements as to synchronization, it is necessary to know the delay in the triggering of the thyratron, i.e., the time from the time of application of voltage to the time when the anode current appears. In case it is necessary to trigger several thyratrons in parallel, it is necessary to know the triggering instability. The studies done have shown that the triggering instability for pulse thyratrons with corresponding stabilization of the heating and triggering voltage amounts to 10^{-9} sec [62]. Table 4-1 gives the basic characteristics of domestic thyratrons, obtained in [27, 62] and those obtained by the authors. An important property of thyratrons is the possibility of increasing the current as compared with its nominal value when the pulse width is reduced. Experimental studies have shown that, when the pulse width is on the order of 10^{-7} sec, the magnitude of the pulse current may exceed the nominal value several times. The criterion for the possibility of varying thyratron parameters, taking into consideration the maximum currents obtained experimentally (see Table 4-1), is provided by the product of parameters $f_{rot} U_{lt} t_{sp} \leq N_{av}$, where N_{av} is the certified value of average power.

As can be seen from Table 4-1, the self-inductance of heavy-duty pulse hydrogen thyratrons with voltages up to tens of kilovolts and

TABLE 4-1

Parameters	Thyratron type						
					Metallic-ceramic		
	TGI-1 325/16	TGI-1 400/16	TGI-1 700/25	TGI-1 2500/35	TGI-1 1000/25	TGI-1 3000/50	TGI-1 500/16
Requirements on stability, %:							
for power source	5	5	8	1.5	8	-	-
for ignition	10	10	10	10	10	-	-
for heating of hydrogen generator	0.4	0.4	0.4	0.8	0.4	-	-
for heating of cathode .	1	1	1	1	1	-	-
for amplitude of firing voltage	1	1	1	2	1	-	-
Delay of discharge in nominal mode, nsec	± 1	± 1	± 1	± 4	± 1	-	-
Front in nominal mode with heating voltage of 6.3 V, nsec	15	20	25	35	20	25	15
Minimum front at U_{heat} V (nsec)	10	12	15	24	15	15	10
Inductance of thyratron (in coaxial case), microhenrys	0.15	0.15	0.35	0.7	0.2	0.3	0.12
Pulse anode current in nominal mode, A	325	400	700	2500	1000	3000	500
Pulse anode current at t_{sp} = 100 (nsec) (experimental data)	10^3	10^3	2.10^3	7.10^3	3.10^3	10.10^3	10^2
Average anode current, A .	0.2	0.5	1	2.5	1	4	0.5
Repetition frequency, Hz..	10^3	450	500	250	700	-	10^3
Maximum anode voltage, kV.	16	16	25	35	25	50	16
Heating current, A	8.5	11	20	55	20	87	15
Maximum amplitude of feedback voltage, kV	16	5	5	5	5	-	3.2
Average output power, kilowatts	-	4	25	43	25	250	8

currents up to several kiloamperes is approximately $L_T \approx 0.3$ microhenrys. If the internal resistance of the generating device is small, $\rho \leq 10$ ohms, the time constant of the current rise L_T/ρ is large, and this makes it impossible to use heavy-duty thyratrons for generating high-voltage nanosecond pulses. At the same time, in

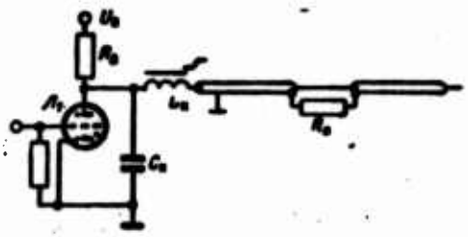

Figure 4-6. Reduction of the switching time by including capacitance and nonlinear inductance into the anode circuit of the thyratron.

contrast with other gas-discharge devices, thyratrons possess a number of extremely valuable properties such as high reliability, simplicity of startup and high pulse repetition frequency. This makes it necessary tc search for new circuit designs that will permit the use of heavy-duty hydrogen thyratrons for generating high-voltage nanosecond pulses.

Figure 4-6 shows one of the designs for a generator of high-voltage nanosecond pulses based on a two-stage coaxial line in which a hydrogen thyratron is used as a switch. The pulse front width at the output of the generator (without considering the parasitic parameters of the output circuit) is determined by the rise time of the current through the thyratron, and depends on the time of discharge development, inductance of the commutator circuit, and the capacitance C_K. To reduce the switching time, an inductive commutator L_K with a small switching time $t_0 << t_f$ is connected in series with the thyratron. The commutator is activated after the thyratron transient is terminated and the current through the thyratron attains a maximum (t_f is the front width without correction). A network of a similar type is used at the output of high-voltage generators [20].

Let us consider the basic concepts involved in selection of the parameters L_K, C_K. The capacitance C_K can be found from the condition that the maximum currents in the $L_T C_K$ circuit and through the generator be equal:

$$C_K = \frac{L_T}{\rho^2},$$

where ρ is the wave impedance of a line stage.

This formula implies that, in the case of heavy-duty thyratrons, the value of C_K may reach several thousand picofarads.

The inductance L_K is selected using the following considerations:

1. The current i_K at which the inductance L_K becomes saturated must satisfy the condition

$$I_{н}\rho \leqslant 0{,}1U_{а}.$$

where U_a is the anode voltage.

This condition means that the active front width is defined as the time of voltage rise from 0.1 to $0.9U_{out}$.

2. The value of the inductance L_{K0} after entering the saturated state must satisfy the condition

$$t_{ф0} \approx \frac{L_{н0}}{\rho} \ll t_{ф}.$$

where t_{f0} is the width of the corrected front.

If one considers that the voltage across the inductance increases linearly, then it is easy to show that in this case

$$L_{н} = \frac{U_{а} t_{ф}}{2I_{н}}.$$

For $I_{н} = 0{,}1U_{а}/\rho$

$$L_{н} = 5t_{ф}\rho. \qquad (4\text{-}17)$$

This assumption is completely justified in rough calculations. The number of turns in inductance L_K can be determined by knowing the value of the saturation field H_K:

$$w = \frac{H_H l_0}{I_H}, \qquad (4\text{-}18)$$

where l_0 is the average length of the magnetic line of force.

The core section is

$$S = \frac{L_0 l_0}{1{,}26 \cdot 10^{-8} w^2 \mu}, \qquad (4\text{-}19)$$

where μ is the magnetic permeability of the core material.

The rise time of the current through L_{K0} which determines the pulse front on the load is

$$t_{f0} = 2{,}2 \frac{L_{K0}}{\rho}. \qquad (4\text{-}20)$$

The ratio $t_f/t_{f0} = k$ is the coefficient indicating the reduction of the switching time.

Given the value of k, the required value of L_{K0} is:

$$L_{K0} = \frac{t_{f0}\rho}{k}. \qquad (4\text{-}21)$$

Thus, the inductive commutator must obey two conditions: up to saturation its magnitude must be L_K, and after saturation — L_{K0}.

Or, in other words, one must select a magnetic material that satisfies the condition

$$\frac{\mu}{\mu_H} \geq \frac{L_H}{L_{K0}}, \qquad (4\text{-}22)$$

where μ_H is the magnetic permeability at saturation.

In the case of nanosecond pulse generation, the most convenient material for a coil core is ferrite.

4-3. Spark Gaps of Nanosecond Range

In this section, we consider spark gaps with nanosecond switching times that are triggered with nanosecond accuracy.

In § 2-1 and in [1, 44], it was shown that, in a static breakdown of a spark gap, the time during which the voltage across the gap decreases from its initial value to one which is close to zero (the switching time t_K) is in proportion to the time constant $\theta = 2p/\alpha E^2$. If the voltage at which the gap is punctured is constant, then the ratio of the field intensity to the pressure is $E/p = \text{const}$. Then

$$\theta = 2(E/p)^{-2}(\alpha p)^{-1}, \tag{4-23}$$

i.e., the value of θ and the commutation time t_K will be smaller in proportion to the increase in gas pressure and the value of E/p. The increase of gas pressure to reduce the switching time of spark gaps was first used in [25]. In [26] a spark gap was immersed in a nitrogen atmosphere at a pressure of 40 at, and the commutation time obtained was $3 \cdot 10^{-10}$ sec. A majority of spark gaps for generators of high-voltage nanosecond pulses were used in an atmosphere of compressed gas [1].

It is well-known that, as the spark gap width d decreases during its static breakdown, the ratio of the field intensity to the pressure, E/p, increases. For example, in the right-hand portion of the Paschen curve in the region near the minimum, we have for the air $E/p = A + \frac{B}{dp}$, where $A = 62 \cdot 10^3$ V/cm · at; B = 340 V [99].

This means that for small spark gap widths d << 1 cm, even at atmospheric gas pressure one can obtain $E/p > 10^3$ V/cm · at, and the time $t_K \approx 10^{-9}$ sec [100]. In [101] this effect was proposed for

building spark switches with a nanosecond switching time. Still another possibility of reducing the switching time, which follows immediately from Equation (4-23), is to use a gas with a large parameter a. For example, if for the air a $\approx$ 1 at $\cdot$ cm^2/V^2 $\cdot$ sec, then for argon it is larger than 20 at $\cdot$ cm^2/V^2 $\cdot$ sec [102]. This is due to the small (on the order of several nanoseconds) switching time of spark gaps in argon even at atmospheric gas pressure and gap widths on the order of 1 mm [103].

In [5, 137] use was made of spark gaps filled with transformer oil, and the commutation time obtained was on the order of 10^{-9} sec. Such arrangements, however, have not been popular due to their instability and short service life. It is also possible to obtain switching times on the order of 10^{-9}-10^{-10} sec using gas spark gaps operating with spark gaps whose voltage has been preliminarily raised. The overvoltage in spark gaps can also be obtained when spark gaps operate as front sharpening circuits [1] and when a large number of spark gaps are connected in series [104].

Commutators that are capable of being triggered with nanosecond accuracy are usually in the form of trigatrons, spark relays, and three-electrode and multi-electrode spark switches.

The trigatron operates in the following fashion. After the triggering pulse reaches the rod electrode 3 (Figure 4-7, a), a discharge occurs between electrodes 3 and 1. This initiates the breakdown of the main gap between electrodes 1 and 2. In [105], a study was made of the possibility of trigatron triggering with nanosecond accuracy. The trigatron was placed in a freon atmosphere at a pressure of 0.14 at. The maximum operating voltage was 50 kV. It was shown that the delay time between the arrival of a triggering pulse and the operation of the trigatron is less when the polarities of the triggering pulse and the potential on the ungrounded electrode are opposite. For a triggering pulse of amplitude 32 kV and front width of $2 \cdot 10^{-8}$ sec, the delay time was $2 \cdot 10^{-8}$ sec, with a scatter of no more than 1 nsec. In this case, the voltage across the gap was less than the static breakdown voltage by 10% and more.

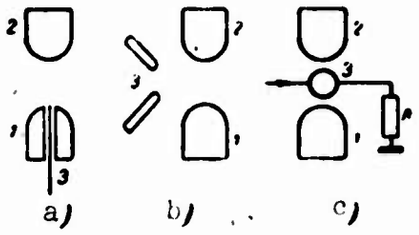

Figure 4-7. a - trigatron spark gap; b - spark relay; c - three-electrode spark gap: 1, 2 - main electrodes; 3 - keep-alive electrode.

In [106], in order to reduce the amplitude of the trigatron triggering pulse, its keep-alive electrode was covered with barium titanate which is a dielectric of a high dielectric constant ($\varepsilon > 1000$). A small gap was created between the dielectric covering of electrode 3 and electrode 1. When the triggering pulse was applied, almost the entire voltage was applied to the gap. In such spark gaps, filled with air at atmospheric pressure, the maximum working voltage was 25 kV, the delay time was 17-65 nsec depending on the required operational mode of the gap, and the scatter of the delay time did not exceed 3 nsec. The amplitude of the triggering pulse was 0.5-1 kV with a front width of 5 nsec. A spark gap using ceramics of high ε was also described in [108].

The spark relay has two spark gaps (Figure 4-7, b): the main one — between electrodes 1 and 2, and the initiating gap 3 [27]. Ultraviolet radiation from a spark in gap 3, incident on cathode 2, results in photocurrent from the cathode, which initiates breakdown of the main gap. In [27] it is shown that, if the voltage across the main gap is too low by 1-2% and the operating voltage is about 10 kV, the delay time t_3 between the breakdown of the initiating and main gap is $\sim$5 nsec.

In [109] for triggering a spark relay in the air, use was made of pulses of ultraviolet radiation 6 nsec in width and 1 nsec in front width. In this case, there is higher stability ($\pm$1 nsec) between the breakdowns of the main gap and auxiliary gap. As the voltage across the main gap approaches its static breakdown value, the time t_3 approaches the time needed for an avalanche breakdown of the main gap.

The basic advantage of a gas spark relay is the fact that the keep-alive and main gaps are completely insulated electrically, and that the time t_3 is highly stable. The disadvantage is that the working voltage is restricted to a narrow range, assuming the inter-electrode distance is constant.

The range of the working voltages of the spark gap increases considerably when vacuum spark relays and spark gaps are used in conjunction with a powerful triggering laser beam and an electron beam. In [110] a study was made of the effect of laser radiation on the gap breakdown. The study involved an investigation of the time delay t_3 between the arrival of the laser pulse and the appearance of the current flowing through the spark gap in air, nitrogen, and elegas. The laser beam had the power up to 80 megawatts, the pressure was 100-1,400 mm Hg, the distance between the electrodes was 0.4-1.5 cm, and the electric field in the spark gap was 10-100 kV/cm. The time t_3 was inversely proportional to the electric field, gas pressure, and the distance of the focus from the surface of the anode.

Reference [111] gives a description of vacuum spark relays. In these switches the breakdown of the main gap is initiated by an auxiliary breakdown on the surface of mica which separates the electrodes of the triggering gap. A use of this insulating lining makes it possible to lower the breakdown voltage of the triggering gap, and thus lower the amplitude of the triggering pulse. For example, VIR-7 operates reliably when the working voltage varies from 10 to 100 kV. The triggering time of the gap and its stability depend on the curvature of the triggering pulse front. If the amplitude of the triggering pulse is 2.2 kV and the front curvature is 225 kV/μsec, the time t_3 for the VIR-7 gap is $(3 \pm 1) \cdot 10^{-8}$ sec. The basic drawback of this type of gaps is the small number of bubbles due to the rapid covering of mica with metal and the vacuum losses in the bulb.

The three-electrode spark gap is built in the following way (Figure 4-7, c). Electrode 2 is connected to a source of high d-c

voltage U_1, and electrode 1 is grounded through the load. The width of the gap 2-3, d_{23}, is chosen such that it will not be punctured at voltage U_1, and the width of the gap 1-3, d_{13}, is such that it will not be punctured by the triggering pulse. When electrode 3 receives a triggering pulse U_2 with polarity opposite to U_1, the gap 2-3 is punctured, and the middle electrode is raised to potential U_1. If the gap widths are in the ratio $d_{23}/d_{13} \approx 2$, then the gap unit has a maximum double range of operating voltages. A study of the operation of the three-electrode gap unit [27] has shown that, in order to reduce the triggering delay time and to increase the stability of this time, one must increase the amplitude and curvature of the triggering pulse front. If the front curvature is 40-50 kV/ /μsec and the amplitude of the triggering pulse is 50-70% U_1, the scatter of the time t_3 obtained is on the order of $\pm 10^{-8}$ sec. The operation of the gap unit is considerably accelerated and stabilized if the gaps 2-3 and 1-3 are irradiated with ultraviolet light. In [112] a suggestion was made that in order to stabilize the operation of the three-electrode gap the gaps 2-3 and 1-3 should be irradiated by a spark from the auxiliary gap connected in series with a cable which carries the triggering pulse. In this case, the stability of t_3 is no less than ± 1 nsec.

Reference [57] proposed a spark gap with high speed triggering (10^{-8} sec) by an electron beam through a thin metal foil in the cathode. Such a spark unit has a wide range of operating voltages, high triggering stability, and, most important, it makes it possible to eliminate localization of a spark channel, and permits a wide area of discharge due to which one can ultimately obtain higher rates of current rise.

Reference [113] describes a single-action discharge unit operating at up to 200 kV which makes use of a discharge in polyethylene. The triggering instability for this discharge unit did not exceed ± 1 nsec.

The three-electrode nanosecond spark gaps provide triggering pulses of high amplitude and a narrow range of operating voltages.

To eliminate these drawbacks, in [100, 101] it was proposed to use multi-electrode spark gaps in which the capacitance between the electrodes and the ground is greater than the interelectrode capacitance. To obtain a switching time on the order of 10^{-9} sec at an atmospheric gas pressure, the spark gaps have narrow gaps (on the order of 0.1 mm).

4-4. Resistors and Capacitors for High-Voltage Nanosecond Pulse Devices

a) Resistors

Ohmic resistors used in high-voltage nanosecond devices must satisfy the following requirements: their resistance must be independent of voltage and frequency within a certain interval, the resistor must have a small parasitic inductance and capacitance, and be thermally stable.

It is not always possible to satisfy these requirements. For this reason, the problem of selecting resistances for nanosecond high-voltage devices cannot be considered as solved. We shall discuss certain features of these resistors.

The resistors used in the nanosecond range are of the following types: carbon, film, metal-film, and composite. Wire resistors are not always applicable, due to their high inductance.

The depth δ of the current penetration into the conductor at which the current density becomes 2.718 times smaller than the maximum density at the conductor surface can be used as a characteristic of the skin effect. The depth δ is given by

$$\delta = \sqrt{\frac{\rho}{\pi \mu f}}, \qquad (4\text{-}24)$$

where f is the frequency; μ_a is the absolute magnetic permeability of the conductor; σ is the specific resistance of the conductor material. Given the depth δ, depending on the frequency, one can determine the variation of resistance for this frequency, and as a result one can find the permissible thickness Δ of the conducting layer. The dependence of the resistance on the frequency is in practice negligible for the entire frequency spectrum of the pulse, assuming that for the maximum frequency $\delta = \sqrt{\frac{\rho}{\pi \mu_a f}}$. The value of δ for conductors at frequencies corresponding to nanosecond pulses can reach tens of microns. Therefore, conducting films must have a thickness on the order of several microns, which does not present any problem when it comes to the fabrication of resistors. When the resistors are subject to voltages of high frequency, the effect of self-capacitance and self-inductance of the line is apparent. The equivalent circuit for resistance at a high frequency is similar to the equivalent circuit for a long line with losses. In addition, we have the effects of the capacitance between the leads of the resistor and their capacitance with respect to the ground. The values of the linear capacitance and inductance L_0 and C_0 are determined by the form factor of the resistor, k_f [114] (it is assumed that the resistor is cylindrical in form):

$$k_\phi = \frac{l}{\pi D},$$

where l is the resistor length; D is its diameter;

$$C_0 \approx 10^{\frac{10.8}{k_\phi} - 2}, \text{ pF/cm} \qquad (4\text{-}25)$$

$$L_0 = 2 [\ln 4\pi k_\phi - 1], \text{ nano henry/cm} \qquad (4\text{-}26)$$

If there is a spiral cut on the resistor which is introduced to increase resistance, the value of L_0 is determined using another formula

$$L_0 = 0{,}9 \frac{w^2}{k_\phi^2}, \text{ nano henry/cm} \qquad (4\text{-}27)$$

where w is the number of turns in the spiral. Since the value of L_0 is much greater for resistors with spiral cuts, such resistors are rarely used in pulse circuits of nanosecond range.

It is difficult in practice to use the above-mentioned equivalent circuit for the resistor. It is considered [114] that if $R > \sqrt{L_0/C_0}$, then the effect of L_0 can be neglected, and the equivalent circuit can be drawn in the form of a parallel RC circuit ($C = C_0 l$). For smaller values of R, the effect of C_0 is neglected, and the equivalence circuit is drawn in the form of a series RL circuit ($L = L_0 l$). The effect of L and C can be neglected if the corresponding time constants L/R and RC are smaller than the front width by a factor of four-fifths.

Under the influence of high voltages, the dependence of the resistance on the voltage is manifested. In this case, starting with a certain voltage the resistance R is reduced, and Ohm's law does not hold. One of the reasons for the nonlinearity of the resistance can be found in the local overheating of the conducting film caused by nonuniform current distribution. In composite resistors, the nonlinearity may be caused by the influence of the conductivity of the clearance between conducting grains, which at field intensities 10^5-10^6 V/cm has a nonlinear character. The maximum permissible operating voltage is restricted by the electric breakdown and sparking on the surface of the resistor. The voltage at which a breakdown along the surface occurs is practically independent of the type of conducting covering, and is determined for a given pressure p only by the distance between the leads, their form, and location. The dependence on the voltage U_{br} at which a breakdown occurs in the resistors without cuts (of MLT, VS and other types), on the resistor length l and pressure p (for $pl > 1$ mm Hg · cm) with sufficient accuracy is given by [114].

$$U_{пр} = 300(pl)^{0.5}, \text{ V} \qquad (4\text{-}28)$$

If the working voltage is less than U_{br} by 20-30%, then in the absence of heating and an external temperature of 15-20°C, the resistor

is guaranteed to operate without any danger. It is necessary to keep in mind that Equation (4-28) is valid for pulses on the order of 10^{-6} sec in width; for pulses on the order of 10^{-9} sec in width, the value of U_{br} turns out to be much higher. The magnitude of U_{br} can be increased by placing the resistor in an insulating liquid.

Designs of resistors operating in pulse circuits in the nanosecond range occur in different forms that are determined by the application of the resistor. Resistors occur as parts and even subunits of constructions. In addition to cylindrical forms, disk and plate resistors are also used. Table 4-2 gives the basic parameters of certain high-frequency cylindrical resistors of the UNU type with a carbon covering [114].

TABLE 4-2

Type	Nominal power, watts	Dimensions		Value of resistance ohms	Limiting voltage at t_{sp} = 1 μsec, V	Maximum test power at pulse, kilowatts
		Length mm	Diameter mm			
UNU-10	10	122	25	50; 75	4,000	212
UNU-25	25	182	29	50; 75	6,500	570
UNU-50	50	252	45	50; 75	8,700	1,000
UNU-100	100	352	64	75	12,500	2,000

In resistors of the metal-film type designed for operating in the high-frequency range, Nichrome is used as a surface covering, which is deposited on a dielectric substrate by spraying in vacuum. Sometimes to obtain high-frequency resistors on the order of one kiloohm and more, resistors are used with composite coverings (mixture of powdered conductor with a dielectric).

When using resistors, it is necessary to keep the fact in mind that the resistance is dependent on temperature, and the latter may increase during operation. To avoid resistor overheating, one must increase the surface area or use forced air or water cooling. For

example, resistors of UNU type increase their nominal power by a factor of 5-10 with intensive air cooling. Metal-film or carbon resistors are sometimes provided with water cooling. In this case, their power is several and even tens of kilowatts [115].

When voltages in the pulse are on the order of hundreds of kilovolts, one can use a water solution of NaCl or other salt solutions as resistors. Such resistors have small inductance and are characterized by a large heat capacity. The skin effect in such resistors is absent if the resistor diameter satisfies

$$D \leqslant 0.1\delta. \tag{4-29}$$

Making use of Equations (4-24) and (4-29), and considering that for water $D \leqslant 0.1\delta$. henry/m, we shall find an expression for the water resistance R at which there will be no skin effect

$$R \geqslant 1.6 \cdot 10^{-4} fl\sigma, \text{ ohm} \tag{4-30}$$

where f is the frequency, Hz; l is the resistor length, m; σ is the specific resistance, ohm/m.

Thus, knowing the uppermost frequency in the pulse frequency spectrum, f_M, and the resistor length l, the required value of R is selected by means of a suitable salt concentration. Disadvantages of water resistors are the following: great dependence of R on external factors, particularly on temperature, large self-capacitance, substantial change in R in the course of time.

In matching long lines, one must include a resistance which is equal to the wave impedance of the line. If an ordinary concentrated resistance is added, the pulse will be distorted due to parasitic parameters, i.e., inductance and capacitance of the resistance and the leads. For this reason, it is better to use a disk type resistance. One can improve the frequency properties of the matching resistance by placing a cylindrical resistance of diameter D and value R, equal to the wave impedance of the line, inside a

cylindrical screen whose length is much longer than its diameter. This produces a line section with losses and with a certain wave impedance Z'. The relationship between R and Z' may be selected using the equality $R=\sqrt{3}Z'$ [6]. The matching unit with a cylindrical screen, however, has a narrow frequency pass band, and can be recommended only if the ratio of the resistor length l to the smallest wavelength λ_M does not exceed 0.1.

In order to better match the resistance with the transmission line, the profile of the screen surrounding the resistance is chosen such that the wave impedance of the entire unit at any cross-section will be equal to the ohmic resistance of the remaining part of the resistor [115]. If the resistor has a uniform film covering, its value does not depend on frequency, and at a distance χ from the end of the load it will be equal to:

$$R_x = R_0 x,$$

where R_0 is the resistance per unit length. The wave impedance of the line without losses in that cross-section is

$$z_x = \sqrt{\frac{L_x}{C_x}}. \qquad (4\text{-}31)$$

where C_χ and L_χ are the inductance and capacitance per unit length at the cross-section χ. There will be no reflections if

$$\sqrt{\frac{L_x}{C_x}} = R_0 x. \qquad (4\text{-}32)$$

We can assume that within a small element $\Delta\chi$ the diameter of the screen is constant. Then

$$L_x = 0.2 \ln \frac{2y}{D}, \ \mu\text{henrys/m}$$
$$C_x = \frac{5.55\varepsilon}{\ln \frac{2y}{D}}, \ \text{pF/m} \qquad (4\text{-}33)$$

where ε is the relative permittivity of the dielectric in the space between the resistance and the screen; y is the ordinate of the profile; D is the resistor diameter. Starting with (4-33) and (4-32), we obtain:

$$\frac{60}{\sqrt{\varepsilon}} \ln \frac{2y}{D} = R_0 x$$

or

$$y = \frac{D}{2} e^{\frac{R_0 x \sqrt{\varepsilon}}{60}}. \qquad (4\text{-}34)$$

This calculation of the screen profile takes into account only the radial components of the electric field, and neglects the axial components. Neglecting this fact, coaxial loads with an exponential screen give good frequency characteristics.

A further improvement of the frequency characteristics of coaxial loads is achieved by making screens with a special profile whose detailed analysis is given in [115].

b) Capacitors

The basic requirement for capacitors used in high-voltage pulse devices is that they must have small inductance. It is also necessary that capacitors be of small size, since otherwise the connecting leads will introduce a large inductance into the discharge circuit.

To obtain pulses with a large current, one needs capacitors with high capacitance. Among high-voltage capacitors those with a paper-oil insulation have the highest capacitance. Their inductance has been calculated in [116, 117].

Capacitors with a paper-oil insulation consist of individual sections wound in reels and connected together into parallel groups

TABLE 4-3

Capacitor type	Inductance, nanohenrys
Air specimen:	
100 pF	10-20
1,000 pF	30-50
Air variable capacitance:	
Of small dimensions	5-20
Of medium dimensions	10-60
Ceramic disk:	
KDK-3	1-1.5
KDK-1, 2	2-4
Ceramic tube:	
KTK-1, 2	3-10
KTK-3, 4, 5	20-30
Press-covered with mica:	
KSO-1	4-6
KSO-11, 12, 13	15-25
Mica specimen, blocked	50-100
Paper:	
Of small dimensions KBG-4	6-11
Of medium dimensions KBG-M, KB	30-60
Of large dimensions (high capacitance)	50-100
Of high capacitance with an irregular location of leads	200 and more

to increase capacitance. The groups are connected in series to increase the operating voltage. The inductance of a capacitor increases as the number of sections in a group becomes larger, and it also increases as the number of groups becomes higher. Table 4-3 gives the values of inductances for capacitors of various types [119].

Ceramic two-plate capacitors possess small inductance. Among domestic ceramic capacitors of greatest interest are barrel-shaped and disk capacitors whose capacitance is relatively large and whose inductance is small.

Their characteristics are listed in Table 4-4.

Reference [118] gives a description of an installation for the study of exploding wires in which a water capacitor is used as an

TABLE 4-4

Parameter	KVI-3	K15U-1	K15-4	K15-5
Capacitance, pF	220-4,700	470-10,000	220-4,700	70-15,000
Operating voltage, kV	16-5	4.8-16	12-40	1.6-6.3
Height, mm	20-14	14-27	38-65	4-7
Diameter, mm ..	20-50	45-185	19-48	8-40
Weight, g	35-70	50-600	30-300	1.5-33

inductance-free reservoir unit. The capacitor is charged in a pulse mode. It is discharged through an exploding wire when the voltage on the capacitor reaches a required value.

4-5. Pulse Electric Resistance of Insulating Materials in the Nanosecond Range

The pulse electric resistance of insulation subject to high-voltage nanosecond pulses has not as yet been sufficiently investigated. However, even today there are several papers available which permit us to estimate for a given pulse width the value of the electric field at which the breakdown of the insulation occurs. It is very important to know this parameter when designing generators of high-voltage nanosecond pulses.

a) Electric resistance of gas gaps

It is known that the breakdown delay time t_3 consists of a statistical component σ, determined by the current of the cathode electrons initiating the breakdown, and the time of discharge formation, τ. The breakdown delay time t_3 has a statistical character, and it is described by the Laue formula according to which the number of breakdowns n_t with a delay time t_3 depends on time t as follows

$$n_t = n_{t=0} e^{\frac{-t-\tau}{\sigma}} \qquad (4\text{-}35)$$

where σ_0 is the mean statistical time of delay; n_0 is the total number of breakdowns.

Reter [121] has shown that in air gaps on the order of several centimeters wide and for overvoltages on the order of 10%, the discharge formation time τ is equal to the time it takes for an avalanche to develop to dimensions for which the avalanche becomes a streamer. A streamer grows much faster than an avalanche, and its time of rise may be neglected. The transition of the avalanche into the streamer occurs at the electron number $N_K \approx 10^8$. Therefore, we have

$$\tau \approx \frac{\ln N_K}{\alpha v}, \tag{4-36}$$

where α is the coefficient of shock ionization; v is the electron drift velocity.

Fletcher [112] attempted to invoke Reter's idea to explain the dependence $\tau(E)$ when the overvoltage on the gap was twice as large and higher. However, as was shown later [123], this attempt encountered a number of difficulties.

The purpose of this section is to consider questions related to the electric resistance of gas gaps during the breakdown with high overvoltage (double and higher). Such overvoltages on spark gaps can be achieved due to the short pulse front which sometimes is approximately $3 \cdot 10^{-10}$ sec [122, 123]. Due to the large magnitude of the electric field, new effects occur which are not important during breakdowns relatively low overvoltages. First of all, the development of a discharge is strongly affected by the effect of self-deceleration of electron avalanches which consists of the following. As the electron avalanche grows $N = \exp \alpha\chi$ (χ is the path length), so does the field of the ion volume charge which lowers the resultant field, reduces the coefficient of impact ionization α and slows down the growth of the number of electrons N and ions in the avalanche [121].

The radius of the avalanche is calculated on the basis of an analysis of diffusion processes, and equals [122] $r_l = (6Dt)^{1/2}$, where t is the time, D is the diffusion coefficient. If we assume that the positive ions are concentrated in a sphere of radius r_l, then the field of the avalanche ions is $E_l = eNr_l^{-2} = eNE(9U_T\chi)^{-1}$, where e is the electron charge; U_T is the thermal energy of electrons, eV; E is the externally applied field. If the equality $E_l = E$ is used as a criterion of self-deceleration, and χ is replaced by N/α, then the number of electrons in the avalanche at which the self-deceleration occurs can be written as:

$$eN_K \approx 9U_T \ln N_K e^{-1}. \qquad (4\text{-}37)$$

The expression on the right depends on the field E to a much lesser extent than α. Consequently, we can assume $N_K \approx \alpha^{-1}$, i.e., the greater the field E, the smaller is the number of electrons which is required to slow down the development of the electron avalanche. For example, if at the atmospheric pressure in air, a gap d is 1 cm wide, and the overvoltage of 10%, the value of N is $N \approx 10^8$ [121], then with an overvoltage of 100% this value decreases by more than one order of magnitude. Of course, the number of excited molecules and the number of ions in the avalanche is in this case reduced by the same numerical factor.

Another important effect involves a small value of the time of development of the electron avalanche up to the beginning of the self-deceleration. This time period is determined by the formula

$$\ln N_K/\alpha v,$$

where v is the electron drift velocity; N_K is the critical number of electrons. At the atmospheric pressure in air and $E \geq 100$ kV/cm, this time is less than $5 \cdot 10^{-10}$ sec. During that short time, only a small number of excited molecules will radiate photons, since the average time of photon emission by the excited molecules, τ_B, is several nanoseconds [121]. Since the number of photons, radiated by

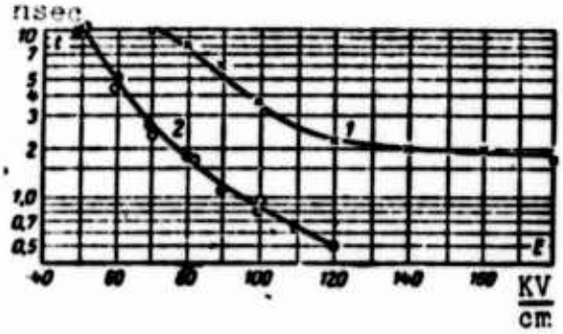

Figure 4-8. Time of discharge formation versus field intensity.

1 - breakdown initiation by single electrons [87];
2 - breakdown initiation by $N_0 \approx 10^4$ electrons.

the avalanche, is $N_f \sim N_K$, and the time of development of the avalanche up to a critical size is much less than τ_B, the number of photons is $N_f \sim \alpha^{-2} v^{-1}$.

Both of the above-mentioned effects slow down the emission of photons by the avalanche, and thus the emission of secondary electrons. This is because, in a breakdown with a large overvoltage, photons of the avalanche produce secondary electrons due to the photoelectric effect on the cathode or the ionization of gas in the gap. This results in a situation where, with single electrons initiating the breakdown, the breakdown delay time for the gap decreases with an increase in the field much more slowly than the time of the avalanche growth up to its critical size. Figure 4-8 (curve 1) gives the plot of the breakdown delay time $t_з$ versus the field E for an air gap 2 mm wide at the atmospheric pressure. The cathode is irradiated with ultraviolet rays simultaneously with the arrival of the pulse [124]. Since the current of the electrons, produced by the ultraviolet radiation incident on the cathode, is $\sim 10^{-10}$ A, the average time between an emission of two electrons turns out to be $\sim$1 nsec, and one may assume that the discharge is initiated by single electrons.

To reduce the breakdown delay time $t_з$, it is necessary to increase the number of the initial electrons that start the breakdown. In [122] the number of the initial electrons initiating the breakdown is approximately 10^4 according to [125]. In that case, the time $t_з$ turns out to be equal to the time for the development of an avalanche up to its critical size (Figure 4-8, curve 2). This is explained by the fact that the growth of current in the gap is due to an avalanche multiplication of electrons. Therefore, the time

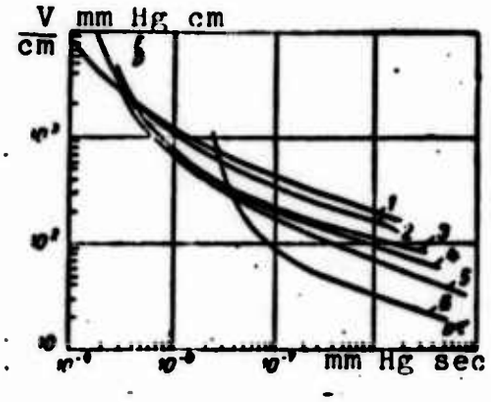

Figure 4-9. Dependence of pτ on E/p for various gases (1-6 are freon 12, elegas, nitrogen, air, argon, helium, respectively).

from the moment of the voltage pulse arrival to the time of breakdown, which is defined as coinciding with the beginning of a rapid current rise, is given by the expression [124]

$$\tau = \frac{1}{\omega_-} \ln \frac{i_K d}{e N_0 v_-}. \qquad (4\text{-}38)$$

where i_K is the minimum value of current, determined by the resolution of the oscilloscope; N_0 is the number of the initial electrons that start the breakdown; d is the gap width. The number of which the logarithm is taken usually varies from 10^7 to 10^8, which is close to the time of the development of an avalanche to its critical size, defined by Equation (4-26). Formula (4-38) implies that the dependence of τ on E can be written in a form which agrees with the law of similarity. In fact, since $\alpha/p = f_1(E/p)$, and $v_- = f_2(E/p)$, then $\tau p = F(E/p)$. This relationship has been confirmed for various gases (Figure 4-9) [138].

b) Electric resistance of vacuum gaps

Pulse electric resistance of vacuum gaps in the nanosecond range has been investigated only for gaps several millimeters in width [126, 127]. Characteristics of vacuum breakdowns were studied at the pressure of 10^{-8} mm Hg in a metal-glass chamber which was heated for 20 hours at a temperature of 420°C. Hemispherical electrodes made of copper, aluminum, lead, molybdenum, and graphite were used. The breakdown delay time depends only on the macro-intensity of the field E at the cathode (Figure 4-10), and does not depend on d.

The plot of $t_з(E)$ is given in Figure 4-10. It confirms the view that the breakdown of a vacuum gap is initiated by an explosion of the micropoints on the cathode due to the autoemission current.

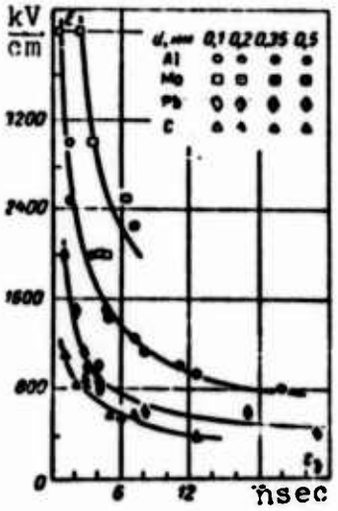

Figure 4-10. Plot of $E(t_3)$ in case of breakdown of vacuum gaps for various electrode materials.

The electric field at the micropoints may be increased hundreds of times and even more as compared with the macrofield E [128]. The appearance of flares on the cathode as a result of an application of a voltage pulse was observed in [129]. The flares would appear chaotically from one breakdown to another at various places on the cathode. They would cross the gap at a speed of approximately $2 \cdot 10^6$ cm/sec. In the process of crossing the gap, the current of the vacuum spark would be increasing. The ratio of the gap width to the time of current rise is close to the velocity of motion of the cathode flare. As shown in [130], the growth of a current in a vacuum gap is due to the stream of electrons from the front of the plasma. This current heats the anode and causes its erosion [131].

The strength of a vacuum gap is considerably reduced by introduction of a dielectric. Figure 4-11 gives the plot $E = f(t)$ in the case of a breakdown over a surface of empty cylinders made of forsterite ceramic measuring 8 mm in outer diameter and 6.8 mm in inner diameter [132]. The cylinders were placed in a vacuum in a uniform field. A detailed oscilloscope and electron-optical study of the development of a discharge over the surface of ceramics in a uniform field was carried out in [133]. The breakdown delay time consists of a statistical component and the time of discharge formation. The first component t_3 is determined by the time necessary for an appearance of an electron capable of initiating a discharge. During the formation time, a discharge develops over the surface of steatite ceramics with the speed $v = (1 - 7) \cdot 10^7$ cm/sec (field $E = (1 - 2) \cdot 10^5$ V/cm). The speed of the discharge development when the residual gas pressure is raised from 10^{-5} to 10^{-2} mm Hg ($E = 120$ kV/cm) increases from 2.2 to $4 \cdot 10^7$ cm/sec.

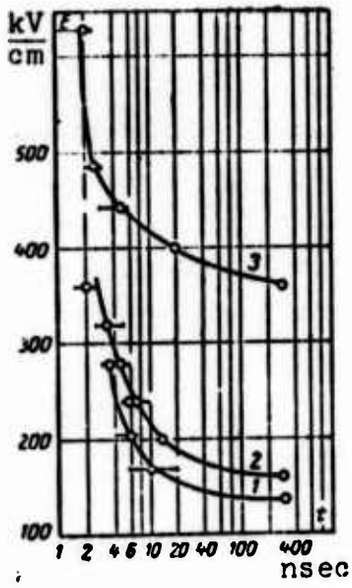

Figure 4-11. Plot of $E(t_з)$ for breakdowns on the surface of forsterite ceramics for gaps of various widths.
1 - d=2 mm; 2 - d=0.9 mm; 3 - d=0.3 mm.

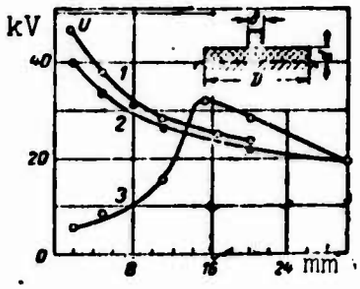

Figure 4-12. Plot of sparking voltage versus the electrode diameter δ with a nonuniform field, D = 11 mm, d = 2 mm.

1 - static voltage of sparking for a nonuniform field at the cathode; 2 and 3 - pulse voltage of sparking, respectively, for a nonuniform field at the cathode and anode.

Of course, the process of discharge development is much more complicated if the field in the cathode region is nonuniform [135]. In this case, there is a strong weakening of the pulse electric resistance. Figure 4-12 gives plots of the amplitude of a rectangular pulse with 1 nsec front and a width of 0.5 μsec for various electrode diameters producing a nonuniform field. The same figure gives an analogous plot for static breakdown voltage. When the diameter of a cathode with sharp edges is less than the diameter of the dielectric, the pulse electric resistance is lowered. This is due to the intensification of the tangential component of the field at the cathode due to the nonuniform distribution of the potential over the surface of the dielectric caused by the presence of surface and volume capacitances [135]. Just as in the case of a uniform field, the discharge is initiated by single electrons, and it propagates at a speed on the order of 10^7 cm/sec (assuming a nonuniform field at the cathode). This velocity increases with an increase in pressure of the residual gas and field intensity. The gas layer

absorbed at the surface of the dielectric [133, 135] plays an important role in the development of a discharge. To increase the pulse electric resistance, one must lower the number of gas molecules on the surface of the dielectric and reduce the electron current toward the surface flowing from the contact between the cathode and the dielectric. The latter can be accomplished by improving the contact between the cathode and the dielectric, for example, by lowering the cathode into the dielectric [136].

c) Electric resistance of liquid dielectrics

The electric resistance of liquid dielectrics in gaps $\delta < 1$ mm in the interaction of voltage pulses with a nonosecond front is 10^6-10^7 V/cm [137-139]. The breakdown delay time is on the order of 10^{-9}-10^{-8} sec. During a breakdown of pure and humidified transformer oil by a voltage pulse front (front width — 15 nsec), it was found that the electric resistance for gap widths of 50-250 microns was almost identical and approximately equal to $2 \cdot 10^6$ V/cm. The electric resistance of the two types of oil in a static breakdown of the same gaps differed by almost four times [139]. According to [137], distilled water had the electric resistance slightly higher than the transformer oil.

In [138] a study was made of the breakdown delay time for gaps 50, 100, 200, 500 microns in width in transformer oil, in distilled water (specific resistance $\sigma \approx 5 \cdot 10^{-6}$ ohm^{-1} · cm^{-1}), and in industrial water ($\sigma \approx 10^{-4}$ ohm^{-1} · cm^{-1}). Studies were made using a pulse generator of amplitudes up to 500 kV and a front of 2 nsec, and a time constant of the voltage drop at the pulse top of 10^{-7} sec. Hemispherical electrodes 2 mm in diameter were made of stainless steel, and the container with the liquid had a volume of 100 cm^2. After each three-fifths of breakdowns, the electrodes were polished, and the liquid was replaced. The relationship between the gap field intensity E and the breakdown delay time t_3 for industrial water and transformer oil is shown in Figure 4-13. The time t_3 was determined as an average of 5-20 measurements. The typical fluctuation of the discharge time is shown for the interelectrode distance of 500 microns.

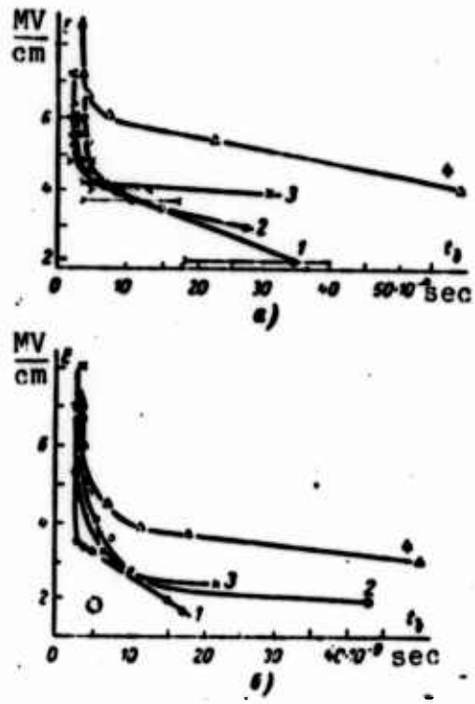

Figure 4-13. Plot of $E(t_3)$ for transformer oil (a) and industrial water (b).

1 - for gap width of 500 microns; 2 - for 200 microns; 3 - for 100 microns; 4 - for 50 microns.

The plots of $E(t_3)$ for distilled water are close to the plots for industrial water [138]. The time t_3 for $E > 6 \cdot 10^6$ V/cm becomes practically identical for all gaps. Figure 4-13 implies that, just as in [137], water and transformer oil have an identical high electric resistance in the nanosecond range.

A study of pulse breakdowns of 61 micron gaps in n-hexane for $E = 3.28 \cdot 10^6$ V/cm has shown [139] that there is a conditioning effect. What this means is that the maximum of the distribution curve for the breakdown delay time in the process of single breakdowns (during five hours of operation) is displaced from 6 to 16 nsec, and the width of the distribution curve increases from 9 to 21 nsec. Pulse ultraviolet irradiation of the gap did not result in stabilization of the time t_3. It was noticed that the value and stability of t_3, as well as the conditioning effect, were strongly affected by a constant auxiliary field in the gap. The magnitude and polarity of the auxiliary field in the range 16.5-82 kV/cm resulted in practically identical effects. Figure 4-14 gives plots of $E(t_3)$ for n-hexane in the presence of and without the auxiliary field.

It should be noted that there are very few papers available on the pulse electric resistance of liquid insulation in the nanosecond range. Thus far, not even a study of the effects of electrode polarity in a nonuniform field and the electrode material on the function $E(t_3)$ has as yet been made.

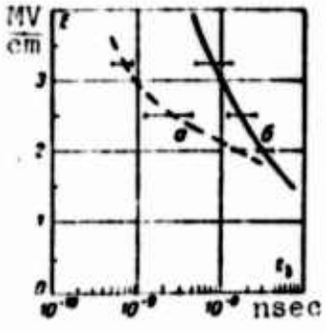

Figure 4-14. Plots of $E(t_3)$ for n-hexane (61 micron gap) in the presence of (a) and without (b) auxiliary constant field of 82 kV/cm.

d) Electric resistance of solid insulators

The problems of the mechanism involved in the breakdown of solid dielectrics (alkali-halide crystals) in the presence of rectangular pulses of nanosecond front were discussed in [140, 141]. We shall consider only those papers in which the relationship between the breakdown delay time and the field intensity for practical insulating materials is given.

The study [142] describes studies of electric resistance for a number of polar and certain nonpolar polymers in homogeneous and nonhomogeneous fields during an exposure of $3 \cdot 10^{-8}$ sec and less. The voltage pulse amplitude was up to 500 kV; front width was 3 nsec. During 30 nsec, the voltage at the top of the pulse was reduced by 7%. A study was made of the electric resistance of organic glass, polystyrene, polyethylene, polyvinylchloride, and Teflon-4. The thickness of specimens during breakdown in an inhomogeneous field was 1.5-3 mm. Breakdowns were accomplished using electrodes of the point-plane type. A needle with a radius of curvature of 65 microns was imbedded into a dielectric to a depth of 3 mm. A homogeneous field in the specimen was produced by using the electrodes of the sphere-plane types. A polished steel sphere 14 mm in diameter, imbedded in a heated state into the dielectric, served as a spherical electrode. The gap width was 0.5 mm. A copper foil, ground into the surface of the dielectric with the aid of vaseline oil, was used as a plane. The specimens were placed in transformer oil. The results were treated statistically according to the Laue technique.

The electric resistance of organic glass and polyvinylchloride in the field of the point-plane is much lower than the electric resistance of nonpolar polymers (Figure 4-15). In a homogeneous field

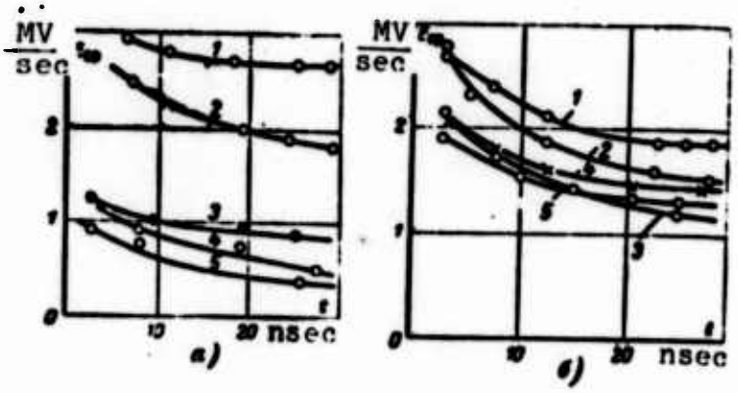

Figure 4-15. Dependence of mean breakdown voltage on the voltage application time for polysterene (1), polyethylene (2), organic glass (3), Teflon-4 (4), and polyvinylchloride (5). a - for negative polarity of the point; b - for positive polarity of the point.

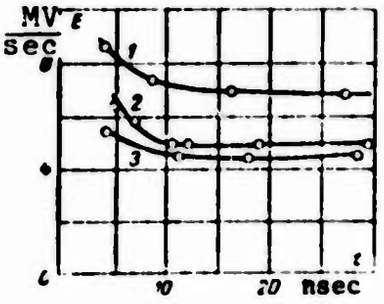

Figure 4-16. Dependence of electric resistance on the voltage pulse width for the sphere-plane electrodes.

1 - organic glass; 2 - polyvinylchloride; 3 - polystyrene.

the electric resistance of polar polymers is much higher than the electric resistance of nonpolar polymers (Figure 4-16).

In [143] a study was made of the relationship between the electric resistance and the voltage arrival time for polysterene, Teflon-4, organic glass, and muscovite mica with exposures of $5 \cdot 10^{-9}$-$3 \cdot 10^{-6}$ sec. The hemisphere-plane electrodes were deposited by evaporation of tin in a vacuum. Specimen thicknesses at the location of breakdowns are given in Table 4-5.

TABLE 4-5

Name of dielectric	Thickness, cm	Fluctuation, mV/cm
Organic glass	0.035	1.5
Polysterene	0.050	1.25
Teflon-4	0.080	0.92
Teflon-4 (film)	0.032	1.18
Polystyrene (film)	0.021	1.45

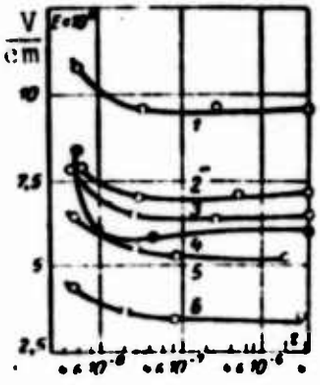

Figure 4-17. Dependence of electric resistance on voltage pulse width for polystyrene (film) (1), mica (2), Teflon-4 (film) (3), organic glass (4), polystyrene (5), Teflon-4 (6).

The same table gives the fluctuations in the electric resistance relative to the average value for a pulse of approximately $5 \cdot 10^{-9}$ sec.

Figure 4-17 shows volt-second characteristics for the dielectric specimens investigated. Figure 4-17 shows that film materials have a higher resistance than strip materials.

CHAPTER V

APPLICATIONS OF NANOSECOND PULSES OF HIGH VOLTAGE

5-1. Applications of High Voltage Nanosecond Pulses in Quantum Radiophysics

a) Semiconductor lasers with electron excitation.

The development of domestic high-voltage nanosecond technology was to a considerable extent stimulated by work done in the area of quantum radiophysics and accelerator technology. In 1961 N. G. Basov proposed the idea of building a semiconductor quantum generator with electron excitation. Successful realization of this idea in the following years depended on the development of nanosecond high voltage generators that would power strong-current injectors. Results of studies on semiconductor quantum generators with electron excitation are given in [144 - 148].

A semiconductor quantum generator with electron excitation consists of a single crystal semiconductor target, a source of electrons, and a generator of nanosecond high voltage pulses. The semiconductor target, which is the active element of the semiconductor quantum

generator, is excited by a beam of fast electrons. To achieve generation, the semiconductor target is the form of an optical resonator. An external mirror [148] can be used to improve the directivity of radiation.

Using the electron method of excitation of semiconductor lasers, it is possible to increase the volume of the active region as compared with the semiconductor laser on the p-n junction, which makes it possible to significantly increase the radiated power. In addition, it is possible to use as the working substance semiconductor materials with a forbidden zone width making it possible to generate radiation at a small wavelength (through vacuum ultraviolet). Using this method of excitation, it was possible to obtain generation from 7 to 0.3 microns [145].

The basic restriction on the power of the pulse is related to the crystal heating by the pulse, and is in practice determined by the heat capacity of the working substance. The maximum permissible density of a stream of accelerated electrons is approximately equal to 10^2 A/cm^2. The energy of the accelerated electrons is about 300 keV. A further increase of the electron energy is not advisable, since at large energies, radiation defects are produced in the semiconductor which increase the probability of nonradiative transitions. The maximum power of photons radiated by a semiconductor laser with electron excitation may be estimated, taking into account the efficiency achieved of 10 - 30% [145]. It amounts to tens of megawatts with a repetition frequency of hundreds of hertz. In building such lasers, one must use large-current sources of electrons and nanosecond high-voltage pulse generators.

The pulsed power for semiconductor quantum generators with electron excitation is usually supplied by generators of pulses having a width on the order of several tens of nsec, and voltages up to several hundred kilovolts. The power ranges from several to hundreds of megawatts and repetition frequency — from tens to hundreds of hertz.

At the P. N. Lebedev Physics Institute, several versions of nanosecond generators have been developed that satisfy the above requirements. For transforming pulses, these generators make use of various networks involving coaxial cables and thyratron commutators. The networks for the three versions of the nanosecond generators used for semiconductor quantum generators with electron excitation are described in Sections 2-3, 2-4, as well as in [70].

b) Gas lasers with pulsed power supplied by nanosecond generators.

At the present time there are quite numerous and diverse types of gas lasers. For this reason there is a wide range of requirements on systems supplying them with power. There is, however, a type of pulsed gas lasers whose efficiency is largely determined by the excitation rate. We have in mind the so-called lasers based on self-limiting transitions. In those lasers, generation is achieved using transitions whose lower level decays very slowly (it may, for example, be metastable). For this reason, an inversion of occupancy during such transitions occurs only in the transition process, and generation takes place at the leading front of the excitation pulse. It is not hard to show that the time during which an inversion exists, and consequently, the length of generation in such systems, is on the order of the lifetime of the upper operational level (in practice, the length of generation turns out to be slightly shorter). For transitions in the optical region of the spectrum, a typical lifetime of the operating level for the allowed transition is 10^{-9} - 10^{-7} seconds. In order that the excitation energy used in the discharge be efficiently utilized, the width of the excitation pulse must not be greater than the width of generation.

This type of laser is interesting, because it permits one to obtain a relatively large value of the peak power generator at substantial pulse repetition frequencies. The power may be generated in a very wide spectrum interval and may encompass the visible and ultraviolet regions.

At the present time, we have already a knowledge of many transitions in various atoms and molecules, for which pulse generation of the type indicated above is obtained. In particular, the largest peak generating power out of all gas lasers is obtained from transitions of nitrogen molecules in the ultraviolet region of the spectrum (λ = 3,371 Å). The power is about 2.3 kW [149]. Considerable peak power can also be obtained, using a different system of nitrogen molecule bands in the near infrared region of the spectrum [150]. In the visible region, the maximum peak power is obtained using the green line of neon λ = 5,400 Å; it amounts to 190 kW [149]. The laser type in question is also of great interest, because it is theoretically possible for it to obtain a high efficiency coefficient. At the present time, the efficiency of a majority of gas lasers is on the order of 10^{-3} and less, which is due to the use of high working levels and the difficulties involved in obtaining a large rate of depopulation for the lower working level. For lasers based on self-limited transitions, both of these difficulties are absent. For this reason, pulse generation can be achieved with high efficiency in principle. In particular, the maximum generation efficiency should apparently be achieved from the resonance to metastable levels: generation using these levels is possible only in the transition process. By now generation in such transitions has already been obtained in several atoms and ions [151 - 153]. Among them the greatest hope from the point of view of high efficiency is to use copper atoms [150] and thallium atoms [152]. The favorable structure of levels in these atoms permits us to hope for an efficiency on the order of 10%. A power of 40 kW was obtained with the average power of 0.5 W and efficiency of about 1% [154] in the corresponding transition of copper in the green region of the spectrum. The lifetime of the working level in thallium is approximately 7 nsec. For this reason, a large power and high efficiency generation for thallium can only be obtained using an excitation pulse 5 - 10 nsec wide.

Let us now consider the requirements on the power and amplitude of the voltage pulse used in gas lasers of the type considered above.

The basic process determining the operation of a great majority of lasers based on the self-limited transitions involves excitation of the working level by the electrons. Optimum conditions for inversion are achieved for the definite mean electron energy during discharge. The latter is given by the ratio E/p, where E is the electric field in the discharge plasma, and p is the pressure of the working gas. For a given size of the discharge cavity, $E/p \sim U/p$, where U is the voltage on the discharge cavity. In present lasers, the pressure of the working gas is usually 1 - 10 torr. With such pressures and usual dimensions of lasers, voltages amounting to several tens of kilovolts are required as a rule. To increase the power and energy of generation, the pressure of the working gas must be increased, which implies an increase in the working voltage. This may apparently be possible with nanosecond generators of high voltage, up to hundreds of kilovolts. In [151] it was shown that, when using a high voltage nanosecond generator, generation may be produced at pressures up to atmospheric pressure.

To increase the average power of radiation, it is desirable to raise the pulse repetition frequency. Since the deionization time of the plasma is 10^{-3} seconds, in principle it is possible to achieve pulse repetition frequencies on the order of one or several kilohertz. Sometimes it is of definite interest to adopt a mode of operation designed to obtain a relatively small peak power coupled with a high pulse repetition frequency [155].

Rectangular voltage pulses on the order of 10^{-7} seconds and less in width, front width of approximately 10^{-9} seconds, and amplitude of several tens of kilovolts are used to control the electro-optical Kerr valve in a network modulating the factor of the resonator in a solid-state laser. The light pulses obtained are 10^{-7} - 10^{-9} seconds in width, and their peak radiated power is up to 10^3 W [9, 156]. By using current pulses of amplitude 10^2 - 10^{-9} A and 10^{-8} - 10^{-9} seconds in width to power semiconductor lasers, it becomes possible to obtain a generated power of tens of watts with nanosecond light pulse width

even at room temperature. In obtaining such current pulses, current pulse generators are used which are based on spark gaps [157].

Summarizing the opportunities of applying high voltages nanosecond pulses in quantum radiophysics, we may state that prospects are opening up in this area. These are based on the applications of powerful nanosecond generators and are extremely interesting. They may result in a new impetus to the development of high voltage nanosecond technology in the near future.

5-2. Application of High Voltage and Super-High Voltage Nanosecond Pulses in Accelerator Technology

a) Production of powerful pulse electron currents.

Powerful pulse currents of accelerated electrons are finding application in studies of the effect of very short intensive flares on materials, in radiation chemistry pulse radiolysis, in laser power supply (see Section 5-1), in heating of plasmas, and in accelerating ions to a high energy.

Reference [158] describes a generator of pulses with an amplitude 50 - 500 kV, width 10 - 40 nsec, pulse repetition frequency from single pulses to 50 Hz, and a pulse front width of 3 nsec. The generator is used to obtain powerful pulse electron currents.

A resonance transformer with inductively coupled circuits (Tesla transformer) is used as a source of the charging voltage. A coaxial line $\mathcal{N}_4$ is used as a reservoir unit, and a cutoff discharge unit P_3 is used to control the pulse width (Figure 5-1).

The resonance transformer (see Section 1-3) consists of two inductively coupled LC circuits in which the natural frequencies are equal ($L_1C_1 = L_2C_2$)(Figures 1-10 and 5-1). If the capacitor C_1 (Figure 5-1) is charged, then after a discharge of the gap P_1 [91],

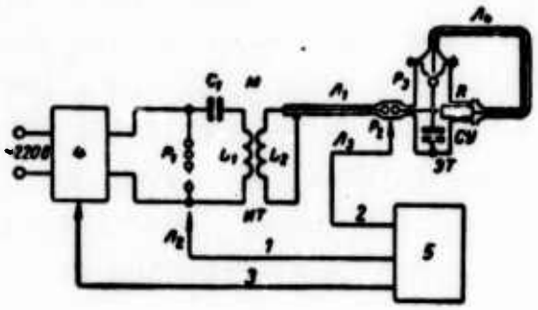

Figure 5-1. Schematic diagram of a generator. 1 - starting of the spark gap P_1; 2 - starting of the spark gap P_2; 3 - voltage regulation; 4 - charging unit; 5 - control panel.

oscillations are set up in the L_1C_1 circuit which are transmitted through the inductive coupling to the L_2C_2 circuit, and vice versa. The capacitance of the coaxial line $Л_1$ is used in the role of C_2. If one neglects transformer windings and takes the coupling coefficient to be k = 0.6, then the voltage on the line $Л_1$ will be in the form of beats. The beat maximum will be in the second half wave, and its value will amount to $U_{h2} = \sqrt{C_1/C_2}U_0$ (U_0 is the initial voltage over C_1). In a transformer actually built, C_1 = 0.23 microfarads, L_1 = 2 microhenrys, L_2 = 1,230 microhenrys, C_2 = 370 pF. The primary had 6 turns and the secondary 230 turns. The transformer was made in the form of two coaxial cylinders (outer one made of bakelite, inner one made of polyethylene). The secondary was wound on the inner cylinder and was made of nichrome wire with an ohmic resistance of 50 ohms. The secondary with the cylinder was placed in transformer oil. Nichrome wire was used to scatter extra energy and thus reduce the wear of the electrodes in the spark gap P_2.

When the required voltage maximum is reached in the line $Л_1$, the spark gap P_2 is triggered (Figure 5-1), due to which the line $Л_1$

is discharged, and a pulse with steep front enters the load in the form of an electron tube. A portion of the pulse through the resistance R = 240 ohms (selite rod [sic]) and a KPV cable of wave impedance 50 ohms is used to trigger the cutoff spark gap P_3. The reservoir line $Л_1$ is made of brass tubes, its wave impedance is 60 ohms and length 4.5 m. The switching gap P_2 is filled with nitrogen at a pressure of 15 at to reduce the switching time.

The cutoff spark gap P_3 clips the pulse by shunting off the load at a suitable time instant. The clipping is determined by the length of the cable $Л_1$ and the width of the discharge gap P_3. The discharge gap is made in the form of a trigatron, and is filled with nitrogen at a pressure of 10 at. The gap P_3 is attached to the matching unit (Figure 5-1) which is necessary to match the gap with the load. A 500 kV electron tube is built into the matching unit, and so is the isolation coil which supplies voltage to the cathode of the electron tube.

The multielectrode gap P_1 in the primary of the transformer contains 8 gaps and permits one to control the voltage between 3 and 30 kV without changing the gap width, and to commutate the maximum current of 15 kA at the switching frequency of 50 Hz.

Reference [28] describes an injector for an iron-free single-turn strong-current 400 MeV synchrotron. The injector produced an electron beam 12 nsec in width and 600 keV in energy. A diagram of the injector is given in Figure 5-2. A segment of line 1 with a wave impedance of 120 ohms is shorted at one end. The other open end contains a cathode unit and a heating filament, to which voltage is fed inside a central tube of the coaxial line. A coaxial line 2 with the wave impedance of 20 ohms is connected to the midpoint of line 1 through a gap P_0. Line 2 is charged by a Marx generator 3 through a resistor 4. Lines 1 and 2 are immersed in transformer oil. After generator 3 is actuated, line 2 is charged for $4 \cdot 10^{-7}$ seconds, which is followed by a breakdown of gap P_0 in the presence of an overvoltage,

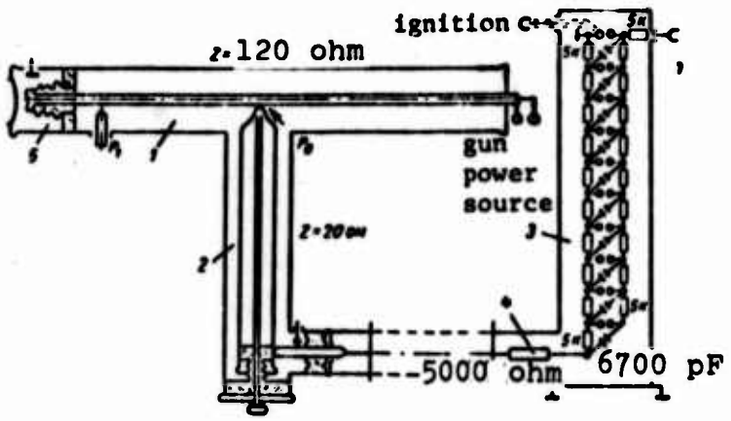

Figure 5-2. A diagram of an injector for a 400 MeV synchrotron.

and a pulse width a 1-2 nsec front goes to line 1. A voltage wave, travelling toward the open end of the line, doubles at the end and produces a rectangular voltage pulse on the cathode. The pulse width can be regulated with the gap width of P_1. The front of the injection pulse is approximately 2 nsec. The functioning of a synchrotron with this injector is described in [159].

Reference [68] describes the development of a pulse generator producing 10^{11} W pulses. The generator consists of a two-stage line with a 50 ohm output resistance which is charged by a Marx circuit through a voltage of $5 \cdot 10^6$ V. The generator was built to produce an electron current from a metallic point. The maximum electron energy was approximately 3 x 10^6 keV, and the current was $5 \cdot 10^4$ A. The pulse width did not exceed 30 nsec. Figure 5-3 shows a schematic diagram of an electron source. In the anode-cathode vacuum chamber, the pressure was $5 \cdot 10^{-5}$ mm Hg, and in the electron beam chamber the pressure could vary in the range 10^{-3} - 760 mm Hg. A large electron current from the point was obtained by producing a field intensity of

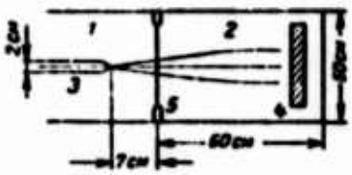

Figure 5-3. A diagram of an electron source.

1 - anode-cathode chamber;
2 - electron firing chamber;
3 - sharp point cathode;
4 - target;
5 - anode (thin foil).

no less than 10^8 V/cm at its end. The cross-section of the electron beam behind the anode was 10 cm^2. Reference [174] gives a description of a pulse electron accelerator designed for the energy of 12 MeV, current of 170 kA, and pulse width of 70 nsec. A two-stage shaping line was used as the reservoir element in the accelerator. The line was insulated with transformer oil. The switching gap was also placed in transformer oil. The reservoir line was charged by a Marx generator which contained 186 capacitor stages designed for 1 μF and 100 kV each. The total amount of energy stored in the capacitors of the voltage pulse generator was about 1 megajoule.

Accelerator tubes ∿ 2 m in size were made of lucite and epoxy resin. The voltage along the tubes was distributed by metallic rings. Tube sparking was observed at a voltage exceeding the level of the electric strength of the vacuum side of the tubes. The cathode was in the form of a metal rod or a system of rods with a hemispherical emitting surface. All the accelerator elements, including the voltage pulse generator, reservoir lines, and the electron tube, were placed in a tank filled with oil.

Reference [12] describes an electron accelerator designed for energies up to 2 MeV with a sharp-point cathode in which a Marx generator with gaps at a high gas pressure was used as a source of nanosecond voltage pulses. To obtain a voltage pulse of amplitude up to 2 MV, 160 stages were used. The generator pulse width was 50 nsec, and the current reached 10 kA.

Reference [48] describes the development of an electron direct action accelerator producing a current beam of 30 kA amplitude and a pulse 25 nsec in width. A sharp-point cathode was also used as a source of electrons. The voltage pulse was produced by a discharge of a coaxial line through a discharge unit. The coaxial line with the wave impedance of 40 ohms was charged to 3.6 MV by a constant voltage source in the form of the Van de Graaff generator. The chief advantage in having the reservoir line charged by a constant voltage source is the possibility of exact control of the pulse amplitude. This is very necessary, for example, when studying the autoelectron emission.

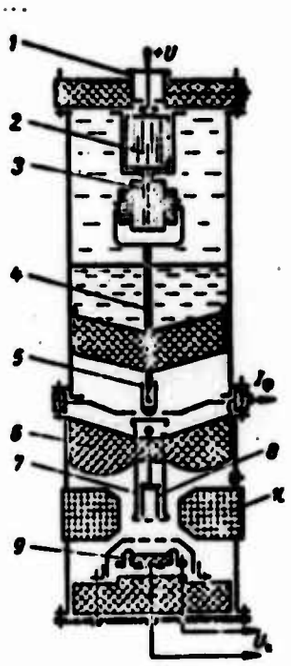

Figure 5-4. A diagram of the 300 kV electron accelerator with a plasma cathode.

1 - discharger; 2 - reservoir capacitance; 3 - pulse transformer; 4 - shaping lines; 5 - widening tube; 6 - insulator; 7 - high-voltage electrode; 8 - Faraday cylinder; 9 - cathode; 10 - focusing magnetic lens.

Figure 5-4 gives a diagram of an electron accelerator with a plasma cathode [161]. The accelerator has the following parameters: energy - 500 keV, current - 10 kA, pulse width - 30 nsec. In the accelerator (Figure 5-4) the shaping element is charged through a pulse transformer. The reservoir capacitance 2 with the aid of an air gap 1 is discharged into the primary of the high-voltage pulse transformer 3. The transformation ratio is equal to 30. The transformer was placed in a tube filled with transformer oil. The shaping element 4 is made in the form of a coaxial line filled with glycerine. The wave impedance of the line is 80 ohms. The leading and trailing fronts of the high-voltage pulse are formed with the aid of

peaking and clipping spark gaps. Both spark gaps are mounted in one chamber, and operate at an air pressure equal approximately to 10 at.

The cathode 9 of the accelerator tube consists of a ceramic plate of height ε, with a silver layer deposited on one side, and a metal net firmly pressed against the other. A pulse voltage $U_K \gtrsim 10$ kV from a special pulse generator is applied between the electrodes of the cathode. At the locations of the junctions between the net and the dielectric, discharges occur which propagate along the dielectric. The plasma in these discharges favors production of large electron currents by the cathode.

In the last version of this accelerator, the polarity of the charging voltage pulse was reversed, and the Faraday cylinder 8 was replaced by cathode 9 (Figure 5-4). Just as in all the other accelerators of this type, the anode was made out of a thin metal foil in order to direct the electron beam away. In a number of electron accelerators [12, 48, 68, 174], sharp-point metallic cathodes were used as electron sources. Reference [175] established the character of electron emission from such sharp points. It was shown that the emitting point always has micropoints with a much smaller radius than the main point. With a large electric field at the micropoints, they explode due to the rapid Joule heating by the electron autoemission current. If the electric field at the tungsten point reaches 10^8 V/cm, then the autoemission electron current is 10^{-9} A/cm^2, and the time necessary for the explosion does not exceed 10^9 seconds. After the points explode, a metal plasma is formed which propagates in all directions at a speed of approximately $2 \cdot 10^6$ cm/sec, just as in the case of a cathode flare during a vacuum discharge (see Section 4-5, b). As the plasma spreads forward, the cathode flare emits electrons. The radius of the surface emitting electrons increases at the same speed as the speed of propagation of the plasma. The electron current in the gap between the front of the plasma and the anode is determined by the Langmuir law. In [176] it was assumed that the emission of electrons into the plasma from the point is due to the autoemission of

electrons amplified by the electric field of the plasma. According to estimates, the magnitude of the field should be on the order of the Debye plasma field.

b) Control of electron beams in accelerators.

In accelerator technology, we are often faced with the problem of rapid control of charged particle beams in the accelerators. Control is achieved by producing a pulsed electric or magnetic field which displaces the particles in the desired direction during a time shorter than the time needed for a particle to move around its orbit once. A description of a pulse generator developed to control a 100 MeV electron beam is given in [29]. The generator forms single voltage pulses 10 nsec in width, 100 kV in amplitude, and a 1 nsec front.

Line $Л_1$ (Figure 5-5) is charged through resistance R_2 by the pulse generator (discharger P_1, capacitance C, resistance R_3). The width of the spark gap P_2 is selected such that its breakdown will occur after the reservoir line $Л_1$ is fully charged for 0.1 - 0.2 μsec after the breakdown of P_1. At the spark gap P_3, the wave branches off, and over line $Л_3$ it travels toward the load. It travels toward the gap P_3 by means of line $Л_4$. After the pulse is reflected from the end of the line $Л_4$ and the voltage on the electrodes of the gap P_3 is redistributed, the latter is actuated and clips the pulse off. If the wave impedance of the lines satisfies $\rho_3>\rho_2>\rho_1$, one can obtain a certain increase in the voltage amplitude.

Two coaxial lines $Л_4$, controlled by the gap P_3, are formed by coaxially located electrodes. The inner line, shorted at the end, is made of a section of RK-6 cable, and the outer one is formed by the cable sheath and a duraluminum tube. The wave impedance of both lines is 45 ohms. The nitrogen pressure in the gaps P_2 and P_3 is 20 at.

The gap of the spark gap P_3 is divided into two identical gaps by the middle electrode. The generator works with a load of 13 ohms.

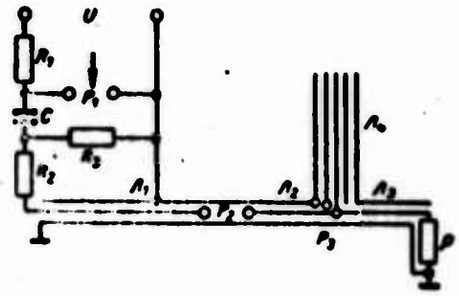

Figure 5-5. A diagram of a generator of 100 kV voltage pulses.

This type of circuit results in a series breakdown of the discharge unit gaps with an overvoltage, and the time fluctuation does not exceed 2 nsec.

5-3. Studies of Discharge Development in Dielectrics

When studying the processes involved in the development of discharges in gases, in a vacuum, and in solid dielectrics, it is customary to have high-voltage pulses 10^{-7} - 10^{-6} sec in width, with fronts on the order of 10^{-9} sec. The top of the pulse is strictly flat.

A pulse with a flat top can be obtained if a line of distributed parameters is used as a reservoir element. For the same length of the reservoir line, the pulse width will increase with an increase in the delay time, which is determined by the value of the linear parameters L_0 and C_0. An increase in the inductance L_0 is achieved by using a spiral winding. The capacitance C_0 can be increased by using a dielectric with a large dielectric constant ε.

In the generator (Figure 5-6), developed at the Nuclear Physics Scientific Research Institute affiliated with the Tomsk Polytechnical

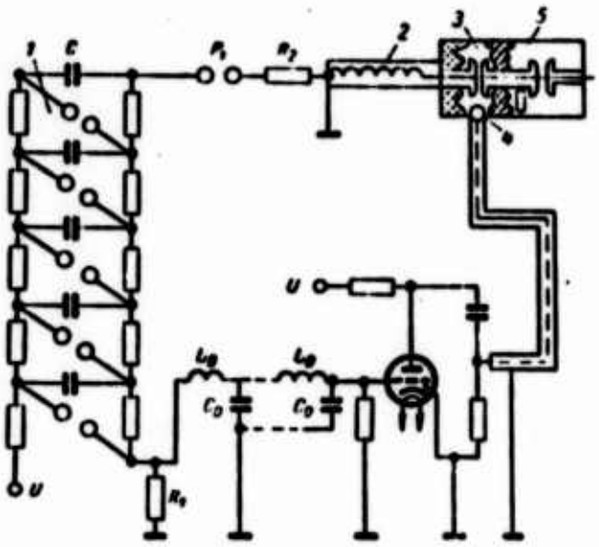

Figure 5-6. A diagram of a 500 kV pulse generator.

1 - Marx generator; 2 - spiral reservoir line; 3 - switching gap; 4 - keep-alive gap; 5 - chamber under study.

Institute [171], the reservoir line 2 was made of coaxial cylinders. The outer one was made of brass and organic glass. A spiral made of tnin brass foil was wound around the inner cylinder of organic glass. Glycerin with $\varepsilon = 40$ was used as the dielectric in the line. The line parameters were the following: line length - 1.5 m, outer cylinder diameter - 15 cm, high-voltage rodd diameter - 2.6 cm, spiral pitch - 1 cm, spiral width - 0.7 cm, wave impedance of the line - 75 ohms, delay - 100 nsec/m.

The reservoir line was charged by a Marx generator of 1 to 500 kV with five stages. After generator 1 was actuated, the spark gap P_1 was punctured, and the shaping line 2 was charged through resistance R_2. The current charging line 2 flowed through resistance R_1 from which L_0C_0 the signal proceeded through the delay line and triggered the thyratron. Resistance R_2 was chosen such that the time

needed to charge the shaping line to a maximum value would be 3 - 5 μsec. Commutator 3 was filled with nitrogen at a pressure of 10 at. By changing the gap width, it could be tuned in such a way that the breakdown between the commutator electrodes would be caused by the breakdown of the initiating gap 4. The delay line was chosen in such a way that the thyratron was actuated after 5.7 μsec from the breakdown of gap P_1. The actuation of the thyratron and gap 4, respectively, is followed by the breakdown between the electrodes of commutator 3. By that time, the reservoir line had already been charged to its amplitude value.

In the design under consideration, the chamber for the study of dielectric breakdown was built as one unit with the commutator. The pulse amplitude was 500 kV; front width was 1.5 nsec. The amplitude at the top of the pulse decreases according to a time constant approximately equal to 10^{-3} sec. Experimental data on the electric strength of various insulators in the presence of high-voltage nanosecond pulses are given in Section 4-5.

5-4. Use of Pulses to Power Spark Chambers

Spark chambers are used in high-energy physics as track detectors. There are several versions of spark chambers in existence. From the point of view of the characteristic features of high-voltage power supplies and the character of the particle tracks, they can be subdivided into three basic types: 1) spark chambers with small inter-electrode gaps of about 1 cm (ordinary spark chambers); 2) spark chambers with large inter-electrode gaps from several to tens of centimeters (tracking spark chambers); 3) streamer chambers.

Neon is most often used to fill chambers, which means that free electrons remain the wake of a particle. We shall dwell in more detail upon questions related to the high-voltage power supply, and the principles of operation of spark chambers of the second and third type.

In track spark chambers with a large inter-electrode gap, the discharge preserves the direction of the particle track up to angles of 50 - 60° C relative to the direction of the electric field. Voltage pulses of hundred of kilovolts are needed to supply them with power. In a majority of experiments, the Marx generators are used for that purpose. These generators, as they are usually constructed, make it possible to obtain pulses whose leading edge is 20 - 30 nsec in width [162]. In [52, 53] it was proposed that, in order to reduce the pulse front width, one should use inductance-free capacitors filled with glycerin or water that would shunt off the shock capacitance of the generator. In normal generators, built according to the Marx design, this makes it possible to obtain front widths equal to several nanoseconds (for more details see Section 2-2). The spark in the chamber is formed after the individual streamers which developed from electrons along the track of the particle, merge together after the application of the field, and form a continuous plasma string coinciding with the direction of the track. For this reason, the spark channel is slightly shifted relative to the true trajectory of the particle and is 0.3 - 0.5 cm [163, 164]. The steeper the leading edge of the pulse, the less the shift, and the higher the accuracy with which the coordinates of the track are determined. An important characteristic of track spark chambers is the value of the maximum angle between the direction of the particle track and the electric field in the chamber at which the spark still maintains the direction of the track. The value of this angle determines the spatial isotropicity of the chamber. In the initial spark chamber of Fukui and Mijamoto [160], a 100% coincidence of the spark and the particle track was observed up to an angle of 15°. In [165], by shortening the front of the high-voltage pulse and reducing the inter-electrode capacitance of the chamber, it was possible to increase the angle up to which the spark followed the particle track up to 30° (with a 100% effectiveness).

Finally, in [166] the angle was 45%. In this study, a specially built generator (see Section 2-2) was used which made it possible to obtain pulses with a 2 nsec leading edge and 500 kV amplitude. The

curvature of the trailing edge and the stability of the pulse width are of no special importance for the operation of track spark chambers. However, in special experiments — for example, in measuring the ionizing ability of particles from the brightness of sparks in the chamber — as was done in [167], the requirements on the stability of pulse width may be high.

In streamer chambers, a mode of operation is achieved such that the development of the spark discharge is stopped in the streamer stage by limiting the width of the high-voltage pulse fed to the chamber. The direction of particles in it is approximately parallel to the electrodes. Tracks in such chambers have the shape of a chain of light points or short lines. The accuracy with which the coordinates are determined depends on the size of the streamers, and the feasibility of track recording on photographic film depends on their brightness. Streamer chambers are most sensitive to forms of high-voltage pulses. In the first few papers [168, 169], chambers were powered by a Marx multiplier network. Two-electrode air clipping gaps were used to regulate pulse widths. As indicated above, Marx networks of usual construction do not permit one to obtain pulses with steep fronts, and two-electrode air clipping gaps do not produce pulses of high width stability. A flat leading front of the pulse does not permit one to produce a field in the chamber of sufficiently high intensity, so that small, but sufficiently bright, streamers could be obtained (field intensity was 10 - 14 kV/cm). Instability in pulse width made it impossible to obtain tracks of identical width and brightness in the chamber from one case to another. In [170] a streamer chamber was supplied with power by the nanosecond pulse generator described in Section 2-2, so that tracks of sufficient brightness were obtained with approximately identical streamer dimensions (2 - 3 mm) both along and across the field. It was shown that for stable operation of a streamer chamber with the field intensity of 25 kV/cm, pulses with a width stability no worse than $\pm$1 nsec are needed (total pulse width was 13 nsec).

Figure 5-7 shows a diagram of a high-voltage nanosecond generator with a streamer chamber [40].

The generator is in the form of a stage strip shaping line which is charged by pulses from the Marx generator (RLC). When the maximum value of the charging voltage is obtained, the gap P is actuated, and a rectangular voltage pulse is formed in the line. Its amplitude is equal to the charging voltage,and the width is equal to twice the time needed for a wave to travel along the line (see Section 2-6). The pulse thus formed propagates along the transmission line with a wave impedance of 2ρ, the composite part of which is a streamer chamber with matching resistances R = 2ρ connected to it. To exclude the occurrence of a pulse voltage on the chamber during the line charging, a bridge network is used to charge the line capacitances C_1 through inductance L_3 (Figure 5-7, b).

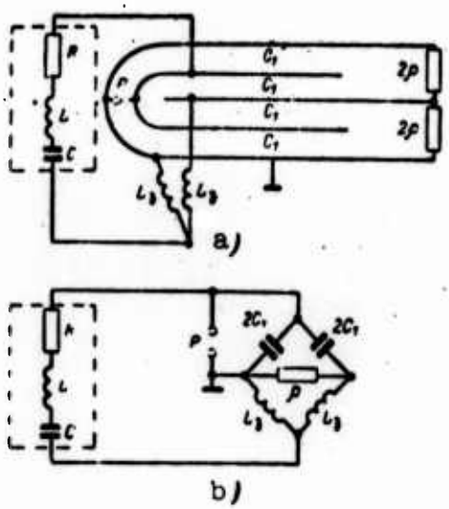

Figure 5-7. High-voltage nanosecond generator with a streamer chamber.

a - generator diagram;
b - pulse charging diagram.

With the help of this generator, a pulse 10 nsec in width, a front of approximately 3 nsec, and an amplitude of about 800 kV was obtained at the streamer chamber. Castor oil was used as an insulator in the shaping line. In order to reduce the front width, a gap was used filled with nitrogen at a pressure of 20 at.

REFERENCES

1. Воробьев Г. А., Месяц Г. А., Техника формирования высоковольтных наносекундных импульсов, Госатомиздат, 1963.
2. Моругин Л. А., Глебович Г. В., Наносекундная импульсная техника, изд-во «Советское радио», 1964.
3. Месяц Г. А. Высоковольтное испытательное оборудование и измерения, сборник, под ред. А. А. Воробьева, Госэнергоиздат, 1960.
4. Цихоки Я. С., Импульсные устройства, изд-во «Советское радио», 1959.
5. Биндер Л., Блуждающие волны в электрических сетях, ОНТИ, 1935.
6. Льюис И., Уэлс Ф., Миллимикросекундная импульсная техника, Изд. иностранной литературы, 1956.
7. Насибов А. С., Импульсный трансформатор с обмотками из коаксиального кабеля, «Электричество», 1965, № 2.
8. Насибов А. С., Кабельный трансформатор для формирования высоковольтных наносекундных импульсов, Препринт № 50, ФИАН, 1967.
9. Басов Н. Г., Амбарцумян Р. В., Зуев В. С., Крюков П. Г., Стойлов Ю. Ю., Оптический квантовый генератор с импульсным включением добротности, ЖЭТФ, т. 47, 1964, № 10, с. 1595.
10. Дружинин В. В., Магнитные свойства электротехнической стали, Госэнергоиздат, 1962.
11. Говорков В. А., Электрические и магнитные поля, Госэнергоиздат, 1960.
12. Charbonnier F. M., Barbour I. P., Brenegier I. L., Dyke W. P., Groundhauger F. I., Intense nanosecond electron beams, IEEE Trans. Nucl. Science v. NS-14, № 3, p. 789, 1967.
13. Recser G. A., New magnetic materials behave at nanosecond pulse widths, Electronics, v. 34, 1961, № 36, p. 72—75.
14. Мейнке Х., Гундлах Ф., Радиотехнический справочник, Госэнергоиздат, 1960.
15. Рабкин Л. И., Высокочастотные ферромагнетики, Физматгиз, 1960.
16. Рабкин Л. И., Эпштейн Б. Ш., Металлические ферромагнетики в аппаратуре связи, Связьиздат, 1955.
17. Евтеев В. И., Ферриты, «Электричество», 1956, № 9.
18. Lewis I. A. D., Some transmission line devices for use with millimicrosecond pulses, Electr. Eng., 1955, № 27, p. 332.
19. Павловский А. И., Склизков Г. В., Получение прямоугольных импульсов высокого напряжения, ПТЭ, 1962, № 2, с. 82.
20. Насибов А. С., Ломакин В. Л., Багранов В. Г., Генератор высоковольтных импульсов малой длительности, ПТЭ, 1965, № 5, с. 133—136.
21. Воробьев П. А., Кремнев В. В., Генератор высоковольтных наносекундных импульсов, Передовой научно-технический и производственный опыт, № 18-65-1637/95, ГОСИНТИ.
22. Кремнев В. В., Месяц Г. А., Анализ импульсного трансформатора на отрезках коаксиальных линий, Известия вузов, «Радиотехника», 1964, № 6, с. 713—722.
23. Месяц Г. А., Кремнев В. В., Теоретическое и экспериментальное исследование импульсного трансформатора на отрезках коаксиальных линий, Труды Томского института радиоэлектроники и электронной техники, т. 2, 1964, с. 54—61.
24. Агрест М. М., Насибов А. С., Чачибая Ц. Ш., Искажение вершины трансформируемого импульса импульсным трансформатором на коаксиальных кабелях, «Электричество», 1967, № 1.
25. Schering H., Raske W., Der Erzeuger des Stoss spanung mit steil stirn 500 kv, ETZ, A-1, c. 87, 7-14, 1936.
26. Fletcher R. C., Production and measurement of ultrahigh speed impulses, Rev. Scient. Instr., v. 20, 1949, № 12, p. 861.
27. Стекольников И. С., Импульсная осциллография и ее применение, Изд-во АН СССР, 1948.
28. Будкер Г. И., Коньков Н. Г. и др., Сильноточные ускорители с однооборотным захватом инжектируемых электронов, Международная конференция по ускорителям, Дубна, 1963.

29. Бродзодинский Б. Г., Бондаренко Л. Н., Приходько В. П., Мостовой Ю. А. и др. Генератор одиночных наносекундных импульсов высокого напряжения, ПТЭ, 1963, № 2, с. 75.

30. Кремнев В. В., Исследование некоторых схем умножения и коррекции высоковольтных наносекундных импульсов, Кандидатская диссертация, Томский политехнический институт, 1965.

31. Heise W., Tesla-transformatoren, ETZ, A-1, 7-14, 1964.

32. Heise W., Tesla-Transformatoren fur hohe Spannungen, VEG Mitteilung, Bd 52, 1962, № 7—8, S. 354.

33. Finkelstein D., Goldberg Ph., Shuchatovitz J., High voltage impulse system, Rev. Scient. Inst., 1966, v. 37, № 2, p. 159—162 (русск. пер. Приборы для научных исследований, 1966, № 2, с. 15—18).

34. Абрамин Е. А., Вассерман С. Б., Сильноточный импульсный ускоритель электронов, «Атомная энергия», 1967, т. 23, вып. 1, с. 44.

35. Воробьев Г. А., Руденко Н. С., Багин В. В., Цветков В. П., Генератор наносекундных импульсов напряжения с амплитудой 1 Мв, ПТЭ, 1968, № 1, с. 126—127.

36. Литвиненко О. Н., Сошников В. Н., Теория неоднородных линий и их применение в радиотехнике, изд-во «Советское радио», 1964.

37. Ковальчук Б. М., Кремнев В. В., Месяц Г. А., Коррекция характеристики искрового коммутатора неоднородной формирующей линией, ПТЭ, 1966, № 6, с. 119—121.

38. Шестеркин Ю. Е., Солоухин Р. Н., Методы скоростных измерений в газодинамике и физике плазмы, изд-во «Наука», 1967.

39. Белоусов Ю. С., Экспериментальное исследование синусного трансформатора импульсов наносекундной длительности, Известия вузов, «Радиотехника», 1962, т. 5, № 1, с. 58.

40. Bulos F., Odian A., Ville F., Sjount D., Streamer chamber development, Technical Report Repared under Contract AT(01—3)—515 for the USAEC San Francisco Operation, June 1967.

41. Смирнов С. М., Терентьев П. В., Генераторы импульсов высокого напряжения, изд-во «Энергия», 1964.

42. Rompe R., Weizel W., Uber das Toeplersche Funkengesetz, Zs. für Phys., Bd 122, 1944, № 636.

43. Месяц Г. А., Коршунов Г. С., Закономерности образования искры в наносекундном диапазоне времени при статическом пробое промежутка, ЖТФ, т. 38, 1968, № 4, с. 646—655.

44. Месяц Г. А., Анализ параметров высоковольтного импульса с крутым фронтом в схеме с формирующей емкостью и искровым разрядником, Труды Томского института радиоэлектроники и электронной техники, 1964, вып. 2, стр. 46—53.

45. Goodman D. H., Sloan D. H., Trau E. A., High voltage high speed square wave surge generator, Rev. Scient. Instr., v. 23, № 12, p. 766, 1952.

46. Broadbent T. E., New high-volfage multi-stage impulse generator circuit, Journ. Scient. Instr., v. 37, 1960, № 7, p. 231—236

47. Smith W. A., An improvement to the multi-stage impulse generator, Journ. Scient. Instrum., v. 35, 1958, № 12, p. 474.

48. Graubill S. E., Nablo S. V., The generation and diagnoses of pulsed relativistic electron beams above 10^{11} watts, IEEE Trans. Nucl. Sci., v. NS-14, 1967, № 3, p. 782—788.

49. Gygi E., Schneider F., A nanosecond pulse generator of 200 kV amplitude, Scient., Rept CERN, 1964, AR 64, 46.

50. Голутвин И. А., Заневский Ю. В., Кирюшин Ю. Т., Устинов В. Н., Генераторы для стримерных камер, ПТЭ, 1967, № 3, с. 74—76.

51. Keller L. P., Walschon E. G., Simple marx high voltage pulse generator for wide gap spark chambers, Rev. Scient. Instrum., v. 37, 1966, p. 1258—1259 (русск. пер. Приборы для научных исследований, 1966, № 9, стр. 151—153).

52. Месяц Г. А., Генератор импульсных напряжений, Авторское свидетельство № 150616, Бюллетень изобретений, 1963, № 16.

53. Месяц Г. А., Кремнев В. В., Увеличение крутизны фронта высоковольтного импульса, получаемого от генератора импульсных напряжений, Изв. АН СССР, ОТН, «Энергетика и транспорт», 1963, № 2, с. 199—204.

54. Воробьев Г. А., Месяц Г. А., Руденко Н. С. Смирнов В. А., Генератор импульсов с амплитудой 150 кв и крутым фронтом, ПТЭ, 1963, № 6, с. 93—94.

55. Месяц Г. А., Генератор импульсных напряжений, Авторское свидетельство № 178854, Бюллетень изобретений, 1966, № 4.

56. Воробьев Г. А., Руденко Н. С., Генератор наносекундных импульсов напряжения 500 кв, ПТЭ, 1965, № 1, с. 109—111.

57. Ковальчук Б. М., Кремнев В. В., Месяц Г. А. Лавинный разряд в газе и генерирование нано- и субнаносекундных импульсов большого тока, ДАН, 1970, т. 191, № 1, с. 76—78.

58. Дульзон А. А., Месяц Г. А., Фурсей Г. Н., Измерение автоэмиссионным диодом малых изменений напряжения на вершине импульса, ПТЭ, 1969, № 6, с. 105—107.

59. Чиковани Г. Е., Ройтинштейн В. Н., Михайлов В. А., Джапаридзе А. К., Трековая искровая камера с многократными свойствами — прибор для изучения высокоэнергетичных ядерных взаимодействий, XII международная конференция по физике высоких энергий, Сборник докладов, т. 2, с. 326—331, Госатомиздат, 1966.

60. Теумин И. И., Экспериментальный анализ переходных процессов в линейных электрических цепях, изд-во «Советское радио», 1956.

61. Глебович Г. В., Искажение наносекундных импульсов при прохождении по коаксиальному кабелю, «Радиотехника», т. 18, 1963, № 10, с. 54—62.

62. Гельцель М. Ю., Панфилов А. Д., Соболев С. С., Юдин Л. Н., Характеристики водородных тиратронов, ПТЭ, 1965, № 2, с. 121.

63. Насибов А. С., Ломакин В. Л., Баграмов В. Г., Авторское свидетельство № 168754, Бюллетень изобретений, 1965, № 5.

64. Насибов А. С., Коррекция фронта высоковольтных наносекундных импульсов, Препринт № 19, ФИАН, 1968.

65. Насибов А. С., Ломакин В. Л., Генератор коротких высоковольтных импульсов, ПТЭ, 1965, № 1, с. 123—126.

66. Месяц Г. А., Методы умножения импульсного напряжения с крутым фронтом, ПТЭ, 1963, № 6, с. 95—97.

67. Blumlein A. D., Patent USA № 589127, 1941 (двухступенчатая линия).

68. Link W. I., Electron beams from 10^{11}—10^{12} watts pulsed accelerators, IEEE Trans. Nucl. Science 1967, NS 14, № 3, p. 777.

69. Fitch R. A., Howell V. T. S., Novel princple of transient high-voltage generation, Proc. IEE, 1964, v. 111, № 4, p. 849—855.

70. Насибов А. С., Генератор высоковольтных наносекундных импульсов, Препринт № 27, ФИАН, 1968.

71. Геллер Б., Веверка А., Волновые процессы в электрических машинах, Госэнергоиздат, 1960.

72. Говард П. Р., Точные электрические измерения, Госэнергоиздат, 1959.

73. Greed F. C., Collins M. M. C., The measurement of short duration impulse votages, IEEE Trans. Commun. and Electr. 1963, № 69, p. 621—630 (русск. пер., Экспресс-информация, серия «Электрические станции, сети и системы», 1964, № 14, с. 53).

74. Arribe H., Gari Cl., La mesure des phenoménes transitoiren technique des hautes tensions, Bull. Soc. trans. electricients. v. 2, 1961, № 21, p. 494—512.

75. Miller C. J., Wittibschlager J. F., Measurements of steep-front impulse waves with a isolated screen room installation. Commun. and Electr., 1958, № 37, p. 262—270.

76. Месяц Г. А., Делитель для регистрации высоковольтных наносекундных импульсов, Известия Томского политехнического института, 1962, № 122, стр. 143—149.

77. Hergenrother R. C., Rudenberg H. G., A direct-reading oscilloscope for 100 kV pulses, Proc. IRE, 1953, № 41, p. 896

78. Wunsch D. C., Erteza A., Kerr cell measuring system for high voltage pulses, Rev. Scient. Instrum., v. 35, 1964, № 7, p. 816—820 (русск. пер. Приборы для научных исследований, № 7, 1964).

79. Ettinger S. Y., Venezia A. C., High voltage pulse measuring system based on Kerr effect, Rev Scient. Instrum., v. 34, 1963, № 3, p. 221—224, (русск. пер. Приборы для научных исследований, № 3, 1963).

80. Zarem A. M., Marchall R. S., Roole F. L., An electric optical shutter for photography, Amer. Inst. Electrical engineering, 1949, № 68, p. 283.

81. Елинсон М. И., Васильев Г. Ф., Автоэлектронная эмиссия, Физматгиз, 1958

82. Волин М. Л., Паразитные связи и наводки, изд-во «Советское радио», 1965.

83. Белорусцев Н. И., Гроднев И. И., Радиочастотные кабели, Госэнергоиздат, 1959.

84. Каляцкий И. И., Дульзон А. А., Желучников Б. П., Искажение высоковольтных униполярных импульсов в коаксиальном кабеле, Известия Сибирского отделения АН СССР, ОТН, т. 10, 1965, № 3, р. 151—154.

85. Литвиненко О. Н., Сошников В. Н., Расчет формирующих линий, Гостехиздат, УССР, Киев, 1962.

86. Жекулин Л. А., Распространение электромагнитных сигналов по коаксиальному кабелю, Известия АН СССР, ОТН, 1941, № 3, стр. 11—24.

87. Таблицы вероятностных функций, т. 1, Вычислительный центр, АН СССР, 1958.

88. Глебович Г. В., Переходные характеристики коаксиальных кабелей с учетом потерь в проводниках и диэлектрике, «Электросвязь», 1961, № 5.

89. Солодовников В. В., Топчиев Ю. И., Крутикова Г. В., Частотный метод построения переходных процессов с приложением таблиц и номограмм, Гостехиздат, 1955.

90. Глебович Г. В., Переходные процессы в однородных линиях передачи импульсов, Труды Горьковского политехнического института, т. 20, 1964, № 2, с. 516.

91. Ковальчук Б. М., Месяц Г. А., Потапицын Ю. Ф. Искровой разрядник для точного включения конденсаторов в мощных конденсаторных батареях, ПТЭ, 1968, № 4, с. 161.

92. Клейн Р. З., Королев В. С., Торбин Н. М., Исследование электрической прочности кабеля с полиэтиленовой изоляцией на импульсном напряжении, Известия Томского политехнического института, т. 149, 1966.

93. Делекторский Г. П., Закономерности пробоя высоковольтных кабелей с полиэтиленовой изоляцией при передаче импульсов напряжения, «Вестник электропромышленности», 1963, № 1

94. Делекторский Г. П., О некоторых закономерностях пробоя полиэтиленовой изоляции, «Электричество», 1961, № 11.

95. Howard P., The effect of electric stress on the life of cables incorporating a polyethylene dielectric, Proc. IEE, v. 98, 1951.

96. Impulse cables for plasma physics, Electrical Review, v. 172, 1956, № 14, p. 555—557.

97. Дульзон А. А., Каляцкий И. И., Чепиков А. Т., Расчет затухания и искажения высоковольтных униполярных импульсов в коаксиальной линии на ЭЦВМ «Минск-1», Известия Томского политехнического института, т. 159, 1968.

98. Бибергаль Л. А., Шаги Э. А., Соломоник С. С., Кабели и провода для электронной аппаратуры, изд-во «Энергия», 1964.

99. Сканави Г. И., Физика диэлектриков, часть II, Физматгиз, 1958.

100. Месяц Г. А., Воробьев П. А., Бычков Ю. И., О применении газовых микрозазоров в высоковольтных наносекундных импульсных устройствах, «Радиотехника и электроника», т. 10, 1965, № 4, с. 780.

101. Воробьев П. А., Месяц Г. А., Потапицын Ю. Ф., Новый мощный управляемый наносекундный коммутатор, ЖТФ, т. 36, 1966, № 8, с. 914.

102. Месяц Г. А., Исследование по генерированию наносекундных импульсов большой мощности. Докторская диссертация. Томский политехнический институт, 1966.

103. Коршунов Г. С., О процессе образования искры при статическом пробое азота и аргона в наносекундном диапазоне времени, Известия вузов, «Физика», 1967, № 3.

104. Воробьев Г. А., Устройство для получения импульсов с коротким фронтом, Авторское свидетельство № 120876, Бюлл. изобр. № 13, 1959.

105. Theophanis G. A., Millimicrosecond triggering of high voltage spark gaps, Rev. Scient. Instrum., v. 31, 1960, № 4, p. 427.

106. Lavoie L., Parker S., Rey C., Schwartz D. M., Spark chamber pulsing system, Rev. Scient. Instrum., v. 35, 1964, № 11, p. 567.

107. Насибов А. С., Генераторы мощных коротких высоковольтных импульсов, Кандидатская диссертация, ФИАН, М., 1966

108. Городинский Г. М., Даманский Е. А. и др., Разрядник для искровой камеры, управляемый импульсом малой амплитуды, ПТЭ, 1967, № 2, с. 68.

109. Godlove T. F. Nanosecond triggering of air gaps with intense ultraviolet light, Journ Appl. Phys., v. 32, 1961, № 8, p. 191.

110. Pendleton W. K., Guenther A. H., Investigation of a laser triggered spark gap. Rev. Scient. Instrum., v. 36, 1965, № 11, p. 1545—1550.

111. Бриш А. А., Дмитриев А. Б. и др., Вакуумные искровые реле, ПТЭ, 1968, № 5, с. 53.

112. Месяц Г. А., Коршунов Г. С., Трехэлектродный искровой разрядник, запускаемый с наносекундной точностью, ПТЭ, 1963, № 4, с. 123.

113. Martin J. C. Английский патент № 988777, 14.4.1965. Make Switch for Fast Electrical Discharge.

114. Гальперин Б. С., Непроволочные сопротивления, Госэнергоиздат, 1958.

115. Слуцкая В. В., Тонкие пленки в технике сверхвысоких частот, Госэнергоиздат, 1962.

116. Дашук П. Н., Расчет эквивалентных параметров высоковольтных конденсаторов, Известия вузов, «Энергетика», 1961, № 3

117. Кучинский Г. С., Иркаева К. М., Индуктивность конденсаторов с рулонными секциями, Вестник электропромышленности, 1961, № 11, с. 38.

118. Взрывающиеся проволочки, Пер. с английского под ред. Рухадзе А. А., Изд-во иностранной литературы, 1963.

119. Репне В. Т., Электрические конденсаторы, Госэнергоиздат, М., 1959.

120. Кукель Дж., Уильямс Е., Спираль с экспоненциальным шагом как трансформатор импульсов длительностью порядка миллимикросекунд, «Вопросы радиолокационной техники», т. 5, 1954, № 23, с. 51.

121. Ретер Г., Электронные лавины и пробой в газах, перевод с английского под ред. Комелькова В. С., изд-во «Мир», 1968.

122. Fletcher R. C., Impulse breakdown in the 10^{-9} sec. range of air at atmospheric pressure, Phys. Rev., v. 76, 1949, № 10, p. 1501—1511.

123. Месяц Г. А., Бычков Ю. И., Статистическое исследование запаздывания пробоя коротких газовых промежутков в сверхвысоких электрических полях в наносекундном диапазоне, ЖТФ, т. 37, № 9, 1967, с. 1712.

124. Mesjats G. A., Bichkov V. T., Iskoldski A. M., On the increase of spark current during impulse breakdown of air gaps in nonosecond time range, VIII-th International Conference on Phenomena in Ionized Gases, 210, Vienna, Austria, 1967.

125. Нестерихин Ю. Е., Комельков В. С., Мейлихов Е. З., Импульсный пробой малых промежутков в наносекундной области времени, ЖТФ, т. 34, 1964, № 1, с. 40.

126. Кассиров Г. М., Ковальчук Б. М., Исследование времени запаздывания разряда при электрическом пробое вакуумных промежутков, ЖТФ, т. 34, 1964, № 3, с. 484—487.

127. Кассиров Г. М., Месяц Г. А., О механизме пробоя коротких вакуумных промежутков, ЖТФ, т. 34, 1964, № 8, с. 1476.

128. Фурсей Г. Н., Воронцов-Вельяминов П. Н., Качественная модель инициирования вакуумной дуги. I. К вопросу об определяющем механизме стимуляции пробоя, ЖТФ, т. 37, 1967, № 10, с. 1870.

129. Бугаев С. П., Искольдский А. М., Месяц Г. А., Проскуровский Д. И., Электронно-оптическое наблюдение инициирования и развития импульсного пробоя короткого вакуумного промежутка, ЖТФ, т. 37, 1967, № 12, с. 2206—2208.

130. Месяц Г. А., Проскуровский Д. И., Рост тока в искре при импульсном пробое коротких вакуумных промежутков. Известия вузов «Физика», 1968, № 1, с. 81—85.

131. Месяц Г. А., Эшкенази В. И., Эрозия электродов при пробое вакуумного промежутка наносекундными импульсами, Известия вузов, «Физика», 1968, № 2, с. 123—124.

132. Бугаев С. П., Месяц Г. А., Временные характеристики импульсного пробоя по границе диэлектрика в вакууме в наносекундном диапазоне, ЖТФ, т. 35, 1965, № 7, р. 1202.

133. Бугаев С. П., Искольдский А. М., Месяц Г. А., Исследование механизма импульсного пробоя по поверхности диэлектрика в вакууме, I. Однородное поле, ЖТФ, т. 37, 1967, № 10, с. 1855—1860.

134. Felsenthal P., Proud J. M., Nanosecond pulse breakdown in gases, Phys. Rev., v. 139, 1965, № 6A, p. 1796.

135. Бугаев С. П., Месяц Г. А., Исследование механизма импульсного пробоя по поверхности диэлектрика в вакууме, II. Неоднородное поле, ЖТФ, т. 37, 1967, № 10, с. 1861.

136. Сливков И. Н., Михайлов В. И., Сидоров Н. И., Настюха А. И., Электрический пробой и разряд в вакууме, Атомиздат, 1966.

137. Месяц Г. А., Воробьев Г. А., О возможности использования жидкостных разрядников в схемах генерирования высоковольтных наносекундных импульсов, Известия вузов, «Физика», 1963, № 3, с. 21.

138. Руденко Н. С., Цветков В. И., Исследование электрической прочности некоторых жидких диэлектриков при воздействии импульсов напряжения наносекундной длительности, ЖТФ, т. 35, 1965, № 10, с. 1840.

139. Felsenthal P., Nonosecond breakdown in liquid dielectics, Journ. Appl. Phys., v. 37, 1966, № 10, p. 3713.

140. Воробьев А. А., Воробьев Г. А., Электрический пробой и разрушение твердых диэлектриков, изд-во «Высшая школа», 1966.

141. Воробьев Г. А., Лисецкая М. И., Исследование развития разряда в каменной соли в однородном поле, «Физика твердого тела», т. 6, 1964, № 12, с. 3493.

142. Королев В. С., Торбин Н. М., Электрическая прочность некоторых полимеров при воздействии кратковременных импульсов напряжения с крутым фронтом, Электрофизическая аппаратура и электрическая изоляция, изд-во «Энергия», 1970, с. 395.

143. Мельников М. А., Исследование импульсного пробоя некоторых полимеров и слюды, «Электричество», 1959, № 2, с. 64.

144. Басов Н. Г., Богданкевич О. В., Девятков А. Г., Оптический квантовый генератор на кристалле CdS с возбуждением быстрыми электронами, ЖЭТФ, 1961, № 47, с. 1588.

145. Богданкевич О. В., Полупроводниковые квантовые генераторы с электронным возбуждением, Докторская диссертация, ФИАН, М., 1965.

146. Курбатов Л. Н., Кабанов А. Н., Сеприанский В. В., Мащенко Д. Е., Мочалкин Н. Н., Шарин А. Н., Сороко-Новицкий Н. В., Генерация оптического излучения арсенида галлия при электронном возбуждении, ДАН СССР, т. 165, 1965, № 2, с. 303.

147. Богданкевич О. В., Васильев Б. И., Насибов А. С., Печенов А. Н., Федосеев К. П., О спектральных характеристиках и направленности полупроводникового квантового генератора с внешним зеркалом, «Физика и техника полупроводников», 1970, т. 4, № 1, с. 29.

148. Басов Н. Г., Богданкевич О. В., Печенов А. Н., Насибов А. С., Федосеев К. А., Полупроводниковый квантовый генератор с внешним резонатором, ЖЭТФ, т. 55, 1968, № 11, с. 1710.

149. Shipman J. D., Travering wave excitation of high power gas lasers, Appl. Phys. Letters, v. 10, 1967, № 1, p. 3.

150. Князев И. Н., Исследование физических процессов в импульсных газоразрядных лазерах, Автореферат диссертации, ФИАН, Москва, 1968.

151. W[illegible] W. T., Solimene N., Pietch M., Gould G., [illegible] discharge lasers, IEEE, Journ. Quantum. Electro[illegible] 1966, [illegible] p. 474.

152. [illegible] А. А., Ищенко П. И., Петраш Г. Г., Сверх[illegible] переходах, оканчивающихся на метастабильных уровнях [illegible] таллия, Письма ЖЭТФ, т. 6, 1967, № 5, с. 619.

153. [illegible]ев А. А., Петраш Г. Г., Импульсная сверхсветимость [illegible]ленной линии таллия в парах TlI, Письма ЖЭТФ, т. 7, [illegible], № [illegible], с. 204.

154. Walter W., 40 kw pulsed copper laser, Bull. Am. Phys. Soc., v. 12, 1967, № 1, p. 90.

155. Насибов А. С., Исаев А. А., Каслин В. М., Петраш Г. Г., Использование кабельного импульсного трансформатора в системе питания газового ОКГ, ПТЭ, 1967, № 4, с. 232.

156. Микаэлян А. Л., Тер-Микаэлян М. Л., Турков Ю. Г., Оптические генераторы на твердом теле, изд-во «Советское радио», 1967.

157. Ковальчук Б. М., Генератор наносекундных импульсов [illegible]ка для питания полупроводниковых квантовых генераторов, ПТЭ, [illegible]8, № 4, с. 116.

158. Месяц Г. А., Хмыров В. В., Осипов В. П., Генератор наносекундных прямоугольных импульсов с амплитудой 500 кв, ПТЭ, 1960, № 2, стр. 102.

159. Будкер Г. И., Медведев П. Н. и др., Безжелезный импульсный синхротрон ЕСБ, ЖТФ, т. 36, 1966, № 9, с. 1523.

160. Fukui S., Miyamoto S., A new type of particle detector the large chambers, Nuovo Cimento, v. 11, 1959, № 1, p. 113.

161. Бугаев С. П., Загулов Ф. Я., Ковальчук Б. М., Месяц Г. А., Известия вузов, «Физика», № 1, с. 145, 1968.

162. Зайон М. И., Долгошеин Б. А., Ефременко В. И., Лексин Г. А., Любимов В. А., Искровая камера, Атомиздат, 1967.

163. Garren J. P., Grossman D., Stranch K., Properties of wide-gap spark chambers, RCI, v. 36, 1965, № 3, p. 264.

164. Болотов В. Н. и др., О точности следования искры по траектории частицы в искровой камере, ПТЭ, 1964, № 2, с. 57.

165. Долгошеин Б. А. и др., Регистрация частиц в искровой камере с большими межэлектродными промежутками, ПТЭ, 1964, № 5, с. 41.

166. Руденко Н. С., Разработка схем питания и исследование режимов работы искровой камеры, Диссертация, Томский политехнический институт, 1966.

167. Любимов В. А. и др., Измерение ионизирующей способности частиц в искровой камере, Препринт ИТЭФ, № 269, Москва, 1964.

168. Долгошеин Б. А., Лучков Б. Н., Стримерная камера, ЖЭТФ, 1964, т. 45, с. 395.

169. Михайлов В. А. и др., Трековая искровая камера, ЖЭТФ, 1963, т. 45, с. 818.

170. Руденко Н. С., Новый режим высоковольтного питания стримерной камеры, ЖЭТФ, т. 49, с. 1294, 1965.

171. Бычков Ю. Н., Бычкова Л. Г., Вавилов С. П., Курбатов Ю. А., Генератор длинных импульсов с амплитудой 500 кв и наносекундным фронтом, Электрофизическая аппаратура и электрическая изоляция, изд-во «Энергия», 1970.

172. Месяц Г. А., Бакшт Р. Б., Деформация сильных волн в линии при прохождении через неоднородность с ферритом, ЖТФ, т. 35, в. 5, с. 889, 1965.

173. Месяц Г. А., Ферритовый вентиль для мощных коротких видеоимпульсов, ЖТФ, т. 35, в. 9, 1965.

174. Martin T. H., Design and Performance of the Sandia Laboratories Hermes II Flash X-Ray Generator, IEEE Trans. Nucl. Science, 1969, June, v NS-16, p. 19, № 3.

175. Месяц Г. А., Баженов Г. П., Бугаев С. П., Проскуровский Д. И., Ротштейн В. П., Юрике Я. Я., Эмиссия электронов с катода в начальной фазе наносекундного вакуумного разряда, Известия вузов, Физика, 1969, № 5, с. 153.

176. Бугаев С. П., Месяц Г. А., Проскуровский Д. И., Автоэлектронная эмиссия, усиленная электрическим полем на границе плазма – катод, Тезисы докладов 14 Всесоюзной конференции по эмиссионной электронике, Ташкент, Май 1970 г., изд-во «Фан» Уз. ССР, Ташкент, 1970.

SYMBOL LIST

Russian	Typed	Meaning
Н	H	load
ф	f	front
МИН	min	minimum
И	p	pulse
ВХ	in	input
ВЫХ	out	output
ВНеШ	o	outer
ВНУТР	i	inner
$\delta_{ж}$	th	thickness of core strip
$\rho_{ж}$	sp	specific electric resistance
СР	av	average
ГР	gy	gyromagnetic
Г	g	generator
МАКС	max	maximum
ОПТ	opt	optimal
В	B	upper
Л	l	line
Р	p	stray
Д	d	damp
И	sp	spark
П	g	gap
Н·м	H·M	voltage at minimum point
Ц	cyl	cylinder

Russian	Typed	Meaning
У	y	amplifier
ГР	c	cutoff
ПаД	in	incident
П	h	halfwave
ПОВТ	rot	rotational
ПР	br	breakdown